PHASE TRANSITIONS IN ANTIFERROMAGNETIC SYSTEMS AT FIELDS UP TO 110 KILO-OERSTEDS

J. W. METSELAAR

PHASE TRANSITIONS
IN ANTIFERROMAGNETIC SYSTEMS
AT FIELDS UP TO 110 KILO-OERSTEDS

INSTITUUT-LORENTZ
voor theoretische natuurkunde
Nieuwsteeg 18-Leiden-Nederland

PHASE TRANSITIONS IN ANTIFERROMAGNETIC SYSTEMS AT FIELDS UP TO 110 KILO-OERSTEDS

PROEFSCHRIFT

TER VERKRIJGING VAN DE GRAAD VAN DOCTOR IN DE WISKUNDE EN NATUURWETENSCHAPPEN AAN DE RIJKSUNIVERSITEIT TE LEIDEN, OP GEZAG VAN DE RECTOR MAGNIFICUS DR. A.E. COHEN, HOOGLERAAR IN DE FACULTEIT DER LETTEREN, VOLGENS BESLUIT VAN HET COLLEGE VAN DEKANEN TE VERDEDIGEN OP DONDERDAG 28 JUNI 1973 TE KLOKKE 14.15 UUR

door

JAN WILLEM METSELAAR

geboren te Alkmaar in 1942

Krips Repro - Meppel

PROMOTOR: DR. D. DE KLERK

STELLINGEN

1. De berekening van de exchange constanten voor $CoCl_2 \cdot 6H_2O$, zoals deze gegeven is door Shinoda et al., is aanvechtbaar.
   Shinoda, T., Chihara, H. en Seki, S., J. Phys. Soc. Japan 19 (1964) 1637.

2. De conclusies uit de susceptibiliteitsmetingen aan $LiCuCl_3 \cdot 2H_2O$ van Abrahams en Williams zijn aan twijfel onderhevig.
   Abrahams, S.C. en Williams, H.J., J. Chem. Phys. 39 (1963) 2923.

3. Magnetisatiemetingen in de buurt van het verzadigingsveld van een antiferromagneet met antisymmetrische exchange kan belangrijke informatie geven over de Dzyaloshinsky-Moriya vectors, welke deze exchange beschrijven.
   blz. 69 van dit proefschrift.

4. Het begrip "easy axis" wordt in de literatuur over magnetisme niet éénduidig gebruikt.
   Zie bijvoorbeeld: Date, M., J. Phys. Soc. Japan 14 (1959) 1244 en Haseda, T., J. Phys. Soc. Japan 15 (1960) 483.

5. Bij het construeren van spoelen, welke pulsvelden moeten produceren boven de 400 kOe, dient men de nodige aandacht te besteden aan de isolatie van het draad waarvan de spoelen worden gewikkeld.

6. De verklaring van het warmtegeleidingsgedrag van een Nb-Ti preparaat, zoals deze is gegeven door Dubeck en Setty, wordt niet voldoende door hun experimenten ondersteund.
   Dubeck, L. en Setty, K.S.L., Phys. Letters 27A (1968) 334.

7. De bepaling van de "zero point spin deviation" met behulp van susceptibiliteitsmetingen verdient in een aantal gevallen de voorkeur boven de methode die gebruik maakt van neutronen diffractie.
   blz. 107 van dit proefschrift.

8. De argumenten, welke Pekalski aanvoert ter ondersteuning van zijn fasediagram voor een eenvoudige antiferromagneet, zoals deze werd verkregen uit de lineare spingolf theorie, zijn twijfelachtig.
Pekalski, A., Acta Physica Polonica A40 (1971) 189.

9. De berekeningen aan eindige lineaire Heisenberg ketens van onder andere Bonner en Fisher, kunnen aanzienlijk vereenvoudigd worden.
Bonner, J.C. en Fisher, M.E., Phys. Rev. 135 (1964) A640.

10. De beschrijving welke Brilouin geeft van de roodverschuiving ten gevolge van een gravitatieveld is discutabel.
Brillouin, L., Relativity Reexamined. Academic Press 1970 New York en London, blz. 75.

J.W. Metselaar Leiden 28 juni 1973.

Aan Tini

Aan Remco, Erwin en Irma

CONTENTS

CHAPTER 1

INTRODUCTION AND SURVEY

1. The research program.

In this thesis the magnetic behaviour of three antiferromagnets: $LiCuCl_3 \cdot 2H_2O$, $CoCl_2 \cdot 6H_2O$ and $CoBr_2 \cdot 6H_2O$ is described. These salts have in common that the spins from which the magnetic properties arise have the value one half and that anisotropic interactions play an important role.

The magnetic susceptibility at low frequencies was measured in the temperature range 1.2 to about 12 K and in magnetic fields up to about 110 kOe. This field value is much larger than what is currently available in physical research laboratories. Details can be found in Chapter 2.

Up to now no clear model for the magnetic interactions in $LiCuCl_3 \cdot 2H_2O$ is available in the literature. The model is greatly extended and improved on the basis of the susceptibility measurements given in Chapter 3, which cover a large part of the magnetic phase diagram. From the discussions as outlined in Chapter 4 it appears that the magnetic behaviour is dominated by an anisotropy of the antisymmetric type, giving rise to a spontaneous canting of the four magnetic sublattices with respect to each other (see section 2). Another consequence of the antisymmetric interaction is the occurrence of several phase transitions (first and second order). These transitions take place far below the field at which the transition to paramagnetism occurs, and are not found in simple two sublattice antiferromagnets.

$CoCl_2 \cdot 6H_2O$ and $CoBr_2 \cdot 6H_2O$ are both examples of simple two sublattice antiferromagnets with a (first order) phase transition and a (second order) transition to paramagnetism. The anisotropy in these salts arises from the combined effect of the spin-orbit coupling and the crystal field and its form is symmetric. The model of the interactions in these Co salts is better established in the literature than for $LiCuCl_3 \cdot 2H_2O$. However, a rigorous treatment, based on recent spin wave theories, was necessary because the spin value is low ($S = \frac{1}{2}$) and the most important interaction takes place between a spin and only four neighbours. This leads to a zero point spin deviation (see Chapter 6) large as compared to the one occurring in most other antiferromagnets.

The experimental results are presented in Chapter 5 and the discussion is given in Chapter 6.

2. Canting mechanisms.

A spontaneous canting or bending of the sublattices in zero magnetic field is encountered in many magnetic systems. If only two sublattices are involved the canting gives rise to a small net magnetic moment. This phenomenon is called "weak ferromagnetism". If more sublattices are involved the canting, in case of a non-zero resulting magnetic moment, is called "overt". It is called "hidden" in the case of more than two sublattices with a vanishing net magnetic moment.

The possibility of canting of the sublattices in magnetic systems was first investigated by Dzyaloshinsky [1], who based his considerations upon symmetry properties of the crystal and on Landau's theory of phase transitions. He suggested an energy term of the form

$$\underline{D}_{ij} \cdot \underline{S}_i \wedge \underline{S}_j$$

between two spins $\underline{S}_i$ and $\underline{S}_j$. This gives rise to a canting of the two spins with respect to each other, if in addition an antiferromagnetic interaction between these spins is present.

According to Dzyaloshinsky spontaneous canting can only exist if the symmetry (magnetic as well as crystallographic) is the same in the canted as in the uncanted state.

The symmetry of $LiCuCl_3 \cdot 2H_2O$ is considered extensively in Chapter 4, section 3, from which it can easily be concluded that the proposed zero field spin arrangement, given in section 5 of the same chapter, satisfies Dzyaloshinsky's requirement. This means that canting is possible in $LiCuCl_3 \cdot 2H_2O$ regardless of the mechanism.

The necessary and sufficient conditions for the existence of weak ferromagnetism have been given by Turov [2]. Two necessary conditions for weak ferromagnetism are:

1°. The magnetic and chemical unit cell must be identical.

2°. The magnetic moments at all lattice sites related by translation or inversion transformations must be parallel.

From neutron diffraction data [3], X-ray analysis [4] and Li nuclear magnetic resonance [5] it is concluded that the chemical unit cell contains four different Cu ions and that the magnetic system consists of four or two sublattices.

If there are two magnetic sublattices, thus two magnetically different Cu spins, then the first condition is not fulfilled. If there are four magnetic sublattices then by definition $LiCuCl_3 \cdot 2H_2O$ can not be a weak ferromagnet. In fact a four magnetic sublattice model appears to describe the behaviour of $LiCuCl_3 \cdot 2H_2O$ satisfactorily according to Chapter 4.

The second necessary condition for weak ferromagnetism is not fulfilled as is clear from the neutron diffraction data [4]. Neighbouring spins which are related by inversion are antiparallel.

So the conclusion is that weak ferromagnetism is not possible in $LiCuCl_3 \cdot 2H_2O$.

The canting in $LiCuCl_3 \cdot 2H_2O$ should be either hidden or overt. In the susceptibility measurements, which are given in Chapter 3 no magnetic moment in zero field was detected and also in the literature this property has never been mentioned. In fact, thus far, all investigators have considered $LiCuCl_3 \cdot 2H_2O$ to be an ordinary two sublattice antiferromagnet. This model appears to be too simple, as follows from the discussions given in Chapters 3 and 4.

So it is concluded that in $LiCuCl_3 \cdot 2H_2O$ only a hidden canting is possible and it follows from the susceptibility data of Chapter 3 that the canting angle is approximately 6°.

In the literature several canting mechanisms may be found.

1°. Moriya's single ion anisotropy mechanism [6]. This mechanism is ruled out in the case of $LiCuCl_3 \cdot 2H_2O$ because $S = \frac{1}{2}$ so that no single ion anisotropy can exist.

2°. Moriya's antisymmetric exchange mechanism [7]. In this case the canting arises from the antisymmetric part of the anisotropic superexchange energy; it is caused by the spin-orbit coupling. The magnitude is estimated to be $\Delta g/g$ times the isotropic superexchange energy (see also Chapter 4, section 2). Here Δg is some mean value of $g - 2$ for the substance considered. In the case of $LiCuCl_3 \cdot 2H_2O$ $\Delta g/g \simeq .1$, giving rise to a canting angle of about 6°, which is quite close to the experimental value. The interaction related to this mechanism is in the literature known as Dzyaloshinsky-Moriya interaction.

3°. Silvera et al. [8] have shown that canting can be produced by the action of anisotropic g tensors, of which the principal axes are tilted with respect to each other at the different magnetic ion sites. The antisymmetric interaction in the description of the magnetic behaviour arises in terms of a fictitious spin $S = \frac{1}{2}$. In case of an isotropic g tensor there is no canting. In the case of $LiCuCl_3 \cdot 2H_2O$ g varies only 10% for the different crystallographic directions and the canting angle does not exceed .06° irrespective of

the tilting angle (if this exists) between the principal axes belonging to different Cu ions. Consequently this mechanism can not account for the experimentally observed angle of 6°.

From the preceding discussion it is clear that only Moriya's antisymmetric exchange mechanism is a possible cause of the canting in $LiCuCl_3 \cdot 2H_2O$. The symmetry considerations related to this mechanism are extensively given in Chapter 4 section 3 and important conclusions are drawn,

The model for $LiCuCl_3 \cdot 2H_2O$ is further developed by using the fact that an ordering process sets in at a finite temperature (4.48 K as follows from the susceptibility measurements given in Chapter 3). The existence of this ordering temperature means that interactions should play a role outside the chain in which the smallest distances occur between Cu spins, because a system of uncorrelated chains does not lead to long range order.

The considerations about the existence of a Dzyaloshinsky-Moriya interaction as well as the occurrence of an ordering temperature together with the restriction that, if an important interaction takes place between two spins, their distance should not be too large, are the main features of the arguments which result into the energy expression (equation 3 of Chapter 4) of $LiCuCl_3 \cdot 2H_2O$. It is expected that this Hamiltonian describes the most important properties of this antiferromagnet. Preliminary calculations show that this Hamiltonian describes the spin-flop transition as well as the first order phase transition which takes place at a higher field. An essential property of the higher first order phase transition is that the sign of the vector product of two of the four magnetic sublattices of $LiCuCl_3 \cdot 2H_2O$ suddenly reverses.

3. Spin waves.

The concept of a spin wave was first used by Bloch [9]. This spin wave is described as a single reversed spin distributed coherently over a large number of otherwise aligned atomic spins in a crystal lattice.

A quantummechanical treatment for an antiferromagnet was first given by Hulthén [10]. He defined coordinates which, in a classical way, represent the small vibrations (considered to be harmonic) of the spin system; then these coordinates were quantized. However, he ignored the zero point energy which should exist in a system of harmonic oscillators, as was pointed out by Klein and Smith [11]. A careful treatment of the ground state, including the zero point energy, was carried out by Anderson [12] for a simple antiferromagnet. The theory in which the spin vibrations are taken to be harmonic is called the

linear spin wave theory.

Anderson [12] and Kubo [13] predicted, on the basis of the linear spin wave theory, a spin reduction in a crystal lattice of the order of $1/zS$, in which z is the number of spins with which one spin interacts. For ordinary antiferromagnets this spin reduction should be experimentally observable e.g. with accurate neutron diffraction. If $S = \frac{1}{2}$ and $z = 4$, which is the case for $CoCl_2 \cdot 6H_2O$ and $CoBr_2 \cdot 6H_2O$, the two salts considered in this thesis, the spin reduction is expected to be very large, viz. 0.5, and this must be reflected in the behaviour of the susceptibility in the flop phase of these antiferromagnets. The reason for this is that the spin reduction does not exist in the paramagnetic phase. So a more than linear increase of the magnetization is expected in the flop phase, resulting into a rise of the susceptibility with increasing field. This rise is not predicted by the molecular field theory.

The assumption that the spin differs only a small amount from its ground state value limits the applicability of the linear spin wave theory to the low temperature region. For this reason Holstein and Primakoff [14] developed a non-linear spin wave theory in which they defined the exact coordinates representing the spin deviations from the ground state value. In terms of these coordinates the Hamiltonian of the system splits into two parts. One quadratic in the spin wave amplitudes and one of the higher order. The quadratic part alone gives a theory of non-interacting spin waves, identical to the linear approximation of Anderson [12]. The non-quadratic part represents the effects of interaction between spin waves. Therefore it is expected that, for the lower temperatures, a consistent treatment of spin wave interactions is possible, taking the quadratic part of the Hamiltonian as a first approximation and dealing with the non-quadratic part by perturbation theory. However, according to Dyson [15], for the case of ferromagnetism it appears that in this perturbation theory the spin wave interactions are largely overestimated and that, for the lower temperatures, the linear spin wave theory gives a much better description. The same result is expected for an antiferromagnet, although an exact proof has not yet been given.

Several authors treated the problem of an antiferromagnet in the different phases. Wang and Callen [16] described the behaviour of an antiferromagnet in the flop phase. In this description the spin wave interactions are taken into account to a certain extent. Feder and Pytte [17] carried out calculations including the three different phases of an anisotropic antiferromagnet including spin wave interactions to the order $1/S$. Kanamori and Yosida [18] approached the problem with the linear spin wave theory.

The experimental results of $CoCl_2 \cdot 6H_2O$ and $CoBr_2 \cdot 6H_2O$ given in Chapter 5 are compared with the spin wave predictions in Chapter 6. Special attention is given to the behaviour of the susceptibility in the flop phase, considering the influence of the spin wave interactions, the temperature and the anisotropy.

References.

1) Dzyaloshinsky, I., J. Phys. Chem. Solids 4 (1958) 241.
2) Turov, E.A., Physical Properties of Magnetically Ordered Crystals. New York: Academic Press 1965.
3) Abrahams, S.C. and Williams, H.J., J. Chem. Phys. (1963) 2923.
4) Vossos, P.H., Jennings, L.D. and Rundle, R.E., J. Chem. Phys. 32 (1960) 1590.
5) Henkens, L.S.J.M. and Diederix, K.M., private communication.
6) Moriya, T., Phys. Rev. 117 (1960) 635
7) Moriya, T., Phys. Rev. 120 (1960) 91.
8) Silvera, I.F., Thornley, J.H.M. and Tinkham, M., Phys. Rev. 136 (1964) A695.
9) Bloch, F., Z. Physik 61 (1930) 206; 74 (1932) 295.
10) Hulthén, Proc. Roy. Acad. Sci. Amsterdam 39 (1936) 190.
11) Klein, M.J. and Smith, R.S., Phys. Rev. 80 (1951) 1111.
12) Anderson, P.W., Phys. Rev. 86 (1952) 694.
13) Kubo, R., Phys. Rev. 87 (1952) 568.
14) Holstein, T. and Primakoff, H., Phys. Rev. 58 (1940) 1098.
15) Dyson, F.J., Phys. Rev. 102 (1956) 1217.
16) Wang, Y-L.W. and Callen, H.B., J. Phys. Chem. Solids 25 (1964) 1459.
17) Feder, J. and Pytte, E., Phys. Rev. 168 (1968) 640.
18) Kanamori, J. and Yosida, K., Prog. Theor. Phys. 14 (1955) 423.

CHAPTER 2

EXPERIMENTAL PROCEDURE

1. Introduction.

The purpose of the experiments is to study the behaviour of antiferromagnetic materials as a function of the magnetic field and the temperature, specially the phase transitions.

In the literature many transitions are described which occur at relatively low field values. Most of them are transitions between two ordered states usually between the so-called "antiferromagnetic" and "spin flop" phases. In these phases the order is brought about by the anisotropic exchange interaction, characterized by the exchange energy J.

In the present investigations special attention has been given to the transitions in higher fields, of which the highest one is the transition to paramagnetic saturation. A simple qualitative consideration leads to an estimate of the necessary field values. In zero field the antiferromagnetic order is destroyed by the energy kT_N, where k is the Boltzmann's constant and T_N the Néel temperature. At zero temperature it is destroyed by the energy $\mu_B H_c$, where μ_B is the Bohr magneton and H_c the transition field at T = 0. Considering only only orders of magnitude we have the relations

$$kT_N \approx \mu_B H_c \approx J$$

since $\mu_B/k = .67 \times 10^{-4}$ emu, a Néel temperature in the liquid helium region, say 3 K, corresponds to an upper transition field of about 40 kOe. Such fields are well within reach of the modern superconducting coil magnets.

The quantity determined in the experiments was the isothermal differential susceptibility $(\partial M/\partial H)_T$. The phase transitions are observed as well defined peaks, jumps and kinks in the experimental curves. From these we can derive the (H,T)-phase diagram.

The Néel temperatures of the substances investigated in this thesis are: 4.48 K for $LiCuCl_3 \cdot 2H_2O$, 2.25 K for $CoCl_2 \cdot 6H_2O$ and 3.14 K for $CoBr_2 \cdot 6H_2O$. The first one was investigated between 1.2 and 12 K, the latter two between 1.2

and 4.2 K. Magnetic fields up to 110 kOe were available.

2. The superconducting coil and the cryostat.

2.1. Construction of the coil. The coil is shown in fig. 1. It consists of three concentric sections, each 140 mm in length. The outer section was wound from 3300 m NbTi wire supplied by IMI (type "Niomax S" 50/80). This section has an external diameter of 160 mm and an inner diameter of 86 mm. The middle section was wound from 1037 m Nb_3Sn ribbon supplied by RCA (type R-60214) and had an outer diameter of 82 mm and an inner diameter of 54 mm. The inner section was wound from 533 m Nb_3Sn ribbon, also from RCA (type SR-2101) with an outer diameter of 50 mm and an inner diameter of 30 mm[2]). The resulting magnet has a clear bore of 28 mm. The sections are shown separately in fig. 2. The outer section was wound without any special precautions, as was (at that time) suggested by IMI. Both Nb_3Sn coils were wound exactly according to RCA's application note. Copper shorting strips were applied over all the layers and mylar-copper-mylar sheets were inserted between layers.

In order to increase the homogeneity of the field [3], a number of turns were omitted in the centre of the inner coil, as shown in fig. 1. The length of the gap is 10 mm and its height 2.3 mm. Holes and grooves were applied in

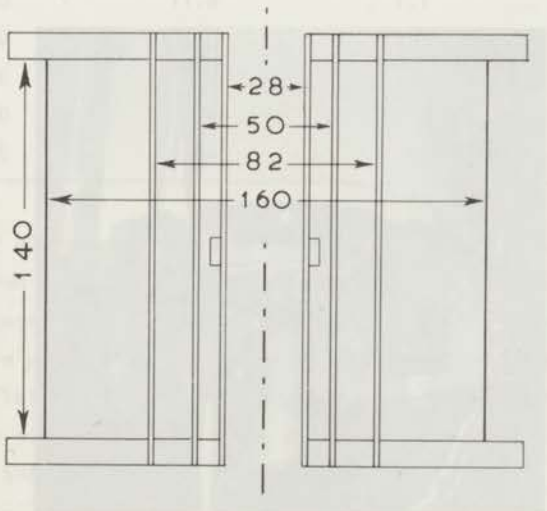

Fig. 1. Cross-section of coil (dimensions in mm).

the flanges of the coils in order to improve the cooling during energizing of

the magnet (see fig. 2).

The connections between the subsequent sections and between the magnet and the current leads were made by means of copper blocks to which strips of Nb_3Sn were soldered. By tightly bolting them to the coil terminals, resistances of the order of $10^{-7}\Omega$ were obtained (see fig. 3). Five soldered connections were

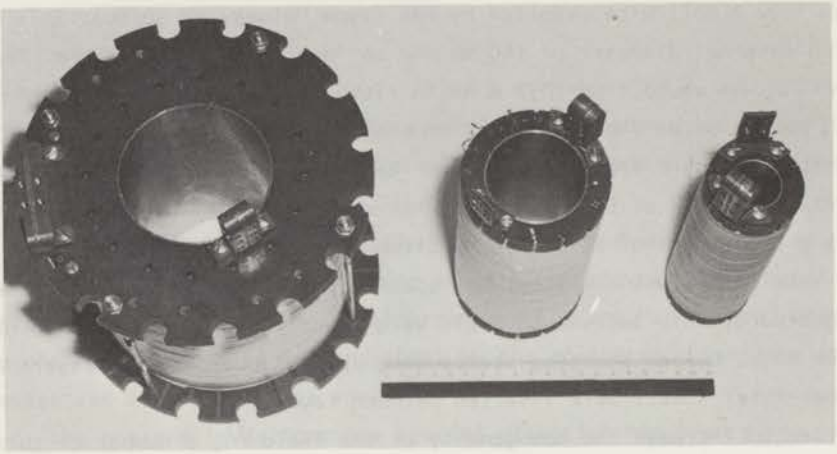

Fig. 2. Photograph of the three separate sections on which the holes and the grooves for cooling can be seen.

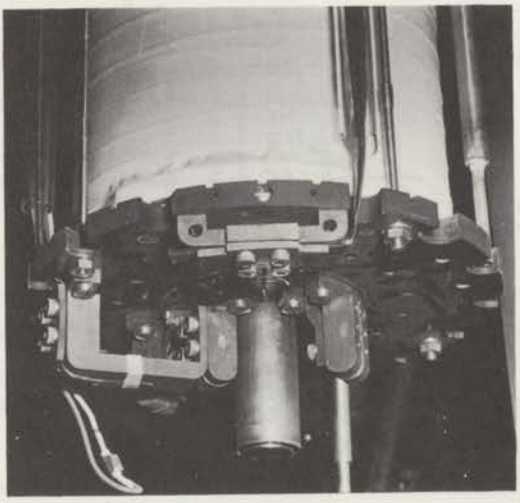

Fig. 3. Photograph showing the coil terminal connections and the tail of the insert dewar.

made inside the sections. Three of them had resistances between 10^{-7} and $10^{-8}\Omega$, and the other two had resistances of the order of $10^{-6}\Omega$ in low fields, increasing to $10^{-5}\Omega$ at 70 kOe 80 A.

2.2. Coil characteristics. The field is measured with a Siemens cryogenic Hall probe, which was calibrated in this coil up to 114 kOe by means of a simultaneous nuclear magnetic resonance experiment. The apparatus for this calibration was kindly put at our disposal by M.W. van Tol from our laboratory.

Table I gives some field values and the deviation from linear behaviour with current. H_{meas} is the experimentally determined field and H_{calc} is the

Table I

Current	Field	Hysteresis
I,A	H_{meas}, kOe	$H_{calc} - H_{meas}$, kOe
0	0	0
5	5.6	0.8
10	11.8	1.1
30	36.5	2.3
50	63.0	1.5
70	89.6	1.0
85	109.4	0.5

field calculated for a copper coil of the same dimensions. After a full run up to 110 kOe and down to zero current, the remanent field is about 3 kOe.

The field homogeneity can be seen in fig. 4, for several field levels. The fully drawn curve was calculated for a copper coil. The dependence of homogeneity on the field strength is caused by the breakdown of the magnetizing currents in the superconducting wire and ribbon of the coil, which is different for Nb_3Sn and NbTi.

2.3. Behaviour of the coil during energizing. Usually rates of field change of about 3 kOe min^{-1} are used. At 4.2 K we observed many small fast

flux jumps (order of magnitude 10 Oe and characteristic time a few millisecond) and a few slow "jumps" (order of magnitude 500 Oe and characteristic time a few second). The small fast flux jumps are probably caused by the quenching of magnetizing currents in the inner Nb_3Sn windings, whereas the large slow jumps are caused by the quenching of magnetizing currents in the outer NbTi windings. The long duration of the latter ones is due to partial compensation by induced currents in the windings of the inner sections which are shorted by copper strips (see above). Below the λ point of liquid helium more jumps occur than at 4.2 K but they are of smaller magnitude (stated wrongly in ref. 1).

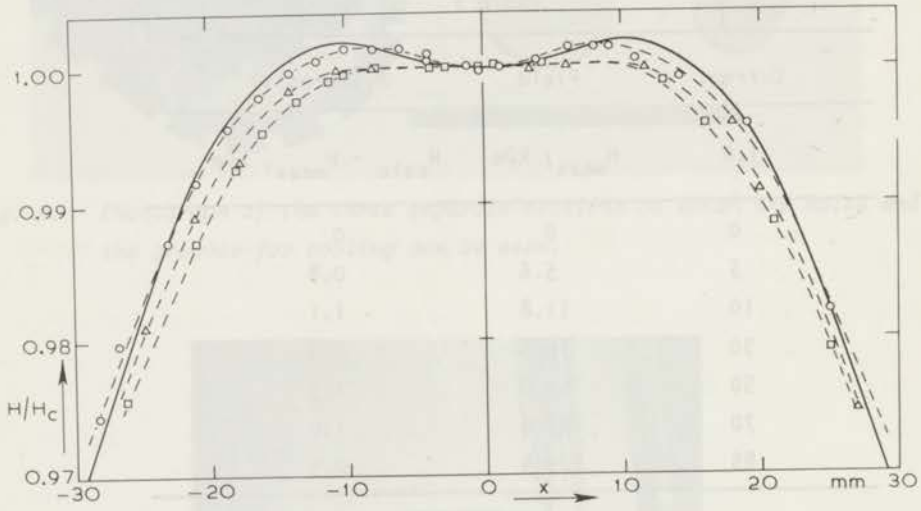

Fig. 4. Field dependent homogeneity; fully drawn curve is calculated for a copper coil of the same dimensions.

○ *Experimental points for 20 kOe*

□ *For 45 kOe*

△ *For 80 kOe*

(H_c is the field in the centre).

Table II gives the maximum fields and currents that could be reached before going normal for different combinations of coil sections. Here section 1 is the outer one, section 2 the middle one, and section 3 the inner one. The maximum current densities for the different sections just before quenching are listed in table III.

The winding densities of the sections proved to be somewhat higher than was expected before winding the magnet. Due to this the expected quench current of 90 A at 4.2 K was not reached, but the necessary current density for 100 kOe below the λ point was easily obtained.

Energizing the coil below the λ point has several advantages.

1. Smaller flux jumps than at 4.2 K.
2. The boil-off rate of helium after quenching is less violent than at 4.2 K.
3. Appreciably higher fields.

The disadvantages are

1. An extra pump is needed.
2. Helium consumption is increased.
3. Extra time is needed to reduce the temperature.

Table II

Combination	Inner diameter mm	Outer diameter mm	4.2 K Field kOe	4.2 K Current A	1.5 K Field kOe	1.5 K Current A
1	82	160	45	77	> 73	>128
1+2	50	160	79	81	90	93
1+2+3	28	160	91	70	114	87

Table III

Section	Type of wire	Current density A cm^{-2} 4.2 K	1.5 K
1	Niomax S 50-80(IMI)	12600	21000
2	R-60214 (RCA)	25700	29400
3	SR 2101 (RCA)	19800	24200

2.4. The cryostat. The cryostat is shown in fig. 5. It has been constructed in the laboratory workshop, and is made entirely from stainless steel. It consists of three concentric vessels. The outer one is filled with liquid

nitrogen, the middle one contains liquid helium which cools the coil, and the inner one is used for the actual experiment during which it may be filled with liquid helium, hydrogen, nitrogen or even neon. Its tail has an inner diameter of 22 mm.

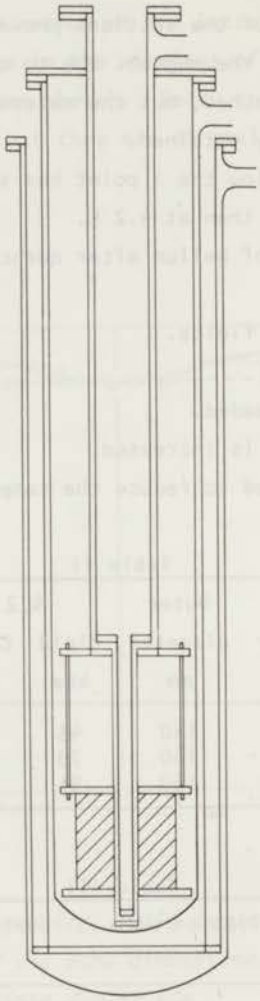

Fig. 5. Cross-section of the cryostat and coil suspension.

The vacuum spaces of the three vessels can be independently evacuated. This has the advantage that, during the filling of the outer vessel with liquid nitrogen, some helium exchange gas can be admitted to the vacuum spaces of the inner two dewars, so that the magnet coil and the experimental equipment can

be cooled down to liquid nitrogen temperature. This takes about eight hours.

In order to reduce the evaporation rate of the helium, we mounted three copper radiation shields in the helium gas stream in such a way that the evaporating gas is forced along the walls of the dewars. This reduces the evaporation rate by a factor of three. At present the total evaporation is 0.35 l h^{-1}.

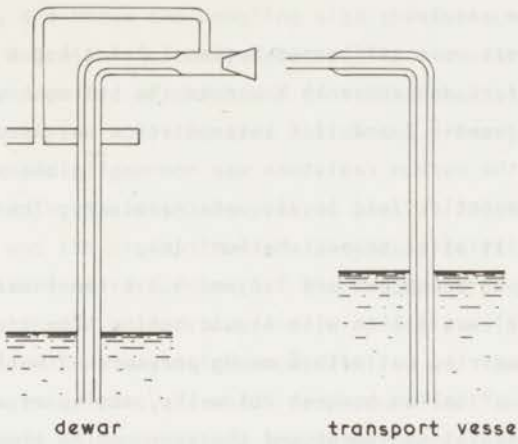

Fig. 6. The helium transfer line, with the interconnection tube required to avoid helium oscillations.

The coil is suspended from a flange which is welded to the lower part of the inner dewar (fig. 5), so there is no extra mounting device which would have its upper part at room temperature. This, again, reduces the helium evaporation.

The current leads to the coil [4,5,6], consist of folded copper sheets, 60 mm wide and 0.1 mm thick, with a superconducting strip soldered to them. They are each mounted in a glass tube which is open at both ends. In this way the leads are effectively cooled by the evaporating helium. A pair of leads, each 1.2 m long, give a total heat dissipation of about 200 mW at 100 A.

In order to cool down the coil (which has a weight of about 20 kg) efficiently from 80 to 4.2 K, a fixed helium transfer line is used. It is double walled down to the bottom of the dewar. Since in such a tube helium oscillations may arise, we mounted a narrow tube, which connects the upper part of the transfer line, to the space above the liquid helium, as shown in fig. 6. In this way the cooling down of the coil from 80 to 4.2 K takes about 6 l of helium. A shorter transfer line is used to replenish the dewar.

3. Temperature measurement and temperature control.

The susceptibility has been measured versus the magnetic field at constant temperature as well as versus the temperature at constant field. The temperature was detected with two Allen-Bradley carbon resistors, mounted symmetrically above and below the sample.

The thermometers were calibrated betwen 1.2 and 4.2 K versus the liquid helium vapour pressure and above 14 K versus the hydrogen vapour pressure. For the experiments between 4.2 and 12 K interpolation was needed. Since the magnetoresistance of the carbon resistors was non-negligible additional calibrations at several magnetic field levels were necessary. The calibrations were repeated periodically after several helium runs.

During the experiments between 1.2 and 4.2 K the inner dewar of the cryostat (see section 2) was filled with liquid helium. The investigations between 4.2 and 12 K were carried out with 8 mm Hg pressure of helium gas in the dewar and a small amount of helium between its walls, acting as an exchange gas between the experimental equipment and the surrounding liquid helium in the dewar containing the superconducting coil. The current through the primary measuring coils and the heat leak from the room temperature top of the inner dewar gave rise to an increase of the temperature of the sample and the thermometers, which could be controlled by adjusting the pressure of the exchange gas between the walls of the dewar.

In the experiments above 4.2 K the temperatures of the crystal and the thermometers were equalized as well as possible by using "coil foil" inside the measuring system. A check on the thermal equilibrium was made by repeating the experiments between 1.2 and 4.2 K with helium gas inside the inner dewar and the helium of the superconducting coil at 1.2 K. Moreover an experiment was made in which the crystal under investigation was replaced by $Cs_2Co(SO_4)_2 \cdot 6H_2O$, a salt which obeys Curie's law very accurately [7]. It turned out that in all these experiments the difference between the mean temperature of the salt (derived from its susceptibility) and the mean temperature of the carbon thermometers never exceeded 0.02 K and it is supposed that, up to 12 K, this uncertainty in the temperature will not be significantly higher.

4. Susceptibility measurement.

The susceptibility of the single crystals of $LiCuCl_3 \cdot 2H_2O$, $CoCl_2 \cdot 6H_2O$ and $CoBr_2 \cdot 6H_2O$ has been measured by means of a mutual induction method[8]. The

crystal under investigation was mounted inside a coil system in the inner dewar, which was surrounded by the superconducting coil magnet, see section 2.

The primary of the mutual inductance consisted of two concentric coils of which the outer one had half the number of turns of the inner one and $\sqrt{2}$ times its diameter, the coils being wound in opposite directions. With this configuration the stray field, and hence the coupling with the surrounding dewar and the superconducting coil magnet, is greatly reduced. The secondary system consisted of two oppositely wound coils, of which one contained the salt. In order to save space the secondary coils were not located inside the primary ones, as is usually done, but between them.

Alternating measuring fields, 3 Oe peak to peak at 225 Hz, were generated in the primary coils and the signal from the secondary coils was detected with the help of a PAR phase sensitive detector. The component of the signal which is 90° out of phase with the primary current is directly related to the real component of the differential magnetic susceptibility χ'. The in phase component is related to the imaginary part χ'', which is proportional to the energy absorption in the sample. None of our crystals showed any detectable χ'' at any temperature or field, so that relaxation effects at 225 Hz may be assumed to be negligible. For a schematic diagram of the measurements see fig. 7.

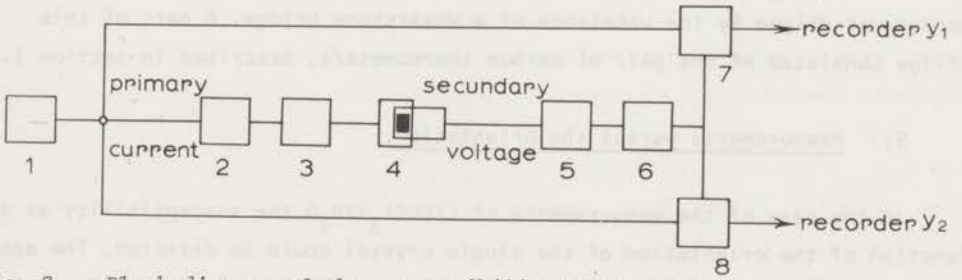

Fig. 7. Block diagram of the susceptibility measurement. 1. oscillator, 2. attenuator, 3. current measuring device, 4. coil system and sample in the cryostat, 5. pre-amplifier, 6. selective amplifier, 7. and 8. phase sensitive detectors.

A correction has to be made to the measured susceptibilities because of a small vibration of the coil system, due to the Lorentz forces on the primary coils. The correction, measured with an empty coil system, appeared to be proportional to the square of the magnetic field, as could be expected. An additional susceptibility peak was found near zero field. This could entirely be ascribed to a coupling between the coil system and the surrounding superconducting coil; a correction could be applied for it.

Only relative values of the susceptibility are measured with our method. The absolute values for $CoCl_2 \cdot 6H_2O$ were obtained by comparing our results with those of Skalyo et al. [9], those for $CoBr_2 \cdot 6H_2O$ by comparing them with those of Garber [10]. The absolute susceptibility values of $LiCuCl_3 \cdot 2H_2O$ were obtained from the calibrations of the Co salts.

Two kinds of experiments were performed. In the regions of the (H,T)-diagrams where a phase transition was represented by a more or less horizontal line the field was slowly varied at constant temperature and the susceptibility (output of the PAR phase-sensitive detector) was plotted on an XY recorder as a function of the field. In opposite cases the temperature was slowly varied at constant field and the susceptibility was plotted against T. The results of the two methods were in mutual agreement.

The field of the superconducting coil was measured with the help of a Hall probe, mounted just below the sample. In the experiments at constant temperature the horizontal axis of the recorder was directly driven by the Hall voltage. This had the consequence of a non-linear field scale of the recorder. For reproducibility of the field scale it proved to be necessary to thermostat the power source of the Hall probe.

In the experiments at constant field the horizontal scale of the XY recorder was driven by the unbalance of a Wheatstone bridge. A part of this bridge consisted of the pair of carbon thermometers, described in section 3.

5. Measurements versus the orientation.

In the case of the measurements of $LiCuCl_3 \cdot 2H_2O$ the susceptibility as a function of the orientation of the single crystal could be detected. The apparatus for reorienting the single crystal is shown in fig. 8. It consists of two concentric frames made from delrin. The outer frame consists of two demountable rings perpendicular with respect to each other. This frame can be rotated over more than 200° around a fixed axis perpendicular to the external field. Inside this frame a smaller similar frame is mounted, in such a way that its axis of rotation is perpendicular to that of the outer one. Rotations of the inner frame (also over more than 200°) with respect to the outer one is accomplished by means of two cotton threads passing through the hollow suspension axes of the outer frame. Because of constructional difficulties the axes of rotation are not exactly perpendicular but 3° off. The whole apparatus is mounted inside a delrin tube of 9.4 mm inner diameter.

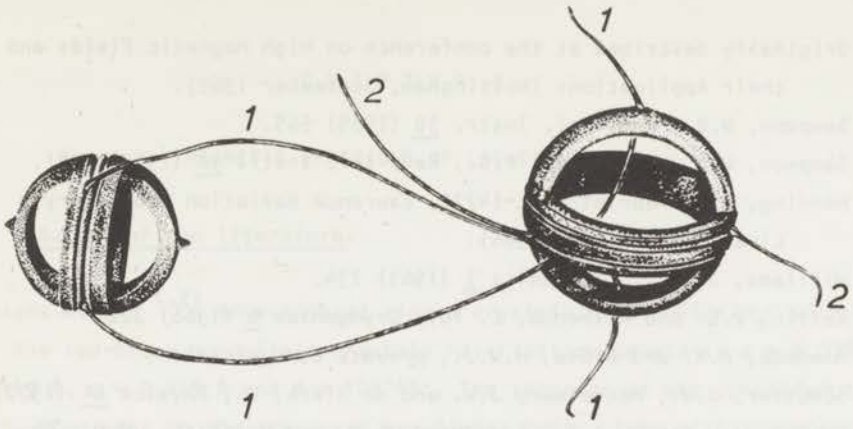

Fig. 8. Apparatus for reorientating the single crystal. The two frames have been taken apart for clarity. With the threads indicated by 1 the inner frame can be rotated with respect to the outer one. With 2 the whole system can be rotated.

References.

1) Originally described at the conference on High Magnetic Fields and their Applications (Nottingham, September 1969).
2) Sampson, W.B., Rev. sci. Instr. 36 (1965) 565.
3) Sampson, W.B. and Kruger, P.G., Rev. sci. Instr. 36 (1965) 1081.
4) Henning, C., Preprint UCRL-14775, Lawrence Radiation Laboratory, Livermore, Calif. (1966).
5) Williams, J.E.C., Cryogenics 3 (1963) 234.
6) Keilin, V.E. and Klimenko, E. Yu., Cryogenics 6 (1966) 222.
7) Miedema, A.R. and Blöte, H.W.J., private communication.
8) Schutter, J.W., Metselaar, J.W. and de Klerk, D., Physica 61 (1972) 250.
9) Skalyo, J., Cohen, A.F., Friedberg, S.A. and Griffiths, R.B., Phys. Rev. 164 (1967) 705.
10) Garber, M., J. Phys. Soc. Japan 15 (1960) 734.

CHAPTER 3

MAGNETIC BEHAVIOUR OF $LiCuCl_3 \cdot 2H_2O$

1. Survey of the literature.

Vossos et al. [1,2] investigated single crystals of $LiCuCl_3 \cdot 2H_2O$ with X-rays. The red-brown monoclinic crystals have lattice constants a = 6.078 Å, b = 11.145 Å, c = 9.145 Å and β = 108°45'. The space group was concluded to be $P2_1/C$. Prominent in the structure are planar $CuCl_6^{--}$ ions with symmetrical Cu-Cl-Cu bridges, giving rise to strongly coupled copper pairs. These pairs will henceforth be referred to as "dimers". The dimers are weakly linked to each other, leading to chains parallel to the a axis. This crystal structure, together with the results of the susceptibility measurements (also performed by Vossos et al.), suggest a ground state triplet. Comparing this structure with that of $CuCl_2$ and $CuCl_2 \cdot 2H_2O$, and taking into account the known exchange interactions of the compounds, it was concluded that in the chains the members of a dimer are parallel and subsequent dimers are oriented oppositely. From the maximum in the susceptibility the ordering temperature was concluded to be 5.9 K.

The heat capacity has been measured in the temperature range 2 - 9 K by Forstat and McNeely [3]. Its behaviour indicated a paramagnetic to antiferromagnetic phase transition at 4.40 K, so appreciably lower than the temperature given by Vossos et al. [1]. The total magnetic entropy change was 1.35 cal/mole degree. This value is very close to the value expected for a $S = \frac{1}{2}$ system, which suggests that the orientation of the members of a dimer is antiparallel, contradictory to the arrangement suggested by Vossos and his coworkers. It was found that 48% of the total entropy change occurs above the Néel temperature, presumably due to the slow diminuation of the short range ordering of the spins. The considerable short range order has also been found in $CoCl_2 \cdot 6H_2O$, $CoBr_2 \cdot 6H_2O$ and other antiferromagnetic salts.

More recently heat capacity measurements by Clay and Staveley [4], however, suggested again that the interaction within a dimer should be ferromagnetic, giving rise to a spin of unity for the pair.

From nuclear resonance of ^7Li and proton resonance by Spence and Murty [5]

a Néel temperature of 4.46 K was found, in good agreement with the value of Forstat and McNeely [3]. The magnetic space group was one of the following three $P2_1/C'$, $P2_1'/C$ or P_a2_1/C.

Spence and Murty [6] derived the sublattice magnetization versus the temperature from the local field at the proton sites by observing the proton resonance. A T^3 dependence was found. The proton spin-lattice relaxation time showed a T^{-4} dependence. The discrepancies between spin wave theory and experiment are much less serious in $LiCuCl_3 \cdot 2H_2O$ than in $CuCl_2 \cdot 2H_2O$.

Antiferromagnetic resonance in $LiCuCl_3\ 2H_2O$ was studied by Date and Nagata [7]. The observed g values along the principal magnetic axes are: $g_{a'} = 2.06$, $g_b = 2.14$, $g_c = 2.22$. it was concluded that the easy spin axis is the a' axis. The spin flop transition takes place at 10.2 kOe at 1.4 K.

From a neutron diffraction experiment on a single crystal in zero field and from magnetic susceptibility measurements performed by Abrahams and Williams [8] the most likely space group was found to be $P2_1'/C$. From the neutron diffraction data it could only be concluded that the spin direction is in the ac plane at approximately 18.8 ± 68° from the c axis. One of these directions (18.8 + 68°) differs only 3° from a' which was the spin direction according to Date and Nagata [7]. From the susceptibility data versus the orientation in the ac plane it was concluded, however, that the correct direction was 18.1 - 68°, although the susceptibility data did not include the a' direction.

Abrahams and Williams could develop a consistent model for the spin arrangement by combining the neutron diffraction data with the susceptibility measurements. They concluded that the spins of the members of a dimer are oriented along the line interconnecting the Cu ions in a dimer and are antiparallel. The antiparallel arrangement of the spins in a dimer is in agreement with the specific heat measurements of Forstat and McNeely [3], but in disagreement with the susceptibility measurements of Vossos et al. [1] and with the specific heat measurements of Clay and Staveley [4]. The susceptibility measurements in zero field between 20 and 100 K indicate a paramagnetic behaviour with an effective paramagnetic moment of 2.04 μ_B, thus corresponding to a spin $S \approx \frac{1}{2}$, in this temperature range.

Forstat et al. [9] investigated the phase boundaries up to 22 kOe by means of adiabatic magnetization experiments for the antiferromagnetic to flop phase transition, and by means of specific heat measurements for the transition to the paramagnetic phase. The Néel temperature found in this way is 4.4 K. By adiabatic rotation in the ac plane the direction of antiferromagnetic alignment was found to be the c' axis in disagreement with both Date and Nagata [7] and

Abrahams and Williams [8].

Electron spin resonance has been performed on $LiCuCl_3 \cdot 2H_2O$ by Zimmerman et al. [10], who found several new modes in addition to the conventional ones in antiferromagnets. The direction of the antiferromagnetic spin alignment was found to coincide with the 101 direction, with an accuracy of 1°.

2. Experimental results.

The red-brown single crystals were grown from an aqueous solution of $CuCl_2 \cdot 2H_2O$ and LiCl. The crystals are elongated along the a axis, and the dominant face is the (011) plane. In moist air the crystals dissolve quickly.

Out of a larger crystal a sphere of 5 mm diameter was ground and mounted inside the coil system in order to measure the differential magnetic susceptibility. The experiments were performed in fields up to 110 kOe and in the temperature range from 1.2 to 12 K.

By observing the susceptibility versus the orientation in fields just below the spin flop field the direction of antiferromagnetic spin alignment ("easy spin axis") was found from the minimum in the susceptibility. For convenience it will further be referred to as the "e direction". Our first experiments were performed in this direction, which is the 101 direction [10].

a. Typical susceptibility curves for the e direction, both versus the field and versus the temperature are shown in figs. 1 and 2.

The curves plotted versus the temperature (fig. 2) show a clear phase transition which is located, for low fields, near 4.2 K and which shifts, with increasing field, to lower temperatures. This transition is readily identified with the upper (second oreder) transition of the curves of fig. 1. The remarkable point is, however, that above this transition, even at the lowest temperatures the susceptibility does not fall to zero. This means that the magnetic system is not yet saturated.

Apart from this transition the curves of fig. 2 above about 50 kOe show another broad maximum, also located near 4.2 K, which depends very little on the field, and which suggests the existence of another phase transition. This anomaly is even more clear for the measurements in the b direction (see fig. 5). It must be emphasized that these broad maxima are much clearer in the original recordings than in the figures as given here, because in these the susceptibility scales have been largely reduced. In sections 5 and 6 of Chapter 4 it will be demonstrated that this broad anomaly is related to a saturation process. This saturation process, however, does not take place via a second order phase

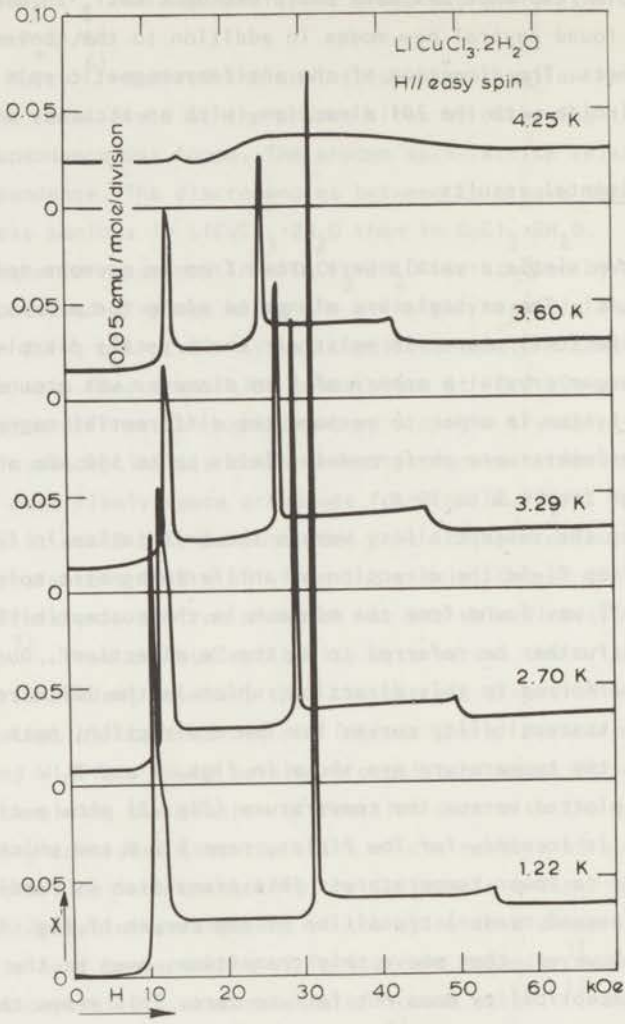

Fig. 1. Susceptibility of $LiCuCl_3 \cdot 2H_2O$ versus the magnetic field at several temperatures. The measurements have been taken along the direction of antiferromagnetic alignment (101 axis). Note the vertical shift of the susceptibility scales.

transition, like a simple two sublattice antiferromagnet, but via a gradual orientation of the spins, which is dominated by the existence of a Dzyaloshinsky-Moriya interaction. Since this broad anomaly is not observed at the lower temperatures in fig. 1 it might approach T = 0 at fields well above 100 kOe.

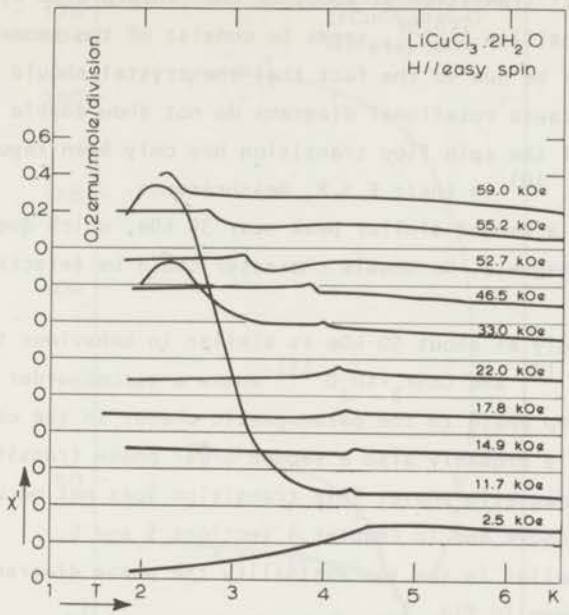

Fig. 2. Susceptibility of $LiCuCl_3 \cdot 2H_2O$ versus the temperature at various field levels, along the direction of antiferromagnetic alignment (101 axis). Note the vertical shift of the susceptibility scales.

The existence of an anomaly in the susceptibility which is related to a saturation process at about 4.2 K and fields which, at the lower temperatures, exceeds 100 kOe is not unlikely because $CuCl_2 \cdot 2H_2O$ shows a transition from the flop phase to the paramagnetic phase in fields up to 150 kOe, and its Néel temperature is 4.3 K, so quite close to the Néel temperature of $LiCuCl_3 \cdot 2H_2O$, which is 4.48 K according to our measurements. The closeness of the two Néel points suggests that the exchange constants, and thus the exchange fields (speaking in terms of the molecular field approximation) are of the same order of magnitude.

For this reason some isothermal magnetization curves were measured on a powdered sample of $LiCuCl_3 \cdot 2H_2O$ by Jordaan [14] in the pulsed magnetic fields installation of our laboratory. A gradual saturation of the magnetic moment was found in fields of the order of 150 kOe, see fig. 1, Chapter 4. These measurements will be discussed and compared with those on $CuCl_2 \cdot 2H_2O$ in Chapter 4 section 2.

The susceptibility versus the magnetic field at intermediate temperatures

(e.g. 2.70 K) as given in fig. 1 shows a few more remarkable facts.

1°. The lowest transition at about 12 kOe, interpreted by most authors as a spin flop transition [7,8,9], seems to consist of two anomalies about 1 kOe apart. This can not be due to the fact that the crystal should not be a perfect single crystal, because rotational diagrams do not show double peaks. The double character of the spin flop transition has only been reported thus far by Zimmerman et al. [10] in their E.S.R. measurements.

2°. There is a second similar peak near 30 kOe, which does not occur in ordinary antiferromagnets. No double character could be detected for this transition.

3°. The anomaly at about 50 kOe is similar in behaviour to the one found in e.g. $CoCl_2 \cdot 6H_2O$ [12] and $CoBr_2 \cdot 6H_2O$ [13] where a second order phase transition occurs from the flop phase to the paramagnetic phase. In the case of $LiCuCl_3 \cdot 2H_2O$, however, it is probably also a second order phase transition but distinctly not to the paramagnetic phase. This transition does not occur in $LiCuCl_3 \cdot 2H_2O$ as discussed above and in Chapter 4 sections 5 and 6.

From the anomalies in the susceptibility the phase diagram is constructed This diagram is shown in fig. 3.
The remarkable points are:

1°. The double transition near 12 kOe (low temperatures).

2°. The bend in the phase boundary near 17 kOe, 4.2 K between the two triple points. Many more points of the phase diagram in this region have been measured than indicated in the figure.

3°. The extra phase transition at about 32 kOe (low temperatures).

4°. The fact that the transition boundary near 56 kOe (low temperatures) is not the one to paramagnetic saturation, although it has the appearance of a second order phase transition.

5°. The anomalies above 4.2 K in the susceptibility versus the temperature, and the anomalies in the magnetization near 150 kOe, which are related to the saturation process. They are connected by a dotted line in fig. 3. It is interesting to note that the slope of this line is positive at fields below about 80 kOe. This point will be discussed further in Chapter 4, section 7.

b. Also other directions than the easy spin axis have been investigated. As an example figs. 4, 5 and 6 show the experiments with the magnetic field parallel to the b axis. In fig. 4 the susceptibility versus the magnetic field is plotted showing one first order phase transition only, with a double character, similar to that found for the transition near 12 kOe with the field parallel to the e direction. No second order phase transition has been found up to

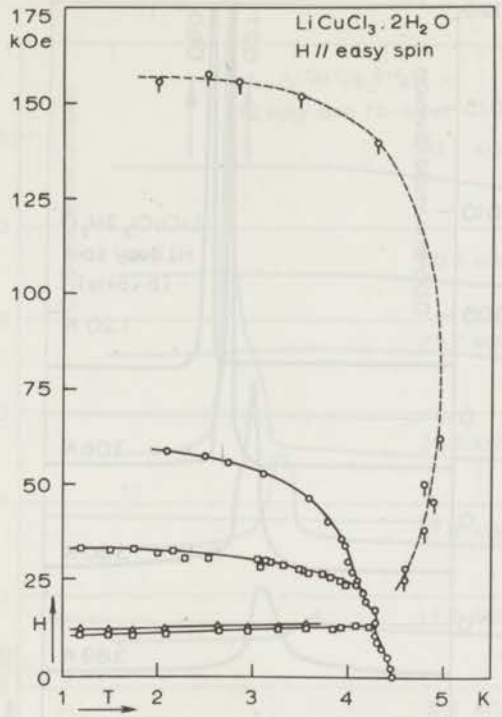

Fig. 3. The magnetic phase diagram of $LiCuCl_3 \cdot 2H_2O$ for the easy spin direction (101 axis).

- O *second order phase transitions*
- ⚲ *anomalies which are, for the lower temperatures, related to saturation*
- □ *first order phase transitions*
- △ *weak anomaly in the susceptibility*

110 kOe for this direction which, again, indicates that the second order phase transition found in the parallel case is not the one to paramagnetic saturation.

Measurements versus the temperature (see fig. 5) at fixed field levels have also been done for this direction. The figure shows clearly the double character of the transition. The high field curves (above about 20 kOe) show a flat region of the susceptibility versus the temperature below, and a broad maximum near, about 4.2 K. This is also observed in the parallel case. Due to the smallness of the susceptibility scales these broad maxima are not too clear from figs. 2 and 5.

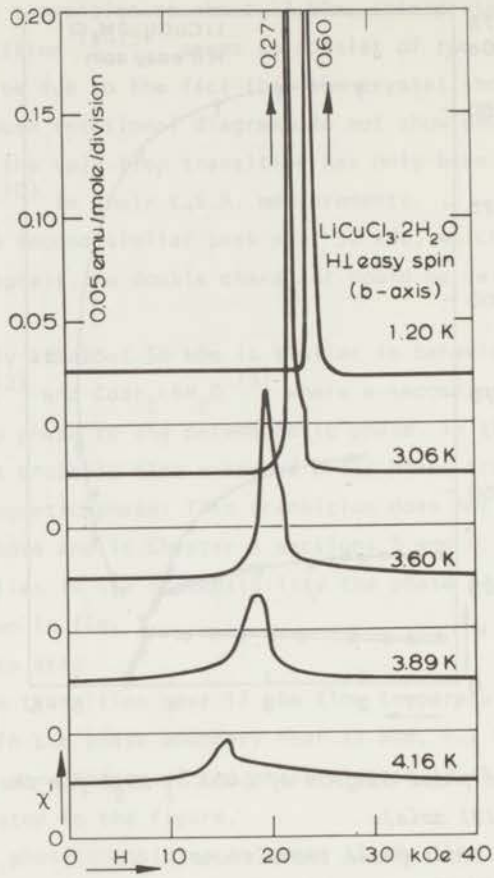

Fig. 4. Susceptibility of $LiCuCl_3 \cdot 2H_2O$ versus the magnetic field at several temperatures. The measurements have been taken along the b axis which is perpendicular to the easy spin direction.

Above about 4.2 K, at any field below 110 kOe, the susceptibility decreases with increasing temperature. This has also been observed in $CoCl_2 \cdot 6H_2O$ [12] and $CoBr_2 \cdot 6H_2O$ [13] when passing the flop-para transition by changing the temperature, in the field region between about 10 and 40 kOe.

A simple calculation concerning the behaviour of a classical paramagnet with $S = \frac{1}{2}$ yields that the susceptibility at constant field versus the temperature shows a maximum at an intermediate temperature. This temperature increases linearly with the field through the relation $\mu_B H \approx 0.8\ kT$. So if we interpret the transition near 56 kOe in the e direction as the one to para-

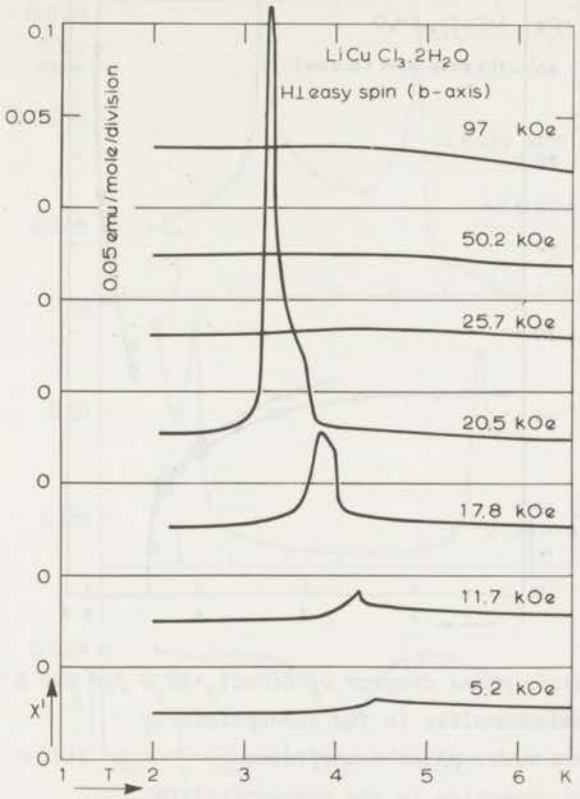

Fig. 5. Susceptibility of $LiCuCl_3 \cdot 2H_2O$ versus the temperature at several field levels along the b axis.

magnetic saturation, we should certainly expect an increase of the susceptibility with the temperature near 4 K and at fields well above 60 kOe. This increase of the susceptibility has in fact been observed in $CoCl_2 \cdot 6H_2O$ and $CoBr_2 \cdot 6H_2O$, at sufficiently high magnetic fields (see the curve for 62.3 kOe in fig. 5 of ref. 13).

In $LiCuCl_3 \cdot 2H_2O$, however, we always find a decrease of the susceptibility up to fields, much higher than 60 kOe as stated above. This, again, is an indication that below 4.2 K and above 60 kOe we are not in the paramagnetic region.

The anomalies for this direction have been assembled in the phase diagram of fig. 6.

c. The susceptibility versus the orientation in the plane perpendicular to the easy spin axis has been measured for some points of the magnetic phase

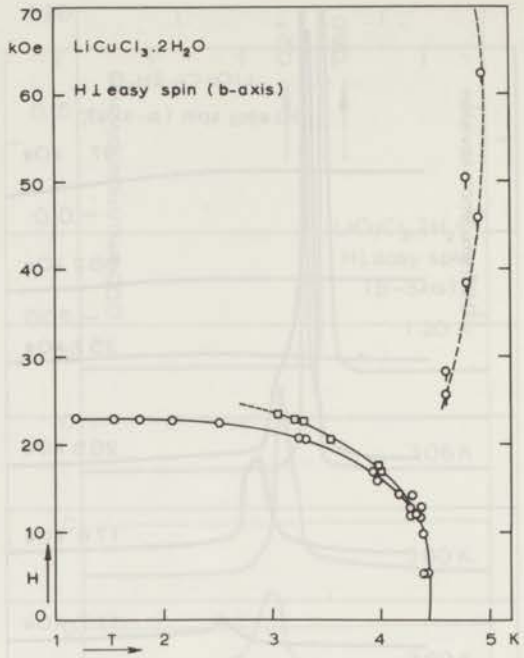

Fig. 6. The magnetic phase diagram of $LiCuCl_3 \cdot 2H_2O$ for the b direction

- ⚲ *broad anomalies in the susceptibility*
- ○ *first order phase transitions*
- □ *weak anomalies in the susceptibility*

diagram. Examples are given in fig. 7 at 3.35 K and different field levels. The anomalies have been assembled in the diagram of fig. 8. The figure is represented (within the accuracy of the experiment) by the critical hyperbola in the (b,⊥e) plane:

$$H_b^2/p^2 - H_{\perp e}^2/q^2 = 1 \qquad (1)$$

where $H_b = \cos\phi$ and $H_{\perp e} = H \sin\phi$ with ϕ the angle between the external field and the b axis. The ⊥e direction is defined as the axis in the ac plane perpendicular to e. We find p = 21.5 ± 1.0 kOe and q = 32 ± 1 kOe. For 26.1 kOe, in the plane perpendicular to the easy spin axis, the temperature dependence of the anomaly versus the orientation is given in fig. 9. Similar behaviour is found for other points of this hyperbola and for points of the curves given in fig. 11.

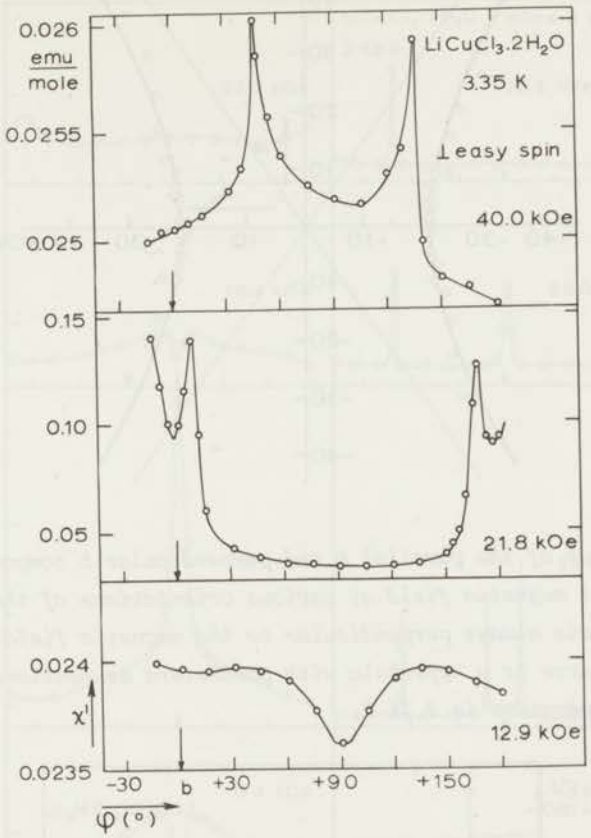

Fig. 7. Angular dependence of the susceptibility of $LiCuCl_3 \cdot 2H_2O$ in the plane perpendicular to the easy spin axis at 3.35 K and several field levels.

d. The susceptibility versus the orientation in a plane through the easy spin axis (e b plane) has been measured for several points in the phase diagram. Some curves are shown in fig. 10.

We first discuss the part in the neighbourhood of the first transition field (left hand half of the figure, H < 23 kOe). These curves are in agreement with the generally accepted fact that the first transition is a spin flop transition. The curves show the behaviour for a rotation in the easy - second easy plane (which is the e b plane) with maxima symmetrically arranged with respect to the easy spin axis. These maxima should not be confused with those which are found in the easy-hard plane (the ac plane in this case) where a

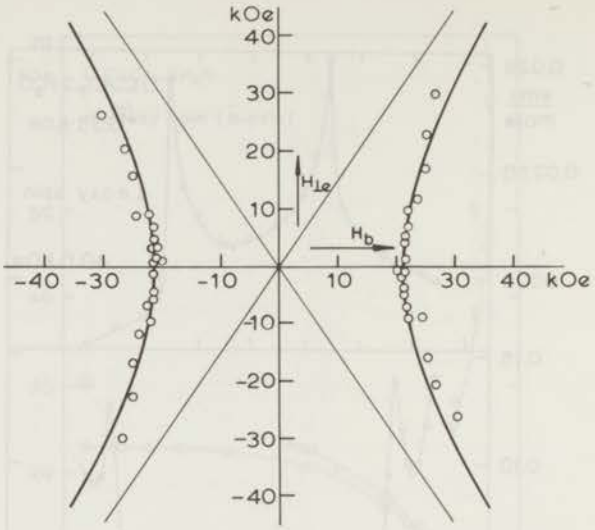

Fig. 8. Behaviour of the parallel b and perpendicular b component of the critical magnetic field at various orientations of the crystal with the e axis always perpendicular to the magnetic field. The fully drawn curve is a hyperbola with parameters as mentioned in the text. The temperature is 3.35 K.

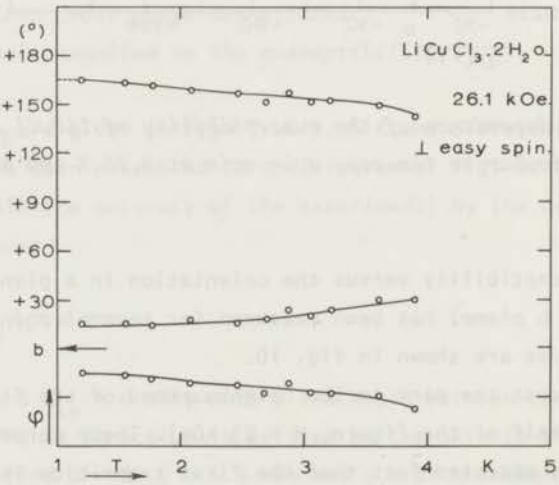

Fig. 9. Critical angle in the plane perpendicular to the easy spin axis versus the temperature at constant field.

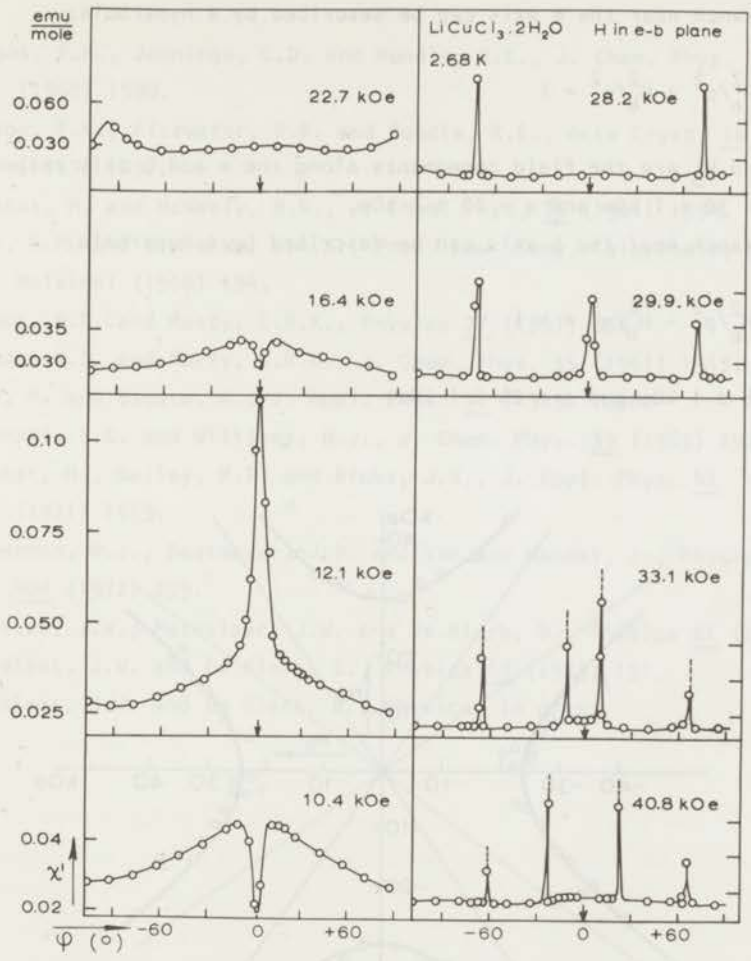

Fig. 10. Angular dependence of the susceptibility of $LiCuCl_3 \cdot 2H_2O$ in the e b plane at 2.68 K and several field levels.

critical hyperbola can be observed [10]. The anomalies in the easy-hard plane, which correspond to a first order phase transition, are generally much more pronounced than those in the easy-second easy plane, which corresponds to a rapid change of the directions of the sublattice magnetization vectors, but not to a first order phase transition.

Above about 23 kOe new peaks appear which are different in nature from those near 12 kOe. They are much more pronounced. The anomalies (corresponding to first order phase transitions) are assembled in fig. 11 for 2.68 K and two

different branches are shown.

The branch near the e axis can be described by a hyperbola:

$$H_e^2/p^2 - H_b^2/q^2 = 1 \qquad (2)$$

where H_e and H_b are the field components along the e and b axis respectively. We find p = 30 ± 1 kOe and q = 20 ± 1 kOe.

The branch near the b axis can be described by a hyperbola:

$$H_e^2/p^2 - H_b^2/q^2 = -1 \qquad (3)$$

with p = 18 ± 1 kOe and q = 24 ± 1 kOe.

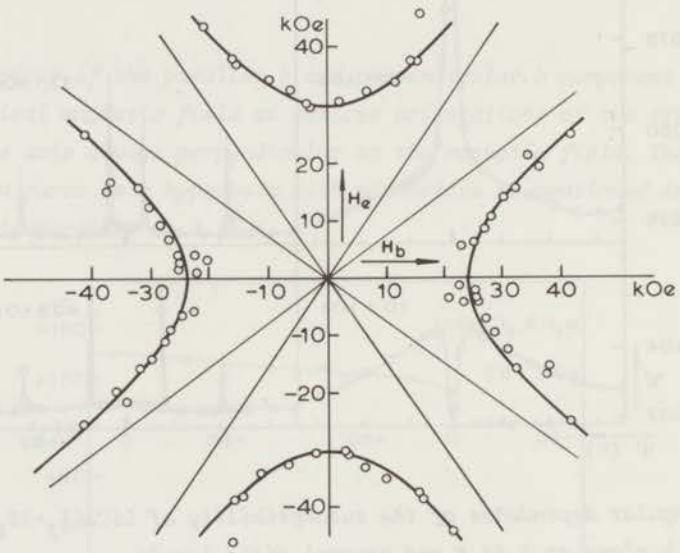

Fig. 11. Behaviour of the parallel b and perpendicular b component of the critical magnetic field at various orientations of the crystal with the ⊥e axis always perpendicular to the magnetic field. The fully drawn curves are hyperbolae with parameters as mentioned in the text. The temperature is 2.68 K.

References.

1) Vossos, P.H., Jennings, L.D. and Rundle, R.E., J. Chem. Phys. 32 (1960) 1590.
2) Vossos, P.H., Fitzwater, D.R. and Rundle, R.E., Acta Cryst. 16 (1963) 1037.
3) Forstat, H. and McNeely, D.R., J. Chem. Phys. 35 (1961) 1594.
4) Clay, R.M. and Staveley, L.A.K., Proc. Low Temp. Calorimetry Conf. Helsinki (1966) 194.
5) Spence, R.D. and Murty, C.R.K., Physica 27 (1961) 850.
6) Spence, R.D. and Murty, C.R.K., J. Chem. Phys. 35 (1961) 1912.
7) Date, M. and Nagata, K., J. Appl. Phys. 34 (1963) 1038.
8) Abrahams, S.C. and Williams, H.J., J. Chem. Phys. 39 (1963) 2923.
9) Forstat, H., Bailey, P.T. and Ricks, J.R., J. Appl. Phys. 42 (1971) 1559.
10) Zimmerman, N.J., Bastmeyer, J.D. and Van den Handel, J., Physics Letters 40A (1972) 259.
11) Schutter, J.W., Metselaar, J.W. and De Klerk, D., Physica 61 (1972) 250.
12) Metselaar, J.W. and De Klerk, D., Physica 63 (1973) 191.
13) Metselaar, J.W. and De Klerk, D., Physica, in press.

CHAPTER 4

DISCUSSION AND THEORY OF $LiCuCl_3 \cdot 2H_2O$

1. Discrepancies in the literature.

From the literature review of Chapter 3 two important conclusions may be drawn.

1° According to some authors the susceptibility [1] and specific heat [2] data indicate that $LiCuCl_3 \cdot 2H_2O$ behaves like a paramagnet with S = 1 in the temperature range 20 K and higher. From this fact it was concluded that the two Cu spins 3.47 Å apart, forming the dimers along the a axis, are parallel and thus ferromagnetically coupled. In contradiction to this other susceptibility [3] and specific heat [4] measurements lead to the conclusion that in $LiCuCl_3 \cdot 2H_2O$ an ordering process sets in at 4.40 K involving a S = $\frac{1}{2}$ spin system. Neutron diffraction measurements [3] finally revealed that the spins within a dimer are antiparallel. Because a neutron diffraction experiment is the most direct way in which the spin arrangement can be detected, it must be concluded that the spins within a dimer are antiparallel.

2° For the direction of spin alignment in zero field four different orientations may be found in the literature: a' from E.S.R. measurements [5]; c' from temperature measurement during adiabatic rotation [6]; the Cu - Cu internuclear line within the $Cu_2Cl_6^{--}$ dimer by combining susceptibility measurements and neutron diffraction data [3]; and the 101 direction from recent E.S.R. measurements [7] (see also fig. 2). The direction as found from the recent E.S.R. measurements seems the most reliable one. The fact that this direction is the correct choice for the easy spin axis is supported by the observation that a clear spin flop transition is found in a Li nuclear resonance experiment if the single crystal is mounted with its 101 direction parallel to the magnetic field (to be discussed further in section 4).

2. Experimental evidence for Dzyaloshinsky-Moriya interaction.

From the data given in the preceding Chapter (see figs. 8 and 11) it is clear that the transitions near 32 kOe in fig. 3 and near 20 kOe in fig. 6

depend strongly on the orientation of the crystal. The same can be said of the transition at about 56 kOe which is found for the easy spin direction (fig. 3) but not for instance for the b direction (fig. 6). This indicates that the anisotropy related to this angular dependence is much larger than what is usally found for exchange constants of this order of magnitude, which can be measured either from the saturation field at low temperatures (about 150 kOe [8]) or from the Néel temperature (4.48 K in the present measurements).

This high anisotropy suggests that a Dzyaloshinsky-Moriya interaction [9][10] should be present in $LiCuCl_3 \cdot 2H_2O$ like in $CuCl_2 \cdot 2H_2O$ [10]. Dzyaloshinsky-Moriya (henceforth D-M) interaction is the antisymmetric part of the super-exchange constant tensor, which describes the quadratic part of the interaction between two spins, and is of the form:

$$\underline{D}_{ij} \cdot \underline{S}_i \wedge \underline{S}_j \qquad (1)$$

where $\underline{D}_{ij}$ is the D-M vector, whose magnitude and orientation depend on the crystal symmetry and the pair of spins under consideration.

One of the effects of the occurrence of D-M interaction in an antiferromagnet is the destruction of the second order phase transition to paramagnetic saturation [13]. This point will be discussed in sections 6 and 7. It is illustrated in fig. 1, which shows the magnetization curves for $LiCuCl_3 \cdot 2H_2O$ and $CuCl_2 \cdot 2H_2O$ at 1.55 K. The lower first and second order transitions of $LiCuCl_3 \cdot 2H_2O$ are not visible in this figure because these experiments were performed on powdered samples. For both salts the saturation occurs at about 150 kOe but the rounding off is much larger for $LiCuCl_3 \cdot 2H_2O$. This shows that in this salt the D-M interaction is much stronger than in $CuCl_2 \cdot 2H_2O$. An even more pronounced anomaly is found in the experiments on $CoCl_2 \cdot 6H_2O$ [11] and $CoBr_2 \cdot 6H_2O$ [12] where D-M interaction is absent.

In fact the rounding off of the magnetization near saturation is also found in the measurements of the susceptibility versus the temperature. See e.g. the curve at 97 kOe in fig. 5, Chapter 3.

A second argument for the existence of D-M interaction is the occurrence of a small ferromagnetic moment at high fields. For instance, integration of the 1.20 K susceptibility curve of fig. 4, Chapter 3 (b direction) gives rise to a jump in the magnetization at about 24 kOe. Extrapolation of the magnetic moment above this field back to zero field yields a ferromagnetic moment of about 6 per cent of the saturation moment. Something similar happens in the e direction. The peaks at about 12 and 32 kOe are followed by regions with

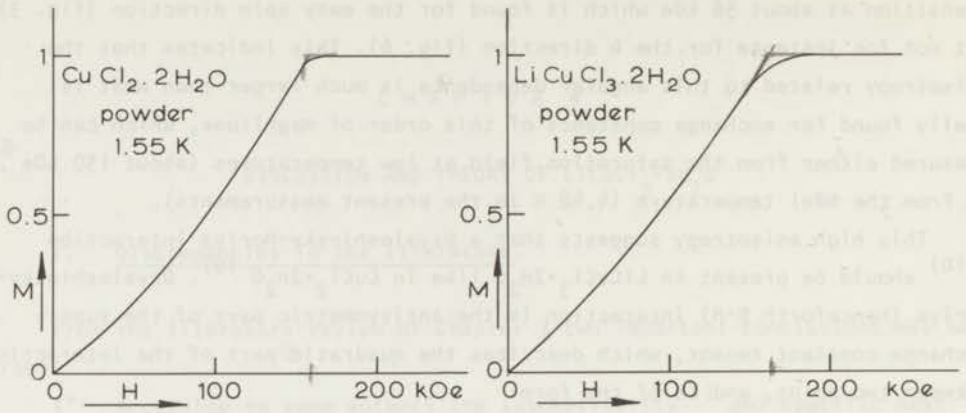

Fig. 1. Isothermal magnetization curves of powder samples of $CuCl_2 \cdot 2H_2O$ (left) and $LiCuCl_3 \cdot 2H_2O$ (right). The measurements have been performed in high pulsed magnetic fields.

higher susceptibilities, in such a way that extrapolation of the magnetization back to zero from these regions leads to zero magnetic moments. But the anomaly at about 56 kOe gives rise to a diminution of the slope of the magnetization versus field above this field and extrapolation back to zero field from here yields a ferromagnetic moment of about 4 per cent of the saturation value. These extrapolated magnetic moments are equivalent with a canting of the spins of approximately 6°.

Because at this point no detailed picture is available of the magnetic interactions in $LiCuCl_3 \cdot 2H_2O$ this canting angle, extrapolated to zero field, must be considered as a preliminary estimation. A final picture will be given in sections 6 and 7.

De Jong [14], making use of the exchange constants given in section 7, made calculations on the spin-spin relaxation frequency. Assuming a D-M interaction large as compared to the dipole-dipole interaction, but small with respect to the isotropic exchange interaction, he came to values in the region 150-500 MHz, the exact numbers depending on the orientation. This was in excellent agreement with the experimental data. For the case D-M interaction was absent, frequencies of about 5 MHz were calculated. This, again, is a strong argument for the presence of an important D-M interaction in $LiCuCl_3 \cdot 2H_2O$.

It was assumed in these calculations that the D-M vector could be

described by:

$$|Di|/J_3 = \alpha \cdot \Delta g_i \qquad (2)$$

with α independent of the direction; i indicates a principal magnetic axis and Δg_i is the deviation of g_i from 2 for the i direction. For the definition of J_3 see below. It turned out that $\alpha = .30 \pm .02$ for any of the three directions mentioned. This magnitude of D/J is half the value given by Moriya, as an order of magnitude, and it differs less than a factor of 2 from D/J = 0.1 which is obtained from the canting angle of 6° mentioned before.

3. Crystal symmetry considerations and D-M interactions.

From the preceding sections it has become clear that an important D-M interaction must play an important role in $LiCuCl_3 \cdot 2H_2O$. In this section this fact will be discussed in more detail.

The crystalline structure of $LiCuCl_3 \cdot 2H_2O$ is represented by figures 2 (projection on the ac plane) and 3 (projection on the bc plane). There are four Cu^{++} and four Li^{+} ions in the unit cell, so in our discussion we will distinguish four crystalline sublattices, numbered 1, 2, 3 and 4, as indicated in figs. 2 and 3. From the Li nuclear resonance data, to be discussed in section 4, it is clear that a four magnetic sublattice model must be adequate to describe the most important features of $LiCuCl_3 \cdot 2H_2O$. These four magnetic sublattices are supposed to coincide with the four crystalline sublattices. The copper ions of sublattices 1 and 2 are approximately in the plane of fig. 2, the ions 3 and 4 are halfway the unit cell above or below the plane, see also fig. 3.

The D-M interaction which must be present in $LiCuCl_3 \cdot 2H_2O$ cannot exist between the Cu spins within the dimer, neither can it exist between the spins 3.84 Å apart from neighbouring dimers (along the a axis), because in both cases the midpoint of the line interconnecting the spins under consideration are inversion centers [10]. Between the spins along the a axis 6.08 Å apart (see fig. 2) a D-M interaction may exist but then, apart from the interaction constants J_1, J_2 and this interaction, all acting inside the same chain along the a axis, a fourth interaction with spins outside the chain is needed because otherwise no long range order can exist.

For the spins 6.6 Å apart in the ac plane along the c axis no D-M interaction is possible again. Between the spins e and b (see fig. 3) belonging to

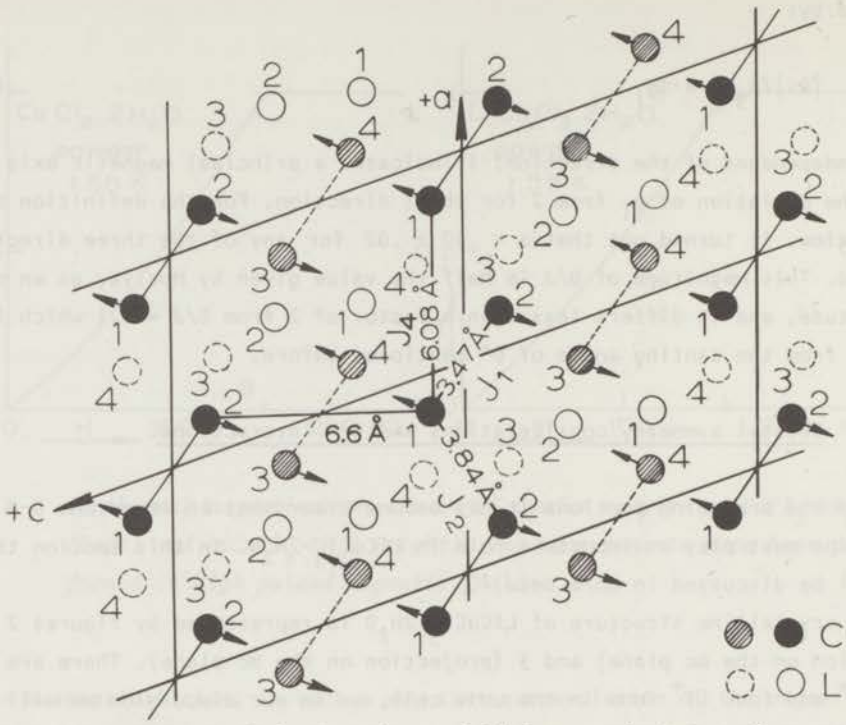

Fig. 2. Arrangement of the Cu spins and Li ions projected on the ac plane. The figure shows also the zero field spin arrangement as deduced from neutron diffraction and E.S.R. measurements.
Black circles : Cu spins near (0,1,0) plane
Shaded circles : Cu spins near (0,2,0) plane
White circles : Li ions near (0,1,0) plane
Dotted circles : Li ions near (0,2,0) plane

sublattices 3 and 2 respectively a D-M interaction may exist, because these spins are related by the two-fold screw axis. The distance between these spins is 6.16 Å. Interactions of the same magnitude occur between e and h, f and k, f and c and so on in chains parallel to the b axis. The spins e and a are related by a glide-mirror plane parallel to the ac plane, so also here a D-M interaction may exist, e and a belonging to sublattices 3 and 1 respectively. The distance between these spins is 7.4 Å. The spins e and g are also related by a glide-mirror plane and belong also to sublattices 3 and 1 respectively. This distance is 7.0 Å. There is no relation at all between the interaction of e and a and of e and g. The interactions between e and a, e and c and so on, however, are equal in magnitude and occur in chains parallel to the c axis;

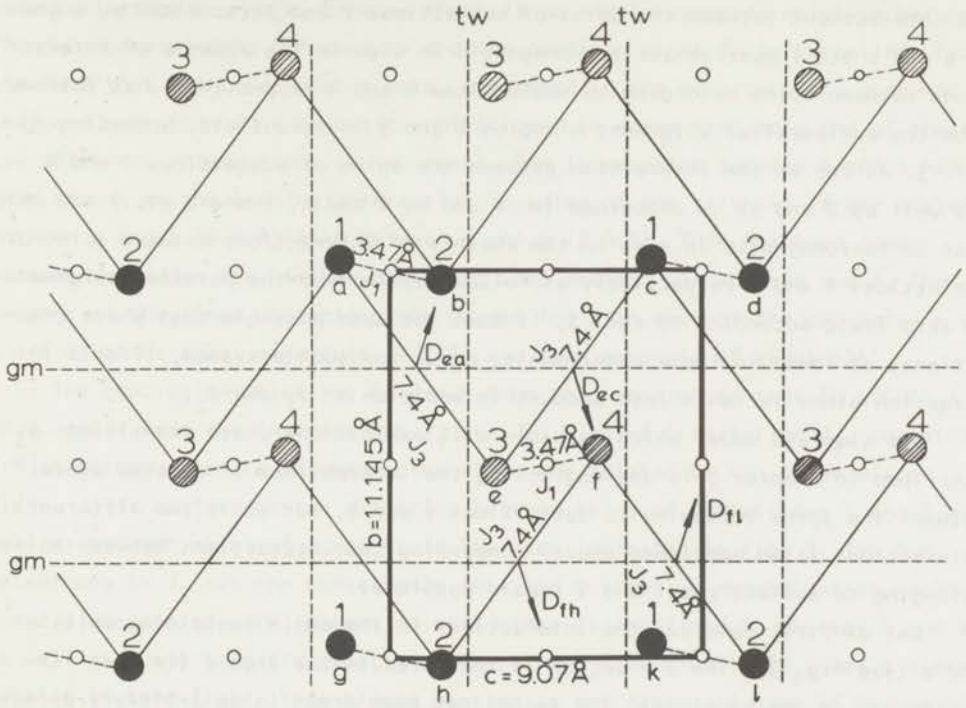

Fig. 3. Arrangement of the Cu spins projected on the bc plane. The interactions as discussed in the text have been indicated.
a, c, g and k belong to sublattice 1
b, d, h and l belong to sublattice 2
e belongs to sublattice 3 and
f belongs to sublattice 4.
The angle between the lines interconnecting the spins in a dimer and the c axis is slightly exaggerated for clarity.
g-m indicates a glide-mirror plane.
tw indicates a two-fold screw axis.
o indicates an inversion center.

interactions of the same magnitude are found between f and h, f and l and so on in chains along the c axis as well. That the magnitude of the interaction between e and a is the same as the one between f and l, is caused by the fact that e and f as well as a and l are related by the same inversion centre.

In section 6 it will be demonstrated that the interaction between the spins belonging to sublattices 1 and 3 respectively, in addition to the exchange constants J_1 and J_2, may result in phase transitions. The net effect of

the interactions between the spins of sublattices 1 and 3 (so e and a, e and g, e and c etc.) must be antiferromagnetic in sign in the absence of interactions between spins belonging to sublattices 1 and 4 respectively, as follows from the antiparallel alignment of spins 1 and 3 in zero field, according to ref. 3. As far as the interaction between the spins of sublattices 1 and 4 (as well as 2 and 3) is concerned (so e and h, f and k, f and c etc.) and which must be ferromagnetic in sign in the absence of interactions between spins of sublattices 1 and 3 respectively as follows again from the parallel alignment in zero field according to ref. 3, it does not seem possible that phase transitions, as found in these experiments, occur for such a system, if this interaction alone is taken into account in addition to J_1 and J_2.

The simplest model which possibly will exhibit the phase transitions as described in Chapter 3 is one neglecting the interactions (indicated above) between the spins belonging to sublattices 1 and 4. But still two different interactions (also mentioned above) concerning the interactions between spins belonging to sublattices 1 and 3 remain possible.

Let us first consider the interactions in the chain containing spins e and a (see fig. 3). The D-M vector is indicated in the figure (in fact its projection on the bc plane). The vector has been drawn in an arbitrary direction. But because the spins e and c can be obtained by the glide-mirror operation from the spins a and e respectively, the D-M vector transforms as indicated in the figure (the D-M vector is an axial vector). The two vectors $\underline{D}_{ea}$ and $\underline{D}_{ec}$ are symmetrically directed with respect to the glide-mirror plane.

In introducing these D-M vectors the spins a and c still belong to the same sublattice, because the components in the ac plane of the D-M vectors give equal canting of the spins a and c out of the ac plane, whereas the canting due to the parallel b components is cancelled. Thus only the components in the ac plane are of importance. This is consistent with the molecular field treatment which allows us to add $\underline{D}_{ea}$ and $\underline{D}_{ec}$ if a and c belong to the same sublattice. $\underline{D}_{13}$ is defined as $\underline{D}_{ea} + \underline{D}_{ec}$ and lies in the ac plane. Similar considerations can be held for the interactions between the spins e and g, e and k, f and b, f and d etc. in chains parallel to the c axis, and also for the interactions between h and e, e and b, k and f, f and c etc. in chains parallel to the b axis. The latter interaction will be neglected as already argued. The D-M vector $\underline{D}_{fh}$ which belongs to f and h is parallel to $\underline{D}_{ec}$ because e and f as well as c and h are related by an inversion centre.

If we introduce an interaction between e and a of about equal magnitude as the interaction between e and g, then possibly a and g do not belong to the

same sublattice any more, because there is no simple symmetry relation between the two corresponding D-M vectors and the canting is not fully cancelled. From the fact that the Li resonance data, discussed in the next section, does not indicate more than four magnetic sublattices, it seems that only one of these two different interactions is important. The interaction between e and a has been chosen as the leading interaction in spite of the slightly larger distance between e and a (7.4 Å) than between e and g (7.0 Å). This has been done because an oxygen ion is favourably situated between the spins e and a. The lengths of the lines connecting the oxygen ion with each of the two spins e and a are of about equal magnitude (4.2 Å) and form an angle of about 124°.

The conclusion which may be drawn from this section is that in $LiCuCl_3 \cdot 2H_2O$, apart from the interactions J_1 and J_2, a third interaction J_3, containing D-M anisotropy, occurs between spins which are related by the glide-mirror plane. J_3 is an interaction occurring between spins of sublattices 1 and 3 as well as between spins of 2 and 4. It has been indicated in fig. 3. The D-M anisotropy in J_3 has the consequence that the sublattice magnetization vectors 1 and 3 are canted with respect to each other as are 2 and 4, whereas 1 and 2 as well as 3 and 4 remain exactly antiparallel. Thus $LiCuCl_3 \cdot 2H_2O$ has a hidden canting in zero field. This hidden canting is not destroyed even if anyone of the other interactions occurring between spins belonging to the sublattices 1 and 3 and to 1 and 4, mentioned in this section, is taken into account.

4. Li nuclear resonance.

In order to get more information about the detailed behaviour of $LiCuCl_3 \cdot 2H_2O$ in the different phases for the e direction preliminary data was taken of Li nuclear resonance [15], with the magnetic field parallel to this direction and with the crystal at 1.3 K. This resonance data is shown in fig. 4. The numbers 1-4 of the curves refer to the numbers of the Li nuclei indicated in fig. 2. These Li nuclei are numbered similarly as the Cu spins.

We,know that in zero field the spins are (or are almost) in the ac plane [3)7)]. Fig. 4 shows that the resonance lines 1 and 4 as well as 2 and 3 coincide at fields well below the spin flop field of about 12 kOe. These coinciding lines must arise from the Li nuclei which are related by the two-fold screw axis, because the corresponding spins are (almost) parallel and in (or near) the ac plane. As far as this Li resonance data is concerned a canting out of the ac plane is permitted, with the restriction that the spins which are related by this screw axis are symmetrically directed with respect to this

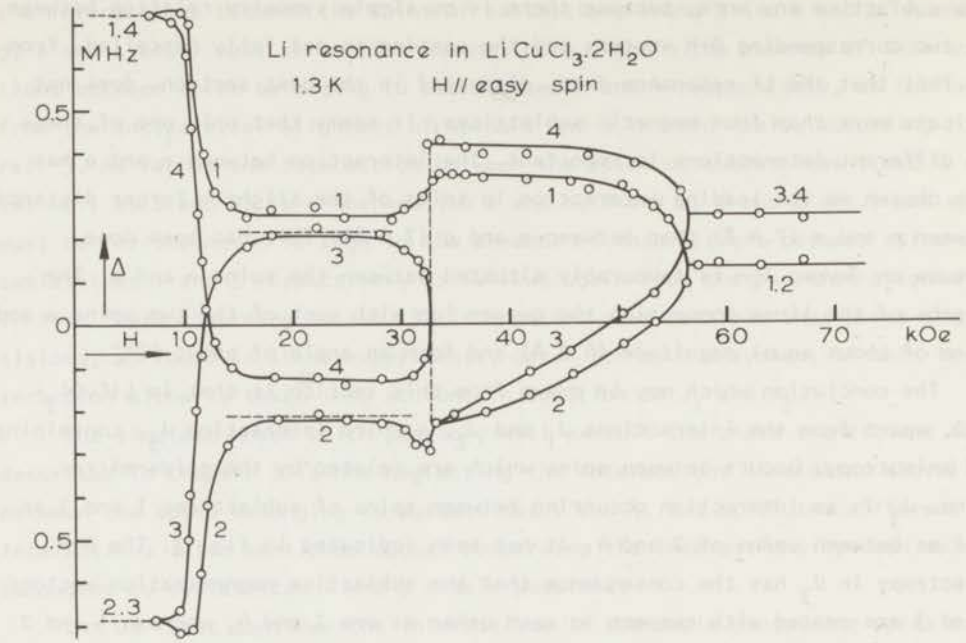

Fig. 4. Li resonance data in $LiCuCl_3 \cdot 2H_2O$. Δ is the deviation of the resonance frequency from the free nucleus value.

plane (see also fig. 5a).

The lines 1 and 2 are symmetrically located around the zero internal field resonance frequency, with a small shift added to it. These lines must arise from the Li nuclei which are related by inversion, because the corresponding spins, which are numbered 1 and 2 respectively (see fig. 2) are antiparallel [3].

Above about 12 kOe the spins flop to a direction near the b axis [7]. From symmetry considerations it follows that the spin arrangement should be symmetrical with respect to the ac plane, if the magnetic field is perfectly aligned in the ac plane. The spins 1 and 3 are connected via a glide-mirror plane, which is parallel to the ac plane. This means that the corresponding Li resonance lines coincide if the spins are symmetrically aligned with respect to the ac plane. The spins 1 and 4 are connected via a two-fold screw axis parallel to the b axis (and consequently perpendicular to the ac plane) and also in this case the corresponding Li lines coincide if these spins are symmetrically directed with respect to the ac plane.

In the experiment, however, four different resonance lines are measured between the threshold field of 12 kOe and the first order phase transition at

about 32 kOe, and also between 32 kOe and the second order phase transition at 56 kOe. This can only be found if the spins 1 and 2 as well as 3 and 4 are symmetrical with respect to the ac plane and other combinations are not symmetric. In such an arrangement, however, any contribution to the energy from the D-M interaction is cancelled. So we are inclined to believe that the splitting of the lines 1 and 3 (and 2 and 4) in the range 12 to 32 kOe as well as the splitting of the lines 1 and 4 (and 2 and 3) in the range 32 to 56 kOe is merely due to a slight misalignment (we estimate about 10°) of the external field with respect to the ac plane. This is also supported by the fact that the transitions as found in this preliminary resonance experiment occur at systematically higher fields than those from the susceptibility measurements. Moreover, the change of the internal fields at the Li sites, at the spin flop transition, seems to be much less sudden than what is usually found for such a transition if the crystal is properly aligned.

The slight misalignment of the external field with respect to the ac plane gives us the opportunity to identify the resonance lines. From this resonance data it can thus be concluded that between 12 and 32 kOe the sublattices 1 and 3, as well as 2 and 4 are symmetrically directed with respect to the ac plane. Between 32 kOe and 56 kOe the sublattices 1 and 4, as well as 2 and 3, are symmetrical with respect to the ac plane.

Coinciding lines 1 and 4 below 56 kOe with the field perfectly aligned in the ac plane necessarily means that only one resonance line should be found above 56 kOe in that case. Full saturation of the spin system occurs at about 160 kOe [8]. This means that above 56 kOe the sublattice magnetization vectors 1 and 2 coincide as well as 3 and 4, whereas 1 and 3 are symmetrically directed with respect to the ac plane, as are 2 and 4, with large angles between the magnetization vectors 1 and 3. See also fig. 5.

5. Mechanism of the transitions.

From the crystal symmetry considerations as given in section 3 it follows that the D-M vectors $\underline{D}_{13}$ and $\underline{D}_{24}$ are parallel, equal in magnitude and lie in the ac plane, giving rise to the spin configuration in zero field with a hidden canting as shown in fig. 5a. After the flopping process at 12 kOe the spins are slightly canted towards the field. See fig. 5b.

As far as the D-M interaction is concerned the sublattice vectors 1 and 3 have lowest energy if the vectors are perpendicular to each other in such a way that the vector product points into the positive e direction. The same is

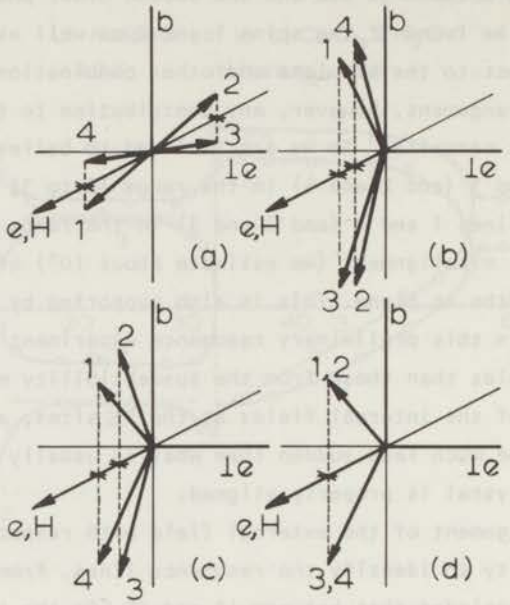

Fig. 5. Proposed spin arrangements of the different phases in $LiCuCl_3 \cdot 2H_2O$ for the external field parallel to the easy spin direction.

(a) 0 to 12 kOe

(b) 12 to 32 kOe

(c) 32 to 56 kOe

(d) 56 kOe and higher

true for 2 and 4. On increasing the field the sublattices cant more and more to the field direction. The D-M contribution to the energy from $\underline{D}_{13}$ decreases this energy, but the D-M contribution $\underline{D}_{24}$ increases it more and more, so that, as far as this interaction is concerned, 2 and 4 must change their directions so that also the D-M contribution from 2 and 4 lowers the energy. See fig. 5c.

This sign reversal of the vector product of the sublattice magnetization vectors 2 and 4 is, of course, only possible if the symmetric interactions allow such a process. The second order phase transition which occurs at higher fields is then due to an antiferromagnetic interaction between the spins 1 and 2. Here the four sublattice system changes into a two sublattice system. See figs. 5c and d.

To understand the process qualitatively only the interactions between 1 and 2 (3 and 4) and between 1 and 3 (2 and 4) are necessary. In that case only one D-M vector ($\underline{D}_{13} = \underline{D}_{24}$) is present which lies in the ac plane. If this

vector makes an arbitrary angle with the field, then the spins are not coplanar in non-zero field. For simplicity in fig. 5 the D-M vector is assumed to be perpendicular to the easy spin axis (thus parallel to $\perp e$).

In order to derive the conditions for these transitions, as well as the values of the interactions which play an important role in $LiCuCl_3 \cdot 2H_2O$, a detailed analysis of the Hamiltonian is necessary. As a start a preliminary analysis of the energy expression at zero temperature and in the molecular field approximation is given in the next section.

6. The energy expression.

On the basis of the preceding sections the spin system of $LiCuCl_3 \cdot 2H_2O$ is a four sublattice magnetic system. If we use subscripts 1, 2, 3 and 4 (indicated in figs. 2 and 3) for the spins belonging to the four magnetic sublattices respectively we may write the energy, corresponding to the Hamiltonian, in the molecular field approximation at zero temperature as follows:

$$
\begin{aligned}
E = &- \tfrac{1}{4} N \underline{S}_1 \cdot (\underline{\underline{J}}_1 + \underline{\underline{J}}_2) \cdot \underline{S}_2 - \tfrac{1}{4} N \underline{S}_3 \cdot (\underline{\underline{J}}_1 + \underline{\underline{J}}_2) \cdot \underline{S}_4 \\
&- \tfrac{1}{2} N \underline{S}_1 \cdot \underline{\underline{J}}_3 \cdot \underline{S}_3 \qquad - \tfrac{1}{2} N \underline{S}_2 \cdot \underline{\underline{J}}_3 \cdot \underline{S}_4 \\
&- \tfrac{1}{2} N \underline{D}_{13} \cdot \underline{S}_1 \wedge \underline{S}_3 \qquad - \tfrac{1}{2} N \underline{D}_{24} \cdot \underline{S}_2 \wedge \underline{S}_4 \\
&- \tfrac{1}{4} N \mu_B \underline{H} \cdot \underline{\underline{g}} \cdot (\underline{S}_1 + \underline{S}_2 + \underline{S}_3 + \underline{S}_4) \qquad (3)
\end{aligned}
$$

Here:

N is the total number of spins.

$\underline{\underline{J}}_1$ is the superexchange constant, which is attributed to the interaction between the spins within a dimer, see figs. 2 and 3.

$\underline{\underline{J}}_2$ is the superexchange constant, which is attributed to the interaction between the neighbouring spins belonging to different dimers along the a axis, see fig. 2.

$\underline{\underline{J}}_3$ is the symmetric part of the superexchange constant, which is attributed to the interaction between the spins which are related by the glide-mirror plane and which are 7.4 Å apart, see fig. 3.

$\underline{D}_{13}$ is the sum of the two D-M vectors which belong to S_1 and its two neighbours, $\underline{S}_3$, the two neighbours $\underline{S}_3$ belonging to the same sublattice, as is indicated by the subscript 3.

$\underline{D}_{24}$ is defined in a similar way.

In order to perform some preliminary calculations we make two more simplifying assumptions:

1°. $\underline{\underline{J}}_1$, $\underline{\underline{J}}_2$ and $\underline{\underline{J}}_3$ are isotropic, though, of course, $\underline{D}_{13}$ and $\underline{D}_{24}$ will be taken into account.

2°. The magnetic field will be taken perpendicular to the D-M vector ($\underline{D}_{13} = \underline{D}_{24}$, as follows from the arguments given in section 3. It will be further referred to as D).

It is obvious that the spins are confined to the plane perpendicular to the D-M vector. From the preceding sections it is clear that we have to consider two different configurations, one with the directions of the spins 1 and 3 (as well as 2 and 4) symmetric with respect to the plane through H and D, which we shall abbreviate as the (1,3) solution, and one with the directions of the spins 1 and 4 (as well as 2 and 3) symmetric with respect to this plane, which we shall refer to as solution (1,4).

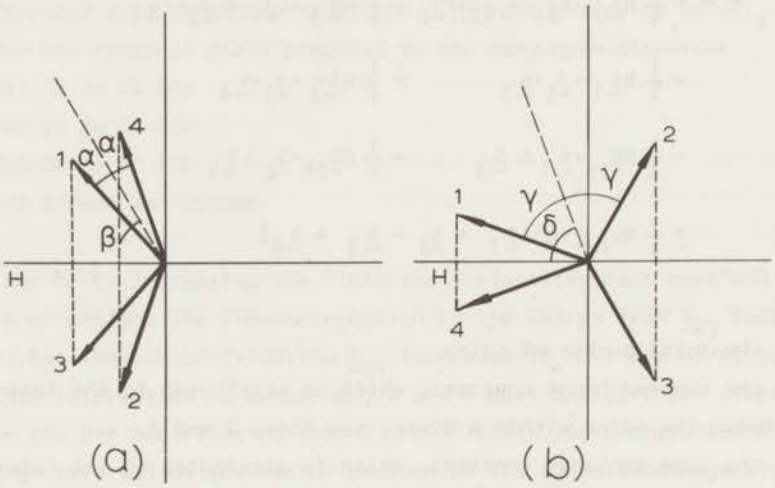

Fig. 6. Definition of the angles α, β, γ and δ for the calculations as carried out in the text. Left: configuration (1,3). Right: configuration (1,4).

Fig. 6a shows configuration (1,3) (as does fig. 5b) and fig. 6b shows configuration (1,4) (as do figs. 5a and 5c).

In the energy expression (3) $J_1 + J_2$ and J_3 are negative, $\underline{D}_{13} = \underline{D}_{24} = D$

will also be taken negative.

6.1. The solution (1,3). See fig. 6a. Using the angles α and β we obtain:

$$e = \cos 2\beta(1 + 2r \cos 2\alpha + 2rd \sin 2\alpha) - 2h \cos\beta \cos\alpha \qquad (4)$$

in which

$$e = -E/\tfrac{1}{2}N(J_1 + J_2)S^2;\ D_{13} = D_{24} = D$$

$$r = J_3/(J_1 + J_2) \text{ which is a positive quantity}$$

$$d = D/J_3 \text{ also a positive quantity}$$

$$h = -g\mu_B H/S(J_1 + J_2)$$

The necessary conditions for the equilibrium values of α and β are that the derivatives with respect to these angles should be zero:

$$\cos 2\beta(-4r \sin 2\alpha + 4rd \cos 2\alpha) + 2h \cos\beta \sin\alpha = 0 \qquad (5)$$

$$-2 \sin 2\beta(1 + 2r \cos 2\alpha + 2rd \sin 2\alpha) + 2h \sin\beta \cos\alpha = 0 \qquad (6)$$

From eq. 6 it follows that two different cases must be considered: $\sin\beta \neq 0$ and $\sin\beta = 0$.

Case a: $\sin\beta \neq 0$

It does not seem possible to obtain α and β explicitly as functions of h from equations 5 and 6. Therefore we treat the equations in such a way that expressions are obtained which are suitable for numerical calculations. Then e as a function of h can be obtained in an indirect way.

Elimination of h from equations 5 and 6 yields

$$\cos^2\beta = \frac{\sin 2\alpha - d \cos 2\alpha}{\rho \operatorname{tang} \alpha - 2d} \qquad (7)$$

with $\rho = (2r - 1)/r$.

The reduced magnetic field can then be calculated either from 5 or from 6:

$$h = 2 \cos\beta \frac{1 + 2r \cos 2\alpha + 2rd \sin 2\alpha}{\cos\alpha} \qquad (8)$$

e can be rewritten in a slightly simpler way:

$$e = -h \cos\alpha \frac{2\cos^2\beta + 1}{2\cos\beta} \tag{9}$$

From equation 7 it is clear that certain values of α cannot be realized, because it is required that $0 \leq \cos^2\beta \leq 1$. The boundary $\cos^2\beta = 0$ corresponds to two values of α, respectively α_1 and α_2, obeying:

$$\sin 2\alpha_1 - d \cos 2\alpha_1 = 0 \tag{10}$$

$$\text{tang } \alpha_2 = \pm \infty \tag{11}$$

The boundary $\cos^2\beta = 1$ gives

$$\frac{\sin 2\alpha_3 - d \cos 2\alpha_3}{\rho \text{ tang } \alpha_3 - 2d} = 1 \tag{12}$$

The right hand side of equation 7 becomes infinite at

$$\rho \text{ tang } \alpha_4 - 2d = 0 \tag{13}$$

A sketch of $\cos^2\beta$ as a function of α is given in fig. 7 (r and d have been chosen 3.51 and .22 respectively).

From equation 8 it can be seen that there must exist a critical value of h above which $|\cos\beta| > 1$ unless $\cos\alpha$ becomes zero simultaneously. From 7, however, it is concluded that if $\cos\alpha = 0$ then $\cos\beta = 0$. This means that this critical value of h is realized as an upper limit and is given by

$$h_{1c} = 2 \frac{1 + 2r \cos 2\alpha_3 + 2rd \sin 2\alpha_3}{\cos\alpha_3} \tag{14}$$

where α_3 obeys equation 12.

The relation between e and h (again for r = 3.51 and d = .22), is represented by the fully drawn curves of fig. 8, of which one ends abruptly at h_{1c}. These curves represent all the solutions of equations 5 and 6 for $\sin\beta \neq 0$, including those with maximum energy.

Case b: $\sin\beta = 0$.

If $\sin\beta = 0$ then $\beta = 0$ or π, which means that spins 1 and 2 coincide as do 3 and 4, so we obtain a two sublattice system. Equation 4 reduces to:

$$e = 1 + 2r \cos 2\alpha + 2rd \sin 2\alpha \mp 2h \cos\alpha \tag{15}$$

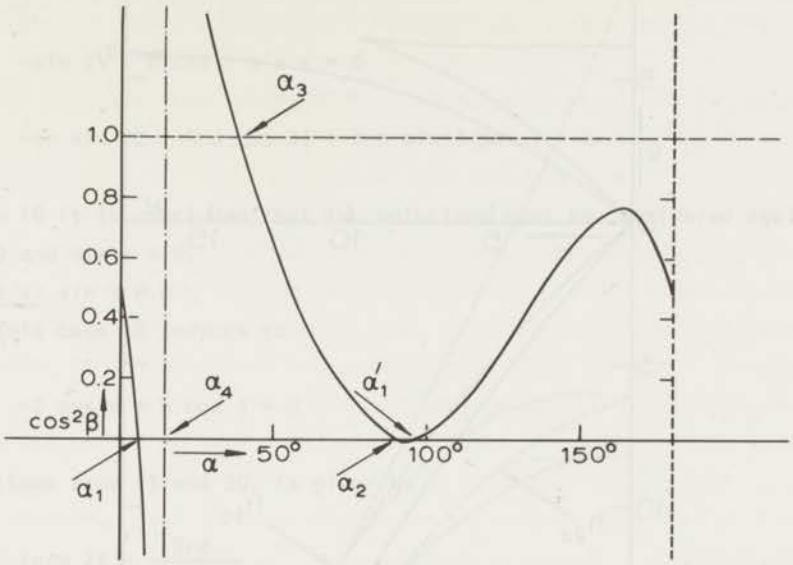

Fig. 7. Plot of $\cos^2\beta$ versus α for configuration (1,3). The periodicity is 180°. α_1, α_1', α_2, α_3 and α_4 are solutions of the equations 10, 11, 12 and 13 respectively. Forbidden ranges of α are: $\alpha_1 < \alpha < \alpha_3$ and $\alpha_2 < \alpha < \alpha_1'$.

which is equivalent with the energy expression for a weak ferromagnet. It reduces to the expression for a simple two sublattice antiferromagnet if $d = 0$. If $d \neq 0$ equation 5 becomes equal to:

$$-4r \sin 2\alpha + 4 rd \cos 2\alpha \pm 2 h \sin \alpha = 0 \qquad (16)$$

If $d = 0$ equation 16 has two solutions, viz. $\sin \alpha = 0$ and $\cos \alpha = h/4r$. The first one is the ferromagnetic solution for a simple two sublattice antiferromagnet. This solution does not exist if $d \neq 0$. Consequently no second order phase transition occurs near saturation. The disturbance of the second order phase transition due to D-M interaction was earlier discussed in ref. 13.

Equation 16 gives the relation between h and α. From this the energy e can be calculated as a function of h. The result ($r = 3.51$ and $d = .22$) is represented by the dashed curves of fig. 8. At h_{1c} cases a and b come together with identical slopes. It should be noted here that h_{1c} does not lie on the lowest energy branch of case b and consequently does not influence the discussions in 6.3.

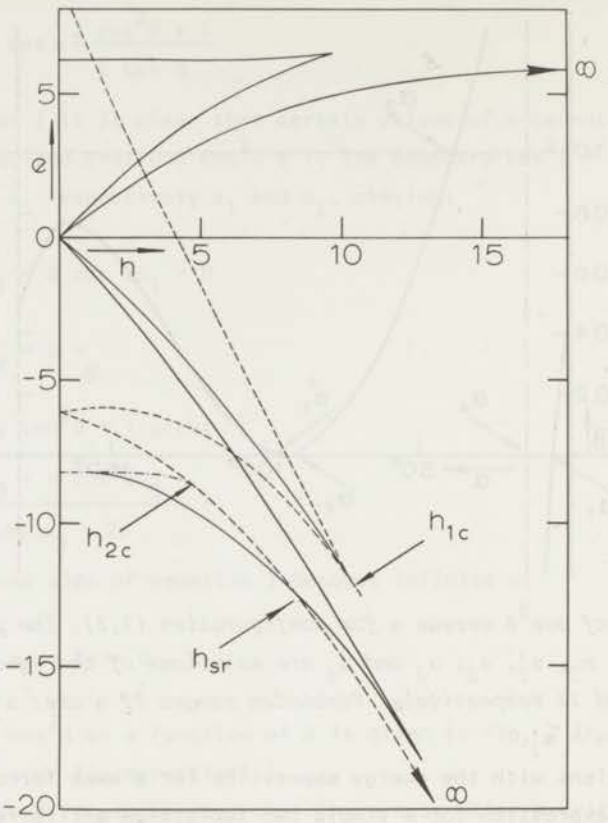

Fig. 8. Plot of the energy e in reduced units as a function of the reduced magnetic field h.
The fully drawn curve belongs to configuration (1,3) for sin β ≠ 0, thus four sublattices, and describes all the solutions of equations 5 and 6 with sin β ≠ 0. The curve ends at $h = h_{1c}$.
The dashed curve belongs to configuration (1,3) with sin β = 0 as well as to configuration (1,4) with sin γ = 0, thus two sublattices, and describes all the solutions from equations 15 and 16.
The dash-dotted curve describes only the lowest energy of configuration (1,4) with sin γ ≠ 0. This curve ends at $h = h_{2c}$.

6.2. The solution (1,4). See fig. 6b. Introducing the angles γ and δ we obtain from equation 3:

$$e = \cos 2\gamma + 2r \cos 2\delta - 2r \sin 2\delta - 2 h \cos \delta \cos \gamma \qquad (17)$$

Necessary conditions for the equilibrium values of γ and δ are

$$-\sin 2\gamma + h \cos \delta \sin \gamma = 0 \tag{18}$$

$$-4r \sin 2\delta - 4rd \cos 2\delta + 2 h \sin \delta \cos \gamma = 0 \tag{19}$$

From 18 it is concluded that two solutions must be considered again: $\sin \gamma \neq 0$ and $\sin \gamma = 0$.

Case a: $\sin \gamma \neq 0$

In this case 18 reduces to

$$-2 \cos \gamma + h \cos \delta = 0 \tag{20}$$

δ, as follows from 19 and 20, is given by

$$\text{tang } 2\delta = \frac{8rd}{h^2 - 8r} \tag{21}$$

γ can then be calculated by combining 20 and 21.

After some calculations it appears that an explicit expression can be obtained for the energy as a function of h:

$$e = -\frac{1}{4}\sqrt{(h^2 - 8r)^2 + 64\, r^2 d^2} - \frac{1}{4} h^2 - 1 \tag{22}$$

From 20 it is clear that this solution exists up to a critical field h_{2c} which is reached for $\cos \gamma = 1$, viz.

$$h_{2c} = \frac{2}{\cos \delta_c} \tag{23}$$

Substituting 22 in 19 and using $\cos \gamma = 1$ we obtain:

$$\frac{\text{tang } \delta_c}{\sin(2\delta_c + \phi)} = \frac{r}{\cos \phi} \tag{24}$$

with tang $\phi = d$.

The solution is represented by the dash-dotted curve of fig. 8.

Case b: $\sin \gamma = 0$

If $\sin \gamma = 0$ then $\gamma = 0$ or π, which means that spins 1 and 2 coincide as do 3 and 4, thus again a two sublattice system. In fact this case is the same as case b of solution (1,3) discussed before, with $\alpha = -\delta$:

$$e = 1 + 2r \cos 2\delta - 2\, rd \sin 2\delta \mp 2\, h \cos \delta \qquad (25)$$

compare equation 15. So it is also represented by the dashed curves of fig. 8. At h_{2c} cases a and b come together with identical slopes.

6.3. Phase transitions. It is clear that for each of the possible spin configurations only the lowest energy branch of fig. 8 can be realized. A cross-over of the lowest fully drawn curve and the lowest dashed curve takes place, so we must expect to observe, in the experiments, one first order transition and no second order transitions. The first order transition may be considered to take place from configuration (1,3) case a to configuration (1,4) case b (see above). It may also be considered to take place, however, from configuration (1,3) case a to case b of the same configuration. From the latter point of view the occurrence of a first order transition seems quite remarkable.

The case of one first order transition and no second order transitions is in agreement with the experiments in the b direction of $LiCuCl_3 \cdot 2H_2O$. In this case we are sure that the field is perpendicular to the D-M vector. The horizontal axes of figs. 6a and b represent the b axis and the D-M vector is perpendicular to the figures.

Thus far, in all our considerations we neglected the symmetric part of the anisotropy. If we take this into account the consequence is that the zero field energy of solution (1,3) case a (the lowest fully drawn curve of fig. 8) is somewhat lowered with respect to the zero field energy of solution (1,4) case a (dash-dotted curve of fig. 8). This is caused by the fact that, near zero field, solution (1,3) belongs to a spin configuration in which all the spins are oriented approximately parallel to the e axis (perpendicular to the field) whereas in solution (1,4), again near zero field, the spins are aligned approximately parallel to the b axis (so parallel to the field). The e axis differs only 16° from the axis along which g reaches its largest value [7]. This energy shift has no consequences for the phase diagram in the b direction, in such a way that still only one first order phase transition is found.

It should be realized that the energies in the solutions (1,3) and (1,4) are exactly equal in zero field if the symmetric part of the anisotropy is neglected. The only difference is that the spin arrangements are mutually perpendicular.

Now consider the case that the field is applied parallel to the e axis,

and suppose that this axis is perpendicular to the D-M vector. If now the symmetric part of the anisotropy is taken into consideration the energy of solution (1,3) for low fields is increased with respect to the energy of solution (1,4). This is because now solution (1,3) belongs to a configuration where near zero field the spins are approximately parallel to the b axis (perpendicular to the field) and in solution (1,4) they are approximately parallel to the e axis (parallel to the field). This shift of the energies gives rise to a second crossing of the energies versus the field which accounts for the first order phase transition which was interpreted as a spin flop transition. It should be realized, however, that in this spin flop transition four sublattices are involved.

The existence of two first order phase transitions for the e direction follows quite naturally from our energy function (equation 3). The explanation of the second order phase transition found for the e direction at higher field gives us more trouble.

From the numerical analysis of equations 21 and 24 which belong to configuration (1,4) case a it appears that 2γ, which is the angle between the spins 1 and 2, changes rapidly just below h_{2c}. For the example ($r = 3.51$, and $d = .22$) we find $2\gamma = 0$ at h_{2c} and $2\gamma \approx 30°$ if h differs only 1% from h_{2c}.

This behaviour seems to be qualitatively in agreement with the actual observations on $LiCuCl_3 \cdot 2H_2O$ at fields just below the second order phase transition in the e direction (about 56 kOe). This is illustrated by the rapid variation of the local fields at the Li sites, which follows from the steep changes of the resonance frequencies just below 56 kOe, see fig. 4. Therefore it seems plausible that for the e direction solution (1,4) case a is realized again above the higher first order transition (as it was below the spin flop transition). It is also supported by the fact that these resonance lines above the higher first order phase transition tend to go back to their original positions found below the spin flop transition.

It is questionable whether the introduction of a symmetric contribution to the anisotropy can influence fig. 8 so much that two crossings arise between the solutions (1,3) and (1,4) below the second order transition field h_{2c} (so between the fully drawn and dash-dotted curves).

Another explanation for the absence of the second order phase transition from our calculations might be the fact that the D-M vector is not perpendicular to the e axis. From equation 2 of section 2 the angle between the e axis and the D-M vector is estimated to be either 4° or 28°. The latter direction seems to be the most probable one, because if the field is parallel to the D-M vector no

transitions are expected at all except the one to saturation, which occurs only for this direction. So our assumption that this angle is 90° may be too crude and it might be useful to perform calculations with the magnetic field at an arbitrary angle with the D-M vector.

6.4. The sign reversing field. Additional calculations have been made in order to find the first order phase transition at which the sign reversal of the vector product of two of the four sublattice magnetization vectors occurs as a function of $1/r = (J_1 + J_2)/J_3$ and $d = D/J_3$. This field, in reduced units, will further be referred to as the sign reversing field h_{sr}.

Three values of d were chosen (d = .06, .10 and .14) which cover the data obtained from various experiments. Equation 2 of section 2 yields d = .065 ± .004, the value from De Jong's calculations [14] (actually the component of d in the ac plane); the magnetization measurements in the b direction near saturation give d = .055 ± .005; the preliminary calculations in section 2 lead to d ≈ .1.

In fig. 9 h_{sr}/h_s has been plotted versus 1/r for the three d values. h_s is the field, again in reduced units, at which full saturation occurs if the D-M interaction is absent (d = 0). According to equations 15 and 16 we have $h_s = 4r$. For the b direction H_{sr} = 24 kOe and $H_s \approx$ 150 kOe. These are values extrapolated to zero temperature which follow from the phase diagrams in Chapter 3 figs. 3 and 6. The two critical fields lead to h_{sr}/h_s = .16. This value is indicated by the horizontal dotted line of fig. 9. It leads to extremely low values of $1/r = (J_1 + J_2)/J_3$. For instance if d = .06 we find 1/r = .022, which means that $J_1 + J_2$, the sum of the interactions in a chain along the a axis, is very small as compared to J_3, the interaction in chains parallel to the c axis. This result might change somewhat if the symmetric anisotropy were taken into account, but this leads to much more complicated calculations, which have not yet been carried out.

The low value of 1/r is somewhat unexpected in view of the interatomic distances.

Two possibilities exist.

1°. J_1, J_2 and J_3 are the only important interactions in $LiCuCl_3 \cdot 2H_2O$. In that case J_1 and J_2 (which must both possess the antiferromagnetic sign) are actually so small as was concluded from the preceding calculations.

2°. In addition to J_1, J_2 and J_3 and fourth interaction J_4 must be taken into account, which stabilizes the structure with the four magnetic sublattices, so that a ferromagnetic J_1 and an antiferromagnetic J_2 are allowed, without

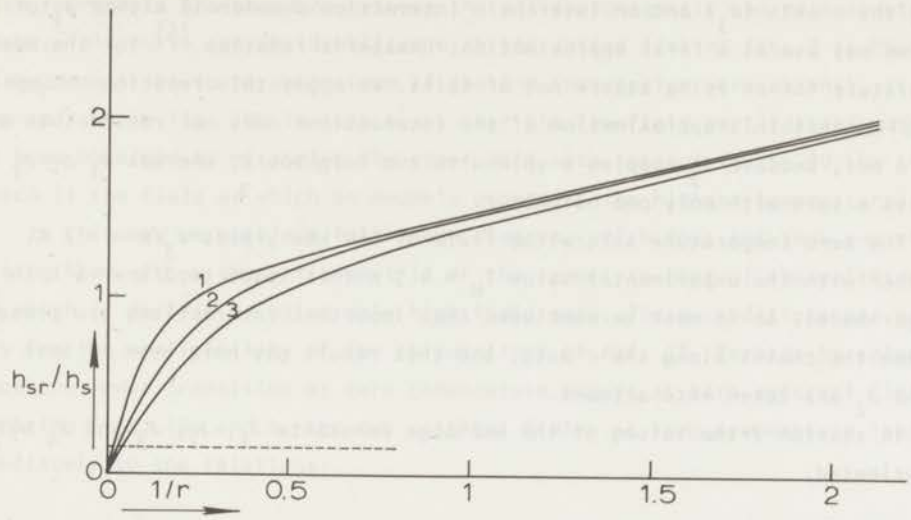

Fig. 9. Plot of the sign reversing field to saturation field ratio versus 1/r at several d values. The sign reversing field exists for any value of 1/r. The curves 1, 2 and 3 belong to d values .06, .10 and .14 respectively. The dotted line represents $h_{sr}/h_s = .16$.

affecting the alternating arrangement of the spins along the a axis in zero field, which has been found with neutron diffraction [3]. (An antiferromagnetic J_1 and a ferromagnetic J_2 is also a possibility but there are argumunts, to be given in section 7, that J_1 is ferromagnetic). A strong ferromagnetic interaction between the spins 6.08 Å apart, which are related by translation along the a axis (see fig. 2), fulfills this requirement. This interaction is ineffective in the four magnetic sublattice model, the only effect being that it stabilizes this model. Even the D-M interaction which may be present in J_4 is cancelled in this four sublattice model. So, as far as the zero temperature behaviour is concerned no inconsistencies are introduced by taking J_4 into account.

The second possibility seems to be sustained by the fact that also in certain antiferromagnetic iron group halides strong ferromagnetic interactions exist [1]. In these halides similarly bridged structures are present as in the dimers in $LiCuCl_3 \cdot 2H_2O$.

Another argument for the existence of strong interactions in the chains along the a axis follows from the value of the Néel temperature.

If we approximate the interactions in $LiCuCl_3 \cdot 2H_2O$ by those in the chains along the c axis (J_3) and an interchain interaction J which is either J_1 or J_2, then we may use as a first approximation, Onsager's relation [16] for the Néel temperature for an Ising square net of spins. We apply this relation though we realize that this approximation of the interactions does not result into a square net, because J_3 couples a spin with two neighbours, whereas J_1 or J_2 couples a spin with only one neighbour.

The zero temperature saturation field of 160 kOe yields $J_3/k = -12$ K. Together with the experimental value $T_N = 4.5$ K this leads to $J/k = -6$ K in the Onsager model. So it must be concluded that important interactions are present between the chains along the c axis, and this result may hold even if both J_1 and J_2 are taken into account.

In section 7 the values of the exchange constants J_1, J_2, J_3 and J_4 will be estimated.

7. Estimation of the exchange constants.

Tachiki and Yamada [17] made some calculations, in the molecular field approximation, on the behaviour of a two sublattice system of identical spin pairs with some interpair exchange interaction. They assumed that the interaction between the members of a pair (with an antiferromagnetic sign) is large as compared to the interpair interactions and that all interactions are isotropic. Since pairs of spins occur in $LiCuCl_3 \cdot 2H_2O$ between which an important antiferromagnetic interaction is expected (J_2 in fig. 2), as was argued in section 6.4, the possibility exists that their theoretical results may lead to at least approximate J values. It should be emphasized that these pairs of spins do not coincide with the dimers as introduced before, but are the neighbours 3.84 Å apart.

If the exchange interactions between the spin pairs along the a axis (J_1 and J_4) are neglected and only J_3 is taken into account as an interpair interaction, then we are dealing with a system of identical spin pairs. If we neglect J_3 instead of J_1 and J_4 the situation is similar, but from section 6 it has become clear why J_3 is so important. Moreover, if only J_1, J_2 and J_4 were taken into account, there would be no long range order.

From the definitions of α and β, the quantities introduced by Tachiki and Yamada (which are both related to the interpair interactions), we find the relations

$$\alpha = -J_3; \qquad \beta = +2J_3 \tag{26}$$

The considerations of these authors lead to the phase diagram of fig. 10a, which represents the boundary between the antiferromagnetic and paramagnetic phases. This curve can be identified with the dotted line of fig. 3 in Chapter 3 (the transition to paramagnetism if the D-M interaction were absent). It has been redrawn in fig. 10b in such a way that the low field part (dotted part) has been obtained by mirroring the upper part with respect to the 80 kOe line (which is the field at which an anomaly occurs at the highest temperature).

In this way we obtain a full phase diagram, which does not show any effect arising from either the antisymmetric or the symmetric part of the anisotropy and which is derived by using only high field data. These conditions are necessary for the applicability of the calculations of ref. 17. Perhaps by coincidence the lower transition at zero temperature occurs at zero external field. Comparing figs. 10a and b, the two critical fields at zero temperature lead immediately to the relations:

$$J - \tfrac{1}{2}|\beta| = 0 \; ; \qquad J + \alpha + \tfrac{1}{2}|\beta| = g\mu_B H^S \tag{27}$$

in which: J is identical to $-J_2$, the interpair interaction, $g = 2.22$ [7] and H^S is the saturation field, which in our case is equal to about 160 kOe. μ_B is the Bohrmagneton.

A third relation follows from the highest temperature at which a transition occurs:

$$|\beta|/4 = 5\ k \tag{28}$$

with k Boltzmann's constant.

Combination of equations 26 and 27 yields

$$J_2/k = -22\ K; \qquad |J_3|/k = 22\ K \tag{29}$$

so equal in absolute magnitude.

Combining 26 and 28 we obtain a different result

$$|J_3|/k = 10\ K \tag{30}$$

The disagreement between the two $|J_3|$ values demonstrates that probably it is not justified to neglect J_1 and J_4, the interpair interactions along the a axis. Moreover, in the calculations of Tachiki and Yamada it has been assumed

that the interpair interactions are small as compared with the intrapair interaction. Thirdley, calculation of the exchange constants in the molecular field approximation, using the transition fields at zero temperature, gives usually values which differ significantly from the values which can be derived from anomalies at higher temperatures. Therefore these calculations can only give orders of magnitude for the interaction constants.

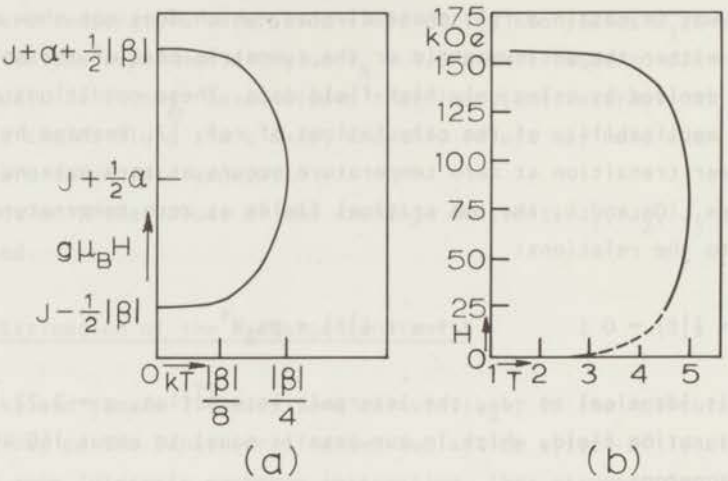

Fig. 10. Left: theoretical phase boundary for a spin-pair system as calculated by Tachiki and Yamada. Right: phase boundary of $LiCuCl_3 \cdot 2H_2O$, omitting any effect as well as all transitions which arise from anisotropy.

Now if we choose $J_3/k = -16$ K (the average of the values derived from equations 29 and 30), the relation $(J_1 + J_2)/J_3 = .022$ of section 6.4 leads to $(J_1 + J_2)/k = -.35$ K. In view of equation 29 this yields $J_1/k = +22$ K and $J_2/k = -22$ K, so that the alternating arrangement of the spins in zero field along the a axis leads to the requirement $J_4/k > +11$ K.

For the calculations of De Jong [14], mentioned in section 2, the values $J_3/k = -16$ K and $J_1/k = +22$ K were adopted, whereas J_2 and J_4 were neglected. Although these calculations are not very sensitive for the exchange model used, they give quite accurate and reliable values of the D-M interaction.

8. Concluding remarks.

So far nothing has been said about the double character of the spin flop

transition as well as about the double character of the first order transition near 24 kOe in the b direction. It is very well possible that the mechanism which causes these small anomalies is a D-M interaction between the spins which are connected via the glide-mirror plane and are 7.0 Å apart (e.f. e and g in fig. 3). This may lead to the existence of at least eight sublattices as has been argued in section 3.

Although the energy expression (equation 3) has not yet been analyzed fully, the first order phase transition, which can be described as a sudden sign reversal of the vector product of two of the four existing sublattice magnetization vectors, occurring at about 32 kOe for the e direction, must be a quite common process in antiferromagnets showing a hidden canting.

It should be very useful to determine the spin directions in a direct experimental way, especially near the second order phase transition (which is found at 56 kOe for the e direction). Just below this transition four different spin directions must be found, which are probably non-coplanar, while above this field only two spin directions should occur. For the b direction only one first order phase transition was found. Similarly here four sublattices exist below 24 kOe and only two above this field. This can be checked with accurate neutron diffraction investigations or with Li resonance experiments, performed on single crystals. In the case of Li resonance for the b direction, for example, four resonance lines must be found below the first order phase transition and only two resonance lines above this field (certainly above the weak anomaly which occurs at a field slightly above that of the first order phase transition).

Investigations of solution (1,3) case b as well as solution (1,4) case b, which both describe the behaviour of a weak ferromagnet (thus two canted sublattices) as was demonstrated in section 6, reveals that the behaviour near saturation is strongly dependent on the magnitude of the D-M vector. For instance if $d = 0$ then a sharp anomaly occurs at saturation, corresponding to a second order phase transition. If $d \neq 0$ a marked rounding off of the magnetization near saturation is found (see equations 15 and 16 from which the magnetization can be derived by calculating $-de/dh$).

At temperatures low as compared to the Néel temperature and in fields near saturation (so about 160 kOe for $LiCuCl_3 \cdot 2H_2O$) the spins are approximately parallel to the field. The canting of the spins is only due to the component of the D-M vector perpendicular to the plane through the two spin directions. Consequently if the magnetic saturation is measured in a direction perpendicular to the D-M vector (for instance the b direction in $LiCuCl_3 \cdot 2H_2O$) the magnitude of the D-M vector can be derived from the width of the saturation

process. The direction of the D-M vector can be found similarly by searching for a crystallographic orientation in which the saturation shows up as a sharp anomaly (even in the case of four sublattices, which remain in existence in $LiCuCl_3 \cdot 2H_2O$, if it is magnetized in the direction parallel to the D-M vector. This direction must be found somewhere in the ac plane.

The above mentioned method of finding the magnitude as well as the direction of the D-M vector is obviously only applicable if only one direction is present in the crystal in which an important D-M interaction occurs. Moreover certain components of the D-M vector are cancelled in the ordered phase. Measurements of this type are in progress in the pulsed magnetic field installation of our laboratory for $LiCuCl_3 \cdot 2H_2O$ [8].

Further calculations with the energy expression (equstion 3) can be carried out. For instance, it cannot be very difficult to calculate the orientation of the D-M vector from the angle between the direction of maximum g and and spin direction in zero field [7] if the magnitudes of the anisotropies are known. Secondly the calculations of section 6 can be extended to magnetic field directions at arbitrary angles with the D-M vector. Thirdly it must be interesting to find the stability regions of the two solutions, considered here, as a function of r (the ratio of the exchange constants) and d (the ratio of the D-M interaction and the exchange energy which it belongs to).

References.

1) Vossos, P.H., Jennings, L.D. and Rundle, R.E., J. Chem. Phys. 32 (1960) 1590.
2) Clay, R.M. and Staveley, L.A.K., Proc. Low. Temp. Calorimetry Conf. Helsinki (1966) 194.
3) Abrahams, S.C. and Williams, H.J., J. Chem. Phys. 39 (1963) 2923.
4) Forstat, H. and McNeely, D.R., J. Chem. Phys. 35 (1961) 1594.
5) Date, M. and Nagata, K., J. Appl. Phys. 34 (1963) 1038.
6) Forstat, H., Bailey, P.T. and Ricks, J.R., J. Appl. Phys. 42 (1971) 1559.
7) Zimmerman, N.J., Bastmeyer, J.D. and Van den Handel, J., Physics Letters 40A (1972) 259.
8) Jordaan, H.A., private communication.
9) Dzyaloshinsky, I., J. Phys. Chem. Solids 4 (1958) 241.
10) Moriya, T., Phys. Rev. 120 (1960) 91.
11) Metselaar, J.W. and De Klerk, D., Physica 63 (1973) 191.
12) Metselaar, J.W. and De Klerk, D., Physica, in press.
13) Fairall, C.W. and Cowen, J.A., Phys. Rev. B2 (1970) 4636.
14) De Jong, W.M., private communication.
15) Henkens, L.S.J.M. and Diederix, K.M., private communication.
16) Onsager, L., Phys. Rev. 65 (1944) 117.
17) Tachiki, M. and Yamada, T., Suppl. Prog. Theor. Phys. 46 (1970) 291.

CHAPTER 5

MAGNETIC BEHAVIOUR OF $CoCl_2 \cdot 6H_2O$ AND $CoBr_2 \cdot 6H_2O$

1. $CoCl_2 \cdot 6H_2O$.

Cobalt chloride hexahydrate, $CoCl_2 \cdot 6H_2O$, becomes antiferromagnetic below $T_N = 2.29$ K [1]. The crystal is base-centered monoclinic, the external shape was described by Groth [2]. The dimensions of the unit cell are: a = 10.34 Å, b = 7.06 Å, c = 6.67 Å with $\beta = 122°20'$ [3], the density being 1.924 g/cm^3. The c axis is the direction of antiferromagnetic alignment [4] and the magnetic space group is $C_c 2/c$ [5]. The g factors for different directions obey $g_c = g_b = 4.9$, $g_{\perp b,c} = 2.9$ [4,6]. Above the spin-flop transition field the sublattice magnetizations are parallel to the b axis.

Two conflicting sets of values for the exchange integrals J between interacting spins (J is defined by writing the exchange energy between two spins $\underline{S}_1$ and $\underline{S}_2$ as $J\underline{S}_1 \underline{S}_2$) can be found in the literature. For the c direction Shinoda et al. [7] give $J_1/k = 8.12$ K for nearest neighbours and a much smaller value for the second-neighour interaction. Kimura [8] gives $J_1/k = 2.32$ K for the nearest-neighbour interaction, $J_2/k = 1.75$ K for the second-neighbour interaction and a small fourth-neighbour interaction. These J values lead in the molecular-field approximation (MFA) to exchange fields of 49.2 kOe and 19.4 kOe, for Shinoda et al. and Kimura, respectively. The exchange fields are calculated for zero temperature in the antiferromagnetic phase. Again in the MFA this leads to critical-field values for the transition from the flop phase to the paramagnetic phase at zero temperature of 98.4 kOe and 38.8 kOe, respectively [9].

Single crystals were grown from a saturated aqeous solution. A crystal weighing 0.216 g was used in the experiment. It was mounted with its c axis parallel to the external field.

Some typical curves, showing the susceptibility versus the magnetic field at constant temperature are given in fig. 1. All the curves are on the same scale, but the zero lines have been shifted with respect to each other as indicated in the figure. Two pronounced anomalies are observed at the lower temperatures. The lower one is the transition from the antiferromagnetic to the spin-flop phase, the upper one is assumed to be the transition from the spin-flop

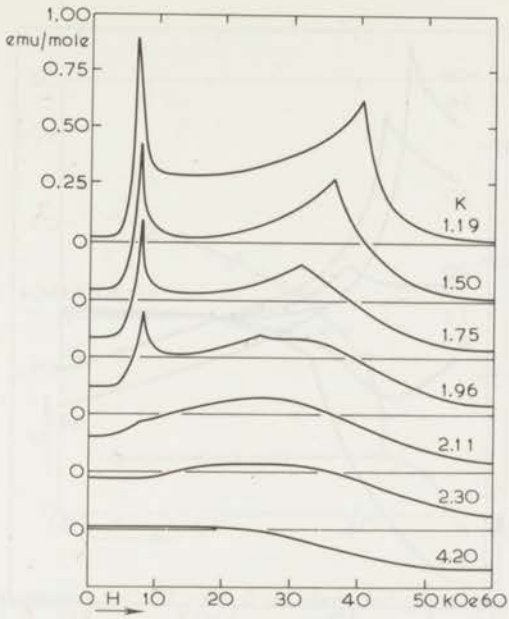

Fig. 1. Typical curves, showing the susceptibility versus the magnetic field at constant temperature. Note the vertical shift of the different curves.

phase to paramagnetism (see below). A small hysteresis of about 1.5% was invariably found in the position of the lower peak (which is a first-order transition), but no such effect could be detected in the case of the upper one.

Curves showing the susceptibility versus the temperature at constant field are shown in figs. 2 and 3. The kinks and peaks in these curves correspond very well with the peaks in fig. 1. Fig. 3 corresponds to a small region of fig. 2. Here, for clarity, the curves have been shifted vertically with respect to each other in an arbitrary way.

From figs. 1, 2 and 3 we constructed the H,T phase diagram of fig. 4. The Néel temperature is observed to be 2.30 ± 0.02 K and the triple point at 2.07 ± 0.02 K and H = 7.9 ± 0.2 kOe. The following criteria were used for the positions of the transitions. For the antiferromagnetic to spin-flop transition: the maxima in the $\chi(H)$ curves; for the antiferromagnetic to paramagnetic transition: the kinks in the $\chi(T)$ curves; for the spin-flop to paramagnetic transition: the maxima in the $\chi(H)$ or $\chi(T)$ curves. In general the transitions become very vague near the triple point.

The diagram of state of $CoCl_2 \cdot 6H_2O$ up to about 12 kOe had been derived before from proton-resonance experiments by Van der Lugt and Poulis [12], from

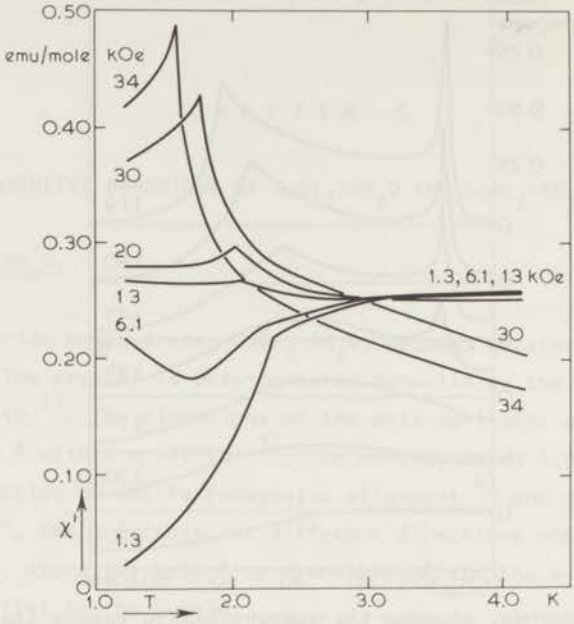

Fig. 2. Typical curves, showing the susceptibility versus the temperature at constant field.

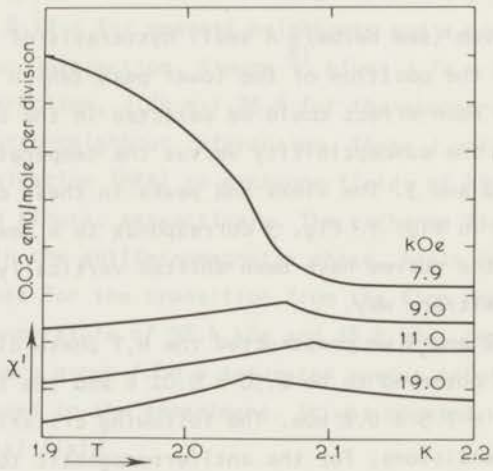

Fig. 3. Detail of the behaviour of the susceptibility versus the temperature at some field levels near the triple point. The negative slope of the transition curve just above the triple point is clearly demonstrated.

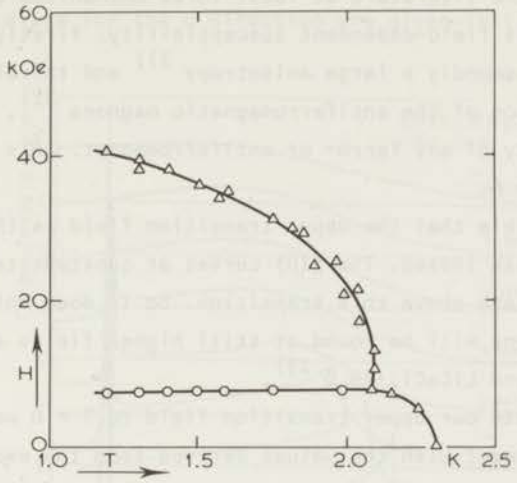

Fig. 4. Phase diagram of $CoCl_2 \cdot 6H_2O$ as derived from anomalies in the susceptibility. ○ First-order phase transition. △ Second-order phase transition.

isothermal magnetization experiments by Schmidt and Friedberg [13] and from isentropic magnetization experiments by McElearney et al. [14]. In general there is good agreement with our results. The positive slope of the upper transition curve just above the triple point was also found in these experiments. It follows clearly from fig. 3.

It is obvious that the low-field transition below the triple-point temperature is the transition from the antiferromagnetic phase (where the spin arrangement is parallel to the c axis) to the flop phase (where the spin arrangement is almost parallel to the b axis).

Considering the transition from the antiferromagnetic to the paramagnetic phase, the $\chi(T)$ curves of fig. 2 for low fields show that there is some short-range order above the Néel point. The susceptibility curves show maxima at temperatures $T_{max}/T_N > 1.8$. This is in agreement with the zero-field specific-heat measurements of Robinson and Friedberg [1].

It should be noted that the susceptibility in the flop phase rises with the field as well as with the temperature, leading to a rather sharp maximum at the transition to the paramagnetic phase. The simple molecular-field calculations show a temperature- and field-independent susceptibility. This field-dependent susceptibility was reported earlier in several other antiferro-

magnetic materials such as $MnCl_2 \cdot 4H_2O$ [15], EuTe [16], $CoCl_2$ [17], $CuCl_2 \cdot 2H_2O$ [18] and $GdAlO_3$ [19]. In the literature at least three mechanisms can be found in order to explain this field-dependent susceptibility: firstly biquadratic exchange effects [20], secondly a large anisotropy [21] and thirdly the existence of a zero-point motion of the antiferromagnetic magnons [22], which is in fact an intrinsic property of any ferro- or antiferromagnet. This will be further discussed in Chapter 6.

It seems plausible that the upper transition field is the transition to the paramagnetic phase indeed. The $\chi(H)$ curves at constant temperature (fig. 1) approach the value zero above this transition. So it does not seem likely that additional transitions will be found at still higher fields as in the cases of $Mn(CHOO)_2 \cdot 2H_2O$ [10] and $LiCuCl_3 \cdot 2H_2O$ [23].

If we extrapolate our upper transition field to T = 0 we obtain 46.0 kOe, which is in disagreement with the values derived from the exchange fields, as calculated from the exchange constants in the MFA of both Shinoda et al. and Kimura (see above). This seems to indicate that molecular-field theories are inadequate to give a description of the behaviour of $CoCl_2 \cdot 6H_2O$. In Chapter 6 we give a more detailed discussion of our results based, for the lower fields, on the two-dimensional Ising model, and for the flop phase, on spin-wave theories. Several authors have already adapted the Ising model in order to explain their experimental results [1,7,11].

2. $\underline{CoBr_2 \cdot 6H_2O}$.

Cobalt bromide hexahydrate, $CoBr_2 \cdot 6H_2O$ becomes antiferromagnetic below $T_N = 3.07$ K [24]. The crystal is isomorphous with the corresponding chloride, which is base-centered monoclinic and whose external shape was described by Groth [2]. The dimensions of the unit cell at room temperature are: a = 11.029 Å, b = 7.178 Å, c = 6.908 Å, each with an accuracy of one part in a thousand and $\beta = 124.71 \pm 0.04°$ [25]. The density is 2.46 g/cm^3. The c axis is the direction of antiferromagnetic spin alignment [26] and the magnetic space group is $C_{2c}^2 2/c$ [27]. The g factors for different directions are $g_b = 5.0$, $g_c = 5.1$, $g_{\perp b,c} = 2.2$ [28]. Above the spin-flop transition the sublattice magnetizations are parallel to the b axis.

Single crystals were grown from a saturated aqeous solution. A crystal weighing 2.36 g was used for the measurements in the b direction and a crystal of 0.902 g was used for the measurements in the c direction. For orienting the single crystals, the morphology as given by Groth [2] was used, and in addition

an X-ray analysis [25] was made in order to check the chosen direction.

Some typical curves, showing the susceptibility versus the magnetic field at constant temperature for the c direction are given in fig. 5. All the curves

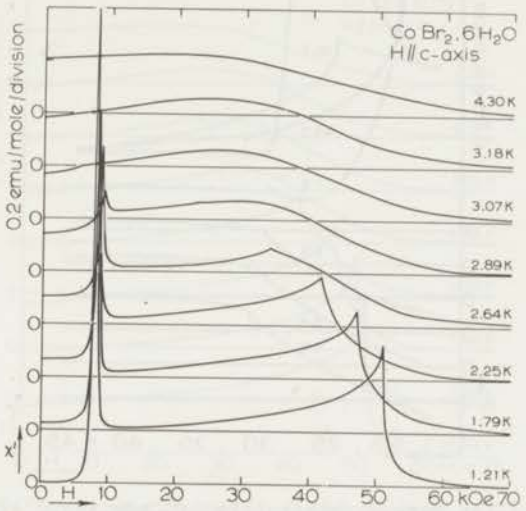

Fig. 5. Susceptibility versus magnetic field of $CoBr_2 \cdot 6H_2O$ single crystal with the external field parallel to the c axis at several temperatures. Note the vertical shift of susceptibility scales.

are on the same scale, but the zero lines have been shifted with respect to each other as indicated in the figure. Two pronounced anomalies are observed at the lower temperatures. The lower one represents the transition from the antiferromagnetic to the spin-flop phase, the upper one corresponds to the transition from the spin-flop phase to the paramagnetic phase. A small hysteresis for the antiferromagnetic to spin-flop phase boundary, ranging from 1 percent at 1.2 K to about 3 percent near the triple-point temperature, was found. No hysteresis could be detected in any of the other phase transitions.

Curves showing the susceptibility versus the temperature at constant field (c direction) are shown in figs. 6 and 7. Fig. 7 corresponds to the region just above the triple point in order to show the positive curvature of the phase boundary as has also been found in e.g. $CoCl_2 \cdot 6H_2O$ [29]. The measurements versus the temperature have been done in addition to those versus the field because close to the Néel temperature the transition temperature is nearly independent of the field, so well-defined anomalies can only be expected by

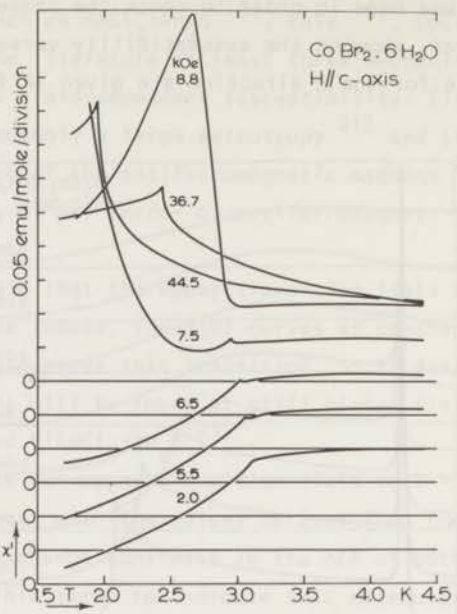

Fig. 6. Susceptibility versus temperature of $CoBr_2 \cdot 6H_2O$ single crystal with the external field parallel to the c axis at several field levels. Note the vertical shift of the susceptibility scales.

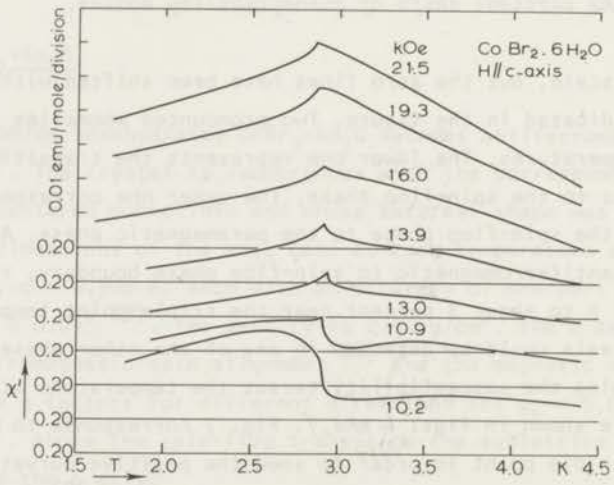

Fig. 7. Susceptibility versus temperature at field levels just above the triple point. Note the vertical shift of the susceptibility scales.

crossing the phase boundary with varying temperature.

The same experiments have been done for the b direction. The results are shown in figs. 8 and 9. No spin-flop transition is found in this direction.

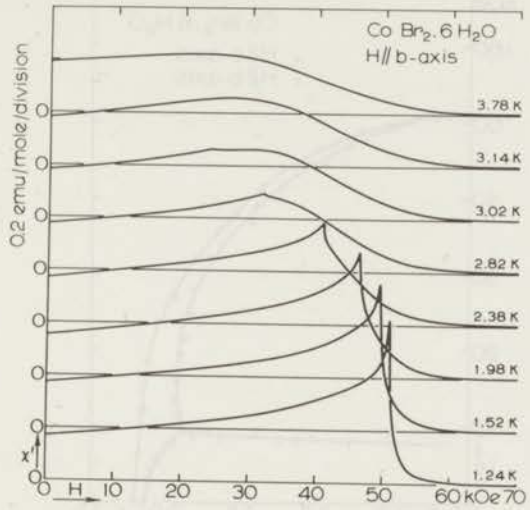

Fig. 8. Susceptibility versus magnetic field of $CoBr_2 \cdot 6H_2O$ single crystal with the external field parallel to the b axis at several temperatures.

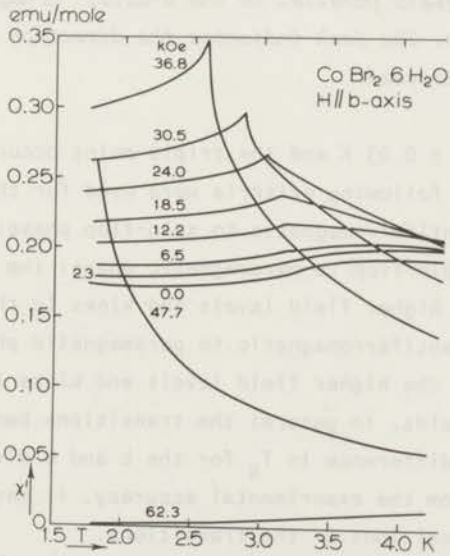

Fig. 9. Susceptibility versus temperature of $CoBr_2 \cdot 6H_2O$ single crystal with the external field parallel to the b axis at several field levels.

From figs. 5, 6 and 7 we constructed the H,T phase diagram for the c

direction. From figs. 8 and 9 we constructed the H,T diagram for the b direction. Both diagrams are given in fig. 10. The Néel temperature (c direction)

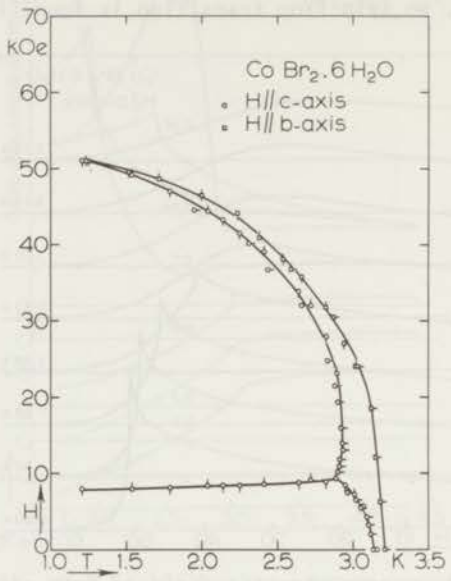

Fig. 10. The magnetic phase diagram of a single crystal of $CoBr_2 \cdot 6H_2O$. ○ Magnetic field parallel to the c axis; □ magnetic field parallel to the b axis. The dash indicates the direction in which the phase boundary is crossed.

is observed to be 3.14 ± 0.03 K and the triple point occurs at 2.89 ± 0.03 K and 9.3 ± 0.2 kOe. The following criteria were used for the positions of the transitions. For the antiferromagnetic to spin-flop phase: the maxima in the $\chi(H)$ curves. For the spin-flop to paramagnetic phase: the maxima in the $\chi(H)$ or $\chi(T)$ curves for the higher field levels and kinks in the $\chi(T)$ curves at the lower fields. For the antiferromagnetic to paramagnetic phase: maxima in the $\chi(H)$ or $\chi(T)$ curves at the higher field levels and kinks in the $\chi(H)$ or $\chi(T)$ curves at the lower fields. In general the transitions become very vague near the triple point. The difference in T_N for the b and c directions of fig. 10 cannot be explained from the experimental accuracy. It may be connected with our criteria for the positions of the transitions.

The diagram of state of $CoBr_2 \cdot 6H_2O$ up to about 10 kOe has been derived before by McElearney et al. [30] by isentropic magnetization and specific-heat measurements. The phase boundaries as detected from the susceptibility measurements correspond within the accuracy of the experiment with those derived from

the isentropic magnetization and specific-heat measurements.

The experimental results will be discussed theoretically in Chapter 6.

References.

1) Robinson, W.K. and Friedberg, S.A., Phys. Rev. 117 (1960) 402.
2) Groth, P., Chemische Kristallographie, 1 Teil, Wilhelm Engelmann (Leipzig, 1906) p. 248.
3) Mizuno, J., J. Phys. Soc. Japan 15 (1960) 1412.
4) Haseda, T., J. Phys. Soc. Japan 15 (1960) 483.
5) Kleinberg, R., J. chem. Phys. 53 (1970) 2660.
6) Flippen, R.B. and Friedberg, S.A., J. appl. Phys. 31 (1960) 338 S.
7) Shinoda, T., Chihara, H. and Seki, S., J. Phys. Soc. Japan 19 (1964) 1637.
8) Kimura, I., J. Phys. Soc. Japan 30 (1971) 1603.
9) See for instance: Martin, D.H., Magnetism in Solids, Iliffe Books Ltd. (London, 1967).
10) Schutter, J.W., Metselaar, J.W. and De Klerk, D., Physica 61 (1972) 250 (Commun. Kamerlingh Onnes Lab., Leiden No. 392b).
11) Skalyo, J., Cohen, A.F., Friedberg, S.A. and Griffiths, R.B., Phys. Rev. 164 (1967) 705.
12) Van der Lugt, W. and Poulis, N.J., Physica 26 (1960) 917 (Commun. Kamerlingh Onnes Lab., Leiden No. 324c).
13) Schmidt, V.A. and Friedberg, S.A., J. appl. Phys. 38 (1967) 5319.
14) McElearney, J.N., Forstat, H. and Bailey, P.T., Phys. Rev. 181 (1969) 887.
15) Rives, J.E., Phys. Rev. 162 (1967) 491.
16) Oliveira Jr., N.F., Foner, S. and Shapira, Y., Phys. Letters 33A (1970) 153.
17) Jacobs, I.S. and Silverstein, S.D., Phys. Rev. Letters 13 (1964) 272.
18) Van der Sluys, J.C.A., Zweers, B.A. and De Klerk, D., Phys. Letters 24A (1967) 637.
19) Blazey, K.W., Rohrer, H. and Webster, R., Phys. Rev. B4 (1971) 2287.
20) Rodbell, D.S. Jacobs, I.S., Owen, J. and Harris, E.A., Phys. Rev. Letters 11 (1963) 10.
21) Carrara, P., De Gunzbourg, J. and Allain, Y., J. appl. Phys. 40 (1969) 1035.
22) Kanamori, J. and Yosida, K., Progr. theor. Phys. 14 (1955) 423.
23) Metselaar, J.W. and De Klerk, D., to be published.
24) Forstat, H., Taylor, G. and Spence, R.D., Phys. Rev. 116 (1959) 897.
25) Verschoor, G.C., private communication.
26) Garber, M., J. Phys. Soc. Japan 15 (1960) 734.
27) Kleinberg, R., Bull. Amer. Phys. Soc. 11 (1966) 759.

28) Murray, T.E. and Wessel, G.K., J. Phys. Soc. Japan 24 (1968) 738.
29) Van der Lugt, W. and Poulis, N.J., Physica 26 (1960) 917 (Commun. Kamerlingh Onnes Lab., Leiden No. 324c).
30) McElearney, J.N., Forstat, H. and Bailey, P.T., Phys. Rev. 181 (1969) 887.

CHAPTER 6

DISCUSSION OF THE MAGNETIC BEHAVIOUR OF $CoCl_2 \cdot 6H_2O$ AND $CoBr_2 \cdot 6H_2O$

1. The model.

Several investigators described their experimental data on $CoCl_2 \cdot 6H_2O$ and $CoBr_2 \cdot 6H_2O$ at low temperatures by using only one important exchange interaction J, where J is defined by writing the exchange energy between two spins $\underline{S}_1$ and $\underline{S}_2$ as

$$E_{ex} = J\, \underline{S}_1 \cdot \underline{S}_2 \quad , \tag{1}$$

see for instance reference 1 for $CoCl_2 \cdot 6H_2O$ and reference 2 for $CoBr_2 \cdot 6H_2O$. This interaction J should occur between a spin and its four neighbours in the (001) or ab plane. These planes are tetragonally occupied by Co spins. In addition to this interaction J a small interaction J', occurring between spins belonging to neighbouring (001) planes, was sometimes introduced.

A more careful investigation of the model of both the chloride and the bromide reveals that both salts are highly anisotropic two dimensional Heisenberg antiferromagnets. The highly anisotropic Heisenberg type of interaction is most clearly demonstrated by the components of the molecular fields as introduced by Date [3] to explain his electron spin resonance data on $CoCl_2\ 6H_2O$. From these molecular field constants an estimation can be made for the anisotropy in the exchange constant. It appears that $J_b = .96\ J_c$; $J_{a'} = .13\ J_c$. From these values it is clear that the anisotropy is of the easy plane type.

The two dimensional character of the interaction is suggested by the crystal structure [4]. Moreover the experimental data as given in the literature as well as the data given in Chapter 5 can be described satisfactorily using only one exchange constant (see also section 4).

The occurrence of a Néel point entails some diffuculties in the anisotropic Heisenberg antiferromagnet. If the model is strictly two dimensional then the Néel temperature T_N is related to the anisotropy, because a two dimensional isotropic Heisenberg antiferromagnet does not order, as has been proved by Mermin and Wagner [5]. In this case it seems reasonable to calculate T_N using the Ising approximation. However, if, in the other limiting case, the exchange

energy is isotropic T_N is related to the interaction between planes, which causes three dimensional order. The former picture appears to be more fruitful, at least in zero field.

A neutron diffraction experiment, carried out by Kleinberg revealed unambiguously that a two sublattice model is adequate in describing the behaviour of $CoCl_2 \cdot 6H_2O$ [6] and $CoBr_2 \cdot 6H_2O$ [7], at least in zero field. The two sublattice models will be adopted throughout this chapter for all field values for both the chloride and the bromide.

The Landé splitting factors g, which have been measured by Haseda [8] and Flippen and Friedberg [9] for $CoCl_2 \cdot 6H_2O$ and by Murray and Wessel [2] for the corresponding bromide, are largely anisotropic and show tetragonal symmetry. The g values were given in Chapter 5 and the anisotropy in g will be further discussed in section 2. The g values indicate that both salts are easy plane antiferromagnets, the easy plane being the bc plane. A small anisotropy in this plane, with the c axis as the easy spin axis, is reflected in the existence of a spin flop phase transition for the c direction as mentioned in Chapter 5.

2. The energy level scheme of Co^{++} in $CoCl_2 \cdot 6H_2O$.

In this section the energy level scheme of Co^{++} in $CoCl_2 \cdot 6H_2O$ will be discussed briefly. Apart from slight quantitative differences it can also be applied to Co^{++} in $CoBr_2 \cdot 6H_2O$.

The lowest state of a free Co^{++} ion is ^4F ($L = 3$, $S = \frac{3}{2}$) [10,11]. The first exited state is ^4P ($L = 1$, $S = \frac{3}{2}$) and lies about 1500 cm^{-1} above the ground state.

In a crystalline field of cubic symmetry the ground state splits into a lowest orbital triplet Γ_4, a higher triplet Γ_5 and a still higher singlet Γ_2, the energy separation between Γ_4 and Γ_5 being of the order of 10^4 cm^{-1}. If we neglect the spin-orbit coupling the tetragonal component of the crystalline field gives rise to a further splitting of Γ_4 into a doublet (denoted by Γ_4' and Γ_4'') and a singlet (Γ_4'''). A substantial tetragonal component can be expected on the basis of the crystal structure [4], because the Co^{++} ion is situated in the centre of an octahedron, on the corners of which four water molecules are situated in a square [12], and two chlorine ions on the tops of the octahedron,

A small orthorhombic contribution is added to the tetragonal and cubic components of the crystal field arising from two more water molecules located near the chlorine ions, which form a slightly distorted octahedron together with the four water molecules mentioned above [10]. This is illustrated in fig. 1.

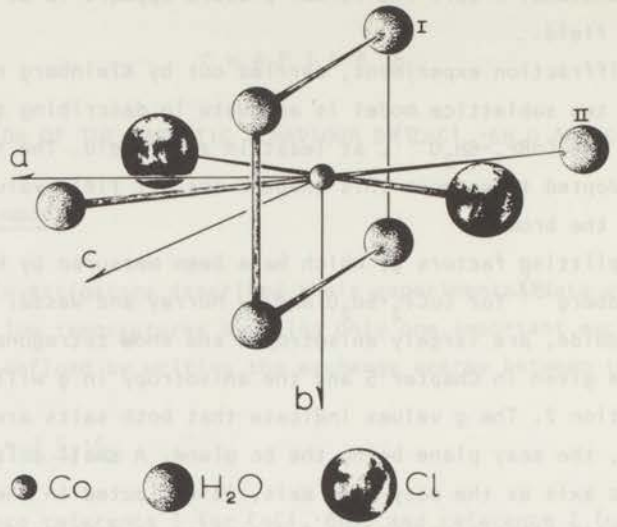

Fig. 1. Schematic representation of the surroundings of a Co^{++} ion in $CoCl_2 \cdot 6H_2O$.
I : $4H_2O$ coordinated tetragonally close to the Co^{++} ion.
II : $2H_2O$ far from the Co^{++} ion.

The combined action of the tetragonal and orthorhombic components of the crystalline field and of the spin-orbit coupling (the latter being of comparable magnitude as the other two) results into the splitting of Γ_4 into six Kramers doublets, of which the lowest two lie about 150 cm^{-1} apart.

A scheme of the level splittings of the Co^{++} ion is shown in fig. 2, which was redrawn from ref. 11.

The tetragonal and orthorhombic components of the crystal field are responsible for the anisotropy in the effective splitting factor g.

$CoCl_2 \cdot 6H_2O$ and $CoBr_2 \cdot 6H_2O$ show transitions to the paramagnetic phase at about 48 kOe and 55 kOe respectively at zero temperatures. The Zeeman splitting $g\mu_B H$ in the paramagnetic phase in fields of the order of 60 kOe is about 13 cm^{-1}, which is small as compared to the level splitting between the ground state and the first excited Kramers doublet (for $CoBr_2 \cdot 6H_2O$ this splitting is slightly larger than for $CoCl_2 \cdot 6H_2O$, about 180 cm^{-1}). Therefore a change in g due to the magnetic field is expected to be small and the effect will be neglected. In fact the value of g in high fields can be determined by integrating the susceptibility curve. For the chloride g_c in 70 kOe is somewhat higher than the

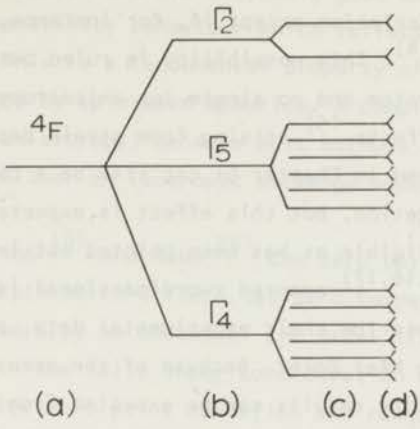

Fig. 2. Scheme of the level splitting for a Co^{++} ion under the influence of a crystalline field and spin orbit coupling.
(a) free ion state ^4F.
(b) splitting in cubic field only.
(c) splitting in tetragonal field with spin orbit coupling.
(d) under the external magnetic field where all degeneracies are removed.

literature value, which has been determined in zero field, but the effect hardly exceeds the experimental accuracy. For the bromide no difference was found between the literature value and its value in 70 kOe.

The degree of saturation of the sample can be estimated by comparing kT with $g\mu_B H$. At 1.2 K we find $kT \simeq .8$ cm^{-1} and since at 60 kOe $g\mu_B H \simeq 13$ cm^{-1}. We have $kT \ll g\mu_B H$ so that the magnetization may be considered as fully saturated.

3. Theories.

A molecular field treatment is not adequate to describe some of the dominating features in the measurements given in Chapter 5. One example is the rise of the zero field susceptibility with the temperature above the Néel point. The molecular field theory predicts a decreasing susceptibility in this region (see for instance Nagamiya, Yoshida and Kubo [13]), since in this theory it is assumed that no short range order exists above T_N. Secondly the rise of the susceptibility with the field in the flop phase (see for instance the curves

at 1.19 K in fig. 1 and at 1.21 K in fig. 5 of Chapter 5) is not predicted in the molecular field description except if, for instance, a large single ion anisotropy is present [14]. This possibility is ruled out here because we are dealing with a $S = \frac{1}{2}$ system and no single ion anisotropy occurs in that case. Biquadratic exchange effects [15] arising from strain dependence of the exchange energy (already mentioned in Chapter 5) can also be a cause of non-linear behaviour of the magnetization, but this effect is expected to be small. The field dependence of g is negligible as has been pointed out in section 2.

Several authors [1,16,17] adopted two-dimensional Ising models for the chloride in order to describe their experimental data, particularly the specific heat behaviour near the Néel point. Because of the occurrence of the spin flop transition no satisfactory results can be expected from the Ising approximation at fields exceeding about 7 kOe, but in section 5 the zero field experimental data will be compared with the results from a two-dimensional super-exchange Ising antiferromagnet, a case which has been exactly solved [18]. This theory also predicts a rise of the susceptibility with the temperature above the Néel point.

In the preceding discussion it appears that a duality exists in the description of the experimental data as given by several authors. On the one hand $CoCl_2 \cdot 6H_2O$ is considered to be a two-dimensional Ising antiferromagnet and on the other hand the Heisenberg type of interaction is adopted. This is not very surprising in view of the discussion given in section 1.

As the Ising model cannot be used in higher fields we have to adopt the two-dimensional anisotropic Heisenberg model.

Spin-wave theories may account for the rise of the susceptibility with the field in the flop phase. These theories, however, are usually developed for three-dimensional systems (simple cubic, thus six neighbours and body centered cubic, thus eight neighbours) with an uniaxial anisotropy. It is interesting to investigate whether these theories can be extended and applied to two-dimensional systems of which both $CoCl_2 \cdot 6H_2O$ and $CoBr_2 \cdot 6H_2O$ are thought to be examples (the number of neighbours being equal to four). In calculating the susceptibility according to these spin-wave theories it appears that the summation over the $\underline{k}$-space ($\underline{k}$ being the wave number of a spin wave), which in this case is two-dimensional, does not lead to divergences except if the magnetic field approaches the value at which saturation occurs. The quantitative agreement between the results from these calculations and the experimental susceptibility is a further indication that these spin-wave theories may also be used for two-dimensional systems.

The two salts considered here are extremely good examples of magnetic substances showing a susceptibility behaviour which reflects the existence of zero point spin deviations. This is a fundamental property of magnetic substances and can only be described by spin-wave theories. A complicating factor, however, is the high easy plane anisotropy, because most authors who treated spin-wave theories thus far used either an isotropic exchange model or an uniaxial (easy axis) exchange model.

According to Anderson [19] and Kubo [20] the zero point spin deviation gives rise to an "effective" spin which differs (at zero temperature and in zero field) from its saturation value S by an amount of the order $1/zS$. Here z is the number of nearest neighbours. In the salts under consideration we have $z = 4$ and $S = \frac{1}{2}$, which means that S and its zero point deviation are roughly of the same magnitude. Accurate neutron diffraction measurements may be used to investigate this in a quite direct way. However, also susceptibility measurements can give accurate and important information about the effective spin value and its field dependence, though this method is less direct and cannot be applied for every magnetic substance. This point will further be discussed in section 6.4.

4. Calculation of the exchange constant.

In order to carry out further calculations using spin-wave theories we have to specify our model for the two salts in more detail. Because in the literature different numerical values are used for J by different authors we recalculate it here using several theories.

4.1. Molecular field. In a molecular field treatment the exchange constant can be obtained in two different ways.

1° From the Néel temperature. From the literature (see for instance Nagamiya, Yoshida and Kubo [13]) we have the relation

$$T_N = -\frac{1}{3}\,(J/k)\; z\; S\; (S+1) \qquad (2)$$

yielding

$$J/k = -3.14 \text{ K for } CoBr_2 \cdot 6H_2O$$
$$J/k = -2.30 \text{ K for } CoCl_2 \cdot 6H_2O \qquad (3)$$

2° From the saturation field at zero temperature. It obeys the equation

$$g\mu_B H = 2 z J S \qquad (4)$$

We find

$$J/k = -4.72 \text{ K for } CoBr_2 \cdot 6H_2O$$
$$J/k = -3.97 \text{ K for } CoCl_2 \cdot 6H_2O \qquad (5)$$

4.2. The Ising model. The similarity to the two-dimensional square Ising model has already been indicated. Onsager's relation [21] for the Néel temperature, in the special case of only one exchange constant reduces to:

$$|\sinh 2K| = 1 \qquad (6)$$

with $2K = -J/2kT_N$. This leads to

$$J/k = -5.54 \text{ K for } CoBr_2 \cdot 6H_2O$$
$$J/k = -4.06 \text{ K for } CoCl_2 \cdot 6H_2O \qquad (7)$$

A second way of calculating J/k from T_N makes use of the relation given by Fisher [18]. He gave an exact solution of the magnetic behaviour of a two-dimensional square net of spins in the Ising approximation. He introduced a super-exchange mechanism, which is essential for solving the problem exactly. He found

$$T_N = -(1.30841/4)\,(J/k) \qquad (8)$$

from which it follows that

$$J/k = -9.61 \text{ K for } CoBr_2 \cdot 6H_2O$$
$$J/k = -7.04 \text{ K for } CoCl_2 \cdot 6H_2O \qquad (9)$$

A third way of estimating the value of the exchange constant makes use of the curvature of the boundary between the antiferromagnetic and paramagnetic phases. Bienenstock [22] calculated the field dependence of the transition temperature for the square, simple cubic and body centered cubic lattices of Ising antiferromagnets with one exchange constant. His results could be described very well by the formula

$$T_N(H) = T_N(0)\ (1 - (H/H_c)^2)^{\xi} \tag{10}$$

For low fields this reduces to

$$T_N(H) = T_N(0)\ (1 - \xi(H/H_c)^2) \tag{11}$$

where ξ equals .87, .35 and .36 for the square, simple cubic and body centered cubic lattices respectively. H_c is defined by $H_c = - zJS/g\mu_B$.

According to figs. 4 and 10 of Chapter 5 the phase boundaries for the bromide and for the chloride can be represented by

$$T_N(H) = T_N(0)\ (1 - \alpha H^2) \tag{12}$$

with

$$\alpha = .83 \times 10^{-9}\ \text{Oe}^{-2} \text{ for } CoBr_2 \cdot 6H_2O$$

$$\alpha = 1.6 \times 10^{-9}\ \text{Oe}^{-2} \text{ for } CoCl_2 \cdot 6H_2O \tag{13}$$

The same value for α was found for $CoCl_2 \cdot 6H_2O$ by Skalyo et al. [17].

With $\xi = .87$ we find

$$J/k = - 5.54\ \text{K for } CoBr_2 \cdot 6H_2O$$

$$J/k = - 3.85\ \text{K for } CoCl_2 \cdot 6H_2O \tag{14}$$

With $\xi = .36$ we find

$$J/k = - 3.57\ \text{K for } CoBr_2 \cdot 6H_2O$$

$$J/k = - 2.48\ \text{K for } CoCl_2 \cdot 6H_2O \tag{15}$$

4.3. Spin-wave description. Spin-wave theories, linear [23] as well as non-linear [24], yield the same relation as the molecular field approximation between the saturation field at zero temperature and the exchange constant. This is not surprising because the zero point spin deviation becomes zero at the saturation field. A relation between the exchange constant and a higher temperature property of the antiferromagnet, such as the Néel temperature or the curvature of the phase boundary between the antiferromagnetic phase and the

paramagnetic phase, is not available in the literature. This is caused by the fact that at higher temperatures the spin-wave interactions become very important and mathematical difficulties arise (see also section 6).

Non-linear spin-wave calculations such as carried out by Feder and Pytte[24] result into a temperature dependent transition field from the flop phase to the paramagnetic phase. A $T^{3/2}$ power law is found. In fig. 3 this transition field is plotted versus $T^{3/2}$ for $CoBr_2 \cdot 6H_2O$ (b and c direction) and for $CoCl_2 \cdot 6H_2O$ (c direction). A $T^{3/2}$ dependence for the lower temperatures is not clearly demonstrated (extension of the measurements to lower temperatures would be highly desirable) but it is possible to approximate the low temperature data by straight lines. According to ref. 24 these slopes should obey

$$\partial H/\partial(T^{3/2}) = -\,2.315\ (3^{3/2}/2S\pi^2)\ (-2k/SzJ)^{3/2} \qquad (16)$$

from which we find

$$J/k = -\,8.1\ \text{K for } CoBr_2 \cdot 6H_2O$$
$$J/k = -\,4.8\ \text{K for } CoCl_2 \cdot 6H_2O \qquad (17)$$

4.4. Discussion of the J values. The J values obtained from the various theories have been listed in table 1.

Table 1

	MOL. FIELD		ISING				SPIN WAVES	
			T_N		H dep. AFM-P			T dep.
	T_N	H_s	Onsager	Fisher	ξ=.87	ξ=.36	H_s	FLOP-P
$CoBr_2 \cdot 6H_2O$	3.14	4.72	5.54	9.61	5.54	3.57	4.72	8.1
$CoCl_2 \cdot 6H_2O$	2.30	3.97	4.06	7.04	3.85	2.48	3.97	4.8

J/k values as calculated from the different theories. The numbers below H dep. AFM-P are those obtained from the field dependence of the Néel temperature. The values below T dep. FLOP-P are those obtained from the temperature dependenceof the saturation field.

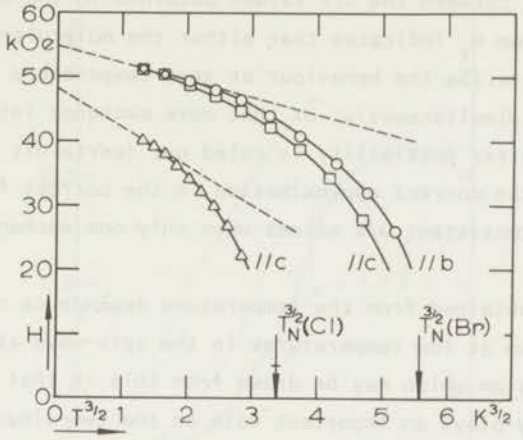

Fig. 3. Plot of the transition field to paramagnetism against $T^{3/2}$. The arrows indicate the Néel temperatures of the chloride and the bromide respectively.

△ $CoCl_2 \cdot 6H_2O$ *parallel c*

○ $CoBr_2 \cdot 6H_2O$ *parallel b*

□ $CoBr_2 \cdot 6H_2O$ *parallel c*

If only one exchange constant is present its value can be obtained in the most reliable way from the saturation field at zero temperature, because both the molecular field theory and the spin-wave theories yield the same relation between these two quantities. For the chloride this J/k value is in nice agreement with the one from T_N using Onsager's relation for T_N and with the J/k value obtained from the curvature of the antiferromagnetic to paramagnetic phase boundary as derived by Bienenstock if we choose $\xi = .87$. This means that the model of the two-dimensional rectangular Ising spin arrangement seems to be a very good approximation in zero field, as must also be expected on the basis of specific heat measurements performed, for instance, by Robinson and Friedberg [16]. For the bromide the correspondence is not so good, indicating that a second neighbour interaction in the bromide is more important than in the chloride.

The values as derived from the superexchange model of Fisher [18] are

significantly higher. This may indicate that his superexchange mechanism does not describe very well the physical situation concerning the superexchange in these salts.

The disagreement between the J/k values obtained in the molecular field theory from T_N and from H_s indicates that either the molecular field treatment is not adequate to describe the behaviour at zero temperature and in zero field at high temperatures simultaneously, or that more exchange interactions should be introduced. The latter possibility is ruled out (certainly for the chloride) because adoption of the correct approximation in the correct field and temperature ranges yields consistent J/k values when only one exchange constant is used.

The J/k values obtained from the temperature dependence of the transition field to paramagnetism at low temperatures in the spin-wave approximation are too high. The conclusion which may be drawn from this is that either the high easy plane anisotropy plays an important role or the two-dimensional character of the antiferromagnets modifies this dependence because, in fact, in reference 24 the temperature dependence of the transition field is derived for the simple cubic case.

From this section it may be concluded that the behaviour of both salts (certainly the chloride) can be described satisfactorily using one exchange constant only. This interaction occurs only in planes, each spin having four neighbours. Introduction of another exchange interaction is not necessary, if the correct approximation is used in the field and temperature region where one wants to describe the magnetic behaviour.

5. Zero field behaviour.

In the present section we give a discussion of the zero magnetic field susceptibility curve of $CoBr_2 \cdot 6H_2O$ in view of the available theories. The only Ising model that could be solved exactly is Fisher's two-dimensional Ising superexchange antiferromagnet. Though it was stated in section 4.4 that this model does not apply too well to our substances we discuss it first. We have chosen J/k = 9.61 K so that the theoretical and experimental T_N coincide (see section 4.2).

It is shown in fig. 4 that the agreement between the experimental and theoretical data is much better below T_N than above it. In this superexchange model an infinite slope of the susceptibility versus the temperature is expected at T_N in zero field and a narrow spike near T_N in finite fields. This

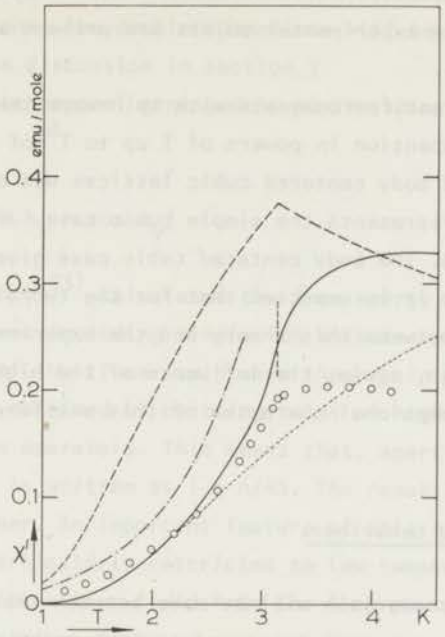

Fig. 4. The experimental parallel susceptibility of $CoBr_2 \cdot 6H_2O$ in zero field compared with different theories.
circles : experimental points.
dashed and dotted curves: molecular field approximation.
fully drawn curve : Ising model from Fisher.
dash-dotted curve : non-linear spin-wave theory.

critical behaviour in zero field does not seem to be sustained by the experiment because the susceptibility shows rather an abrupt change of slope at T_N, the slopes having finite values at either side of T_N. At higher fields, but below the triple point field, a weak maximum, however, is visible in fig. 6 of Chapter 5. This maximum is interpreted as the transition from the antiferromagnetic phase to the paramagnetic one and it may be related to the peak as predicted by Fisher.

The anomaly in the susceptibility as measured here is in qualitative agreement with the approximate treatment of the two-dimensional Ising antiferromagnet by Domb and Sykes (private communication between these authors and Fisher [18]). A numerical comparison has not been made.

The results of the molecular field treatment [13]) have also been represented in fig. 4. The dashed curve corresponds to $J/k = -3.14$ K (derived from T_N,

see section 4.1) and the dotted curve to J/k = - 4.72 K (derived from H_s). Large deviations from the experimental points are present as could be expected according to section 4.4.

Oguchi [25] treated antiferromagnets with spin-wave theory including spin-wave interactions. An expansion in powers of T up to T^6 of the susceptibility for the simple cubic and body centered cubic lattices was obtained. The dash-dotted curve in fig. 4 represents the simple cubic case. J/k was chosen - 4.72 K from H_s, see section 4.3. The body centered cubic case gives slightly lower susceptibility values so it is expected that for the two-dimensional square lattice the difference between this theory and the experimental points will be somewhat larger, although, again, the influence of the high easy plane anisotropy and of the two-dimensional character of this antiferromagnet is hard to estimate.

6. Non-zero field behaviour.

In this section a comparison will be made between the experimental susceptibility data at the lower temperatures and several spin-wave theories. Special attention will be given to the behaviour in the flop phase and the perpendicular susceptibility.

In the different spin-wave theories different approximations are used for the Holstein-Primakoff transformation. Here spin deviation operators are defined using the factor

$$(1 - n/2S)^{\frac{1}{2}} \tag{18}$$

with n the boson number operator. n ranges from 0 to 2S.

6.1. Spin-wave theories. The susceptibility data will be compared with three different spin-wave theories.

In these theories use is made of the quantity $\gamma_{\underline{k}}$ which is defined by:

$$\gamma_{\underline{k}} = \frac{1}{z} \sum_{\rho} \exp\ (i\ \underline{k}\cdot\underline{\rho}) \tag{19}$$

with $\underline{k}$ the wave vector of the spin wave, $\underline{\rho}$ the vectors pointing from a spin to its neighbours and z the number of neighbours. Because in both $CoCl_2 \cdot 6H_2O$ and $CoBr_2 \cdot 6H_2O$ the nearest neighbour interaction takes place in the (001) planes only, one of the three components of the $\underline{k}$ vector does not occur and consequent-

ly all the summations over the $\underline{k}$ space, which will be carried out below, take place in two dimensions. The double summations will be replaced by double integrals. See also the discussion in section 3.

Because of the tetragonal arrangement of the spins in both salts 19 can be rewritten as

$$\gamma_{\underline{k}} = \frac{1}{2}(\cos k_x + \cos k_y) \tag{20}$$

6.1.a. Kanamori [23] calculated the free energy for a simple two sublattice antiferromagnet including single ion anisotropy (which vanishes if $S = \frac{1}{2}$). He made use of the linear spin-wave theory, in which the Hamiltonian of the spin waves is obtained by omitting terms of higher order than quadratic in the spin deviation operators. This means that, apart from other approximations, expression 18 is written as $1 - n/4S$. The resulting spin waves are independent of each other. An important feature of this linear approach is that its application is particularly restricted to low temperatures (where n is small) and that the transition field from the flop phase to the paramagnetic phase is temperature independent.

According to this theory the dispersion relations for the two modes of the spin waves, for zero anisotropy, read:

$$\begin{aligned} \hbar\omega_1 &= -JzS(1 - \gamma_{\underline{k}})^{\frac{1}{2}}(1 + (1 - 2h^2)\gamma_{\underline{k}})^{\frac{1}{2}} \\ \hbar\omega_2 &= -JzS(1 + \gamma_{\underline{k}})^{\frac{1}{2}}(1 - (1 - 2h^2)\gamma_{\underline{k}})^{\frac{1}{2}} \end{aligned} \tag{21}$$

Kanamori derived the susceptibility from the free energy F applying the relation

$$\chi = -(\partial F/\partial H)_T/H \tag{22}$$

Since in our experiments the differential magnetic susceptibility is measured we made use of the formula

$$\chi = -(\partial F/\partial H^2)_T \tag{23}$$

which corresponds to the perpendicular susceptibility from the experiment, because in 23 the anisotropy is assumed to be zero. Equation 23 leads to the following relations:

$$\chi'_r = m/h + (h/(2\pi^2)) \int_0^\pi \int_0^\pi F(\gamma_{\underline{k}},h)dk_x dk_y \qquad (24)$$

with the reduced magnetization

$$m = \frac{1}{2} h + (h/(2\pi^2)) \int_0^\pi \int_0^\pi G(\gamma_{\underline{k}},h)dk_x dk_y$$

$$G(\gamma_{\underline{k}},h) = (2n(\gamma_{\underline{k}},h) + 1)G_o(\gamma_{\underline{k}},h)$$

$$F(\gamma_{\underline{k}},h) = F_o(\gamma_{\underline{k}},h)(2n(\gamma_{\underline{k}},h) + 1) +$$

$$2G_o(\gamma_{\underline{k}},h)(n(\gamma_{\underline{k}},h) + n^2(\gamma_{\underline{k}},h))(2h\gamma_{\underline{k}}/t)((1 - \gamma_{\underline{k}})/(1 + (1 - 2h^2)\gamma_{\underline{k}}))^{\frac{1}{2}}$$

In these expressions:

$$n(\gamma_{\underline{k}},h) = (\exp(((1 - \gamma_{\underline{k}})(1 + (1 - 2h^2)\gamma_{\underline{k}}))^{\frac{1}{2}}/t)-1)^{-1}$$

which is the occupation number of the spin waves

$$G_o(\gamma_{\underline{k}},h) = \gamma_{\underline{k}}((1 - \gamma_{\underline{k}})/(1 + (1 - 2h^2)\gamma_{\underline{k}}))^{\frac{1}{2}}$$

$$F_o(\gamma_{\underline{k}},h) = \gamma_{\underline{k}}(1 + \gamma_{\underline{k}})((1 - \gamma_{\underline{k}})/(1 + (1 - 2h^2)\gamma_{\underline{k}})^3)^{\frac{1}{2}}$$

The reduced magnetic field h is defined by

$$h = -g\mu_B H/2JzS$$

the reduced temperature t by

$$t = -kT/zJS$$

and the reduced susceptibility is defined such that the integral of the susceptibility over h is equal to $\frac{1}{2}$.

6.1.b. Wang and Callen [26] replaced the spin deviation operators appearing in their treatment by simplified ones which give a correct description of the low lying states, but introduce relatively large errors in the higher states. Actually they replaced $(1 - n/2S)^{\frac{1}{2}}$ by $1 - (1 - \xi)n$ with $\xi^2 = 1 - 1/2S$,

which is equivalent to the assumption $n^2 = n$.

In the resulting Hamiltonian expressed in terms of the spin deviation operators third and higher order terms have been replaced by lower order terms, which means that spin-wave interactions are taken into account to a certain extent.

It seems promising to use this approach for $S = \frac{1}{2}$ systems because in that case 18 reads $(1 - n)^{\frac{1}{2}}$ and is exactly equal to $1 - n$ for $n = 0$ and $n = 1$, the only n values which can exist.

The dispersion relations for the two existing spin-wave modes are:

$$\hbar\omega_1 = -zJS(1 - \gamma_{\underline{k}})^{\frac{1}{2}}(1 + (1 - 2h^2)\gamma_{\underline{k}})^{\frac{1}{2}}$$
$$\hbar\omega_2 = -zJS(1 + \gamma_{\underline{k}})^{\frac{1}{2}}(1 - (1 - 2h^2)\gamma_{\underline{k}})^{\frac{1}{2}} \qquad (25)$$

In 25 the anisotropy is assumed to be zero and they coincide exactly with the dispersion relations as given by Kanamori for zero anisotropy, which seems quite surprising.

The perpendicular susceptibility can be obtained from the expression for the sublattice magnetization per spin m_s in the flop phase, which is given by Wang and Callen.

$$\chi_r' = m_s + h(\partial m_s/\partial h)_t \qquad (26)$$

with

$$m_s = 1 - 2(1/2\pi)^2 \int_0^{\pi}\int_0^{\pi} G(\gamma_{\underline{k}},h)dk_x dk_y$$

$$(\partial m_s/\partial h)_t = -2(1/2\pi)^2 \int_0^{\pi}\int_0^{\pi} F(\gamma_{\underline{k}},h)dk_x dk_y$$

In these expressions

$$G(\gamma_{\underline{k}},h) = (2n(\gamma_{\underline{k}},h) + 1)G_o(\gamma_{\underline{k}},h)$$

$$F(\gamma_{\underline{k}},h) = F_o(\gamma_{\underline{k}},h)(2n(\gamma_{\underline{k}},h) + 1) -$$

$$2G_o(\gamma_{\underline{k}},h)(n(\gamma_{\underline{k}},h) + n^2(\gamma_{\underline{k}},h))(2h\gamma_{\underline{k}}/t)((1 + \gamma_{\underline{k}})/(1 - (1 - 2h^2)\gamma_{\underline{k}}))^{\frac{1}{2}}$$

with the definitions:

$$n(\gamma_{\underline{k}},h) = (\exp(((1 + \gamma_{\underline{k}})(1 - (1 - 2h^2)\gamma_{\underline{k}}))^{\frac{1}{2}}/t) - 1)^{-1}$$

which is the occupation number.

$$G_o(\gamma_{\underline{k}},h) = (1 + \gamma_{\underline{k}}h^2)/((1 + \gamma_{\underline{k}})(1 - (1 - 2h^2)\gamma_{\underline{k}}))^{\frac{1}{2}}$$

$$F_o(\gamma_{\underline{k}},h) = 2h\gamma_{\underline{k}}G_o(\gamma_{\underline{k}},h)((1 + \gamma_{\underline{k}}h^2)^{-1} - (1 - (1 - 2h^2)\gamma_{\underline{k}})^{-1})$$

6.1.c. Feder and Pytte [24] treated the simple antiferromagnet (including single ion anisotropy and anisotropic exchange) in the antiferromagnetic, flop and paramagnetic phases. Spin-wave interactions to leading order in 1/2S are taken into account. Their treatment results into a Hamiltonian which contains spin deviation operators up to fourth order. An important feature of this theory is that the spin waves are not independent any more and temperature dependent critical fields are found. For the transition field to the paramagnetic phase a $T^{3/2}$ power law is derived. This dependence has already been compared with the experiment and discussed in section 4.

The expressions for the parallel susceptibility as derived from the expressions for the magnetization given by these authors are the following.

In the antiferromagnetic phase if $h^a_{c1} - h >> t/2$ then

$$\chi'_r = 3.74(h^a_{c1})^{3/2}t^{1/2} \exp(-2h^a_{c1}/t) \cosh(2h/t) \qquad (26a)$$

Here h^a_{c1} is the spin flop field in reduced units.
If $h^a_{c1} - h << t/2 << 2h^a_{c1}$ then

$$\chi'_r = 2.34(h^a_{c1})^{3/2}(h^a_{c1} - h)^{-1/2} - 2.73(h^a_{c1})^{3/2}t^{1/2}h \qquad (27)$$

In the flop phase if $h - h^a_{c1} << t/2$ then

$$\chi'_r = \chi'_r(0) - .8661t^2 + 2.34\,K^{\frac{1}{2}}t(h - h^a_{c1})^{\frac{1}{2}} + 1.17\,K^{\frac{1}{2}}th(h - h^a_{c1})^{-\frac{1}{2}} \qquad (28)$$

In this formula K is related to the anisotropic exchange and can be expressed in h^a_{c1}

$$K = -1 + (1 + 4(h^a_{c1})^2)^{\frac{1}{2}}$$

$\chi'_r(0)$ is the reduced susceptibility at zero temperature and is given by

$$\chi'_r(0) = \frac{1}{2} - S_o(h) - hS'_o(h) \qquad (29)$$

with

$$S_o(h) = 2(1/2\pi)^2 \int_o^{\pi}\int_o^{\pi} G(\gamma_{\underline{k}},h)\, dk_x dk_y$$

$$S'_o(h) = 2(1/2\pi)^2 \int_o^{\pi}\int_o^{\pi} F(\gamma_{\underline{k}},h)\, dk_x dk_y$$

In these expressions for $S_o(h)$ and $S'_o(h)$, $G(\gamma_{\underline{k}},h)$ and $F(\gamma_{\underline{k}},h)$ are given by

$$G(\gamma_{\underline{k}},h) = \gamma_{\underline{k}}((1 + \gamma_{\underline{k}})/(1 - (1 - 2h^2)\gamma_{\underline{k}}))^{\frac{1}{2}}$$

$$F(\gamma_{\underline{k}},h) = -2h\gamma^2_{\underline{k}}((1 + \gamma_{\underline{k}})/(1 - (1 - 2h^2)\gamma_{\underline{k}})^3)^{\frac{1}{2}}$$

If $h - h^a_{c1} \gg t/2$ and $1 - h \gg t/2$ then

$$\chi'_r = \chi'_r(0) + .8547t^4((1 - h^2)^{-5/2} + 5h^2(1 - h^2)^{-7/2} \qquad (30)$$

and if $1 - h \ll t/2$ then

$$\chi'_r = \chi'_r(0) + .8617t^{3/2} - 2.3391t(1 - 1.5h)(1 - h)^{-1/2} \qquad (31)$$

And finally in the paramagnetic phase if $h - 1 \ll t/2$

$$\chi'_r = .825t(h - 1)^{-1/2} - .963t^{1/2} \qquad (32)$$

and if $h - 1 \gg t/2$ then

$$\chi'_r = .659t^{1/2} \exp(2(1 - h)/t) \qquad (33)$$

For the perpendicular susceptibility according to Feder and Pytte equations 29 to 33 are used. Equations 29 and 30 will be applied down to zero field.

The susceptibility versus the magnetic field at zero temperature in the perpendicular case according to all three theories is given in fig. 5.

The field scale h, in agreement with the definition given above, represents the field H in units of $H_c(0)$, the upper transition field at T = 0, which is 55 kOe for $CoBr_2 \cdot 6H_2O$, see fig. 3. The susceptibility scale is chosen in such a way that the integral of χ' over h is equal to $\frac{1}{2}$ (= S).

The curves of Feder and Pytte and of Kanamori coincide as might be expected, because the higher than second order terms in the spin deviation operators

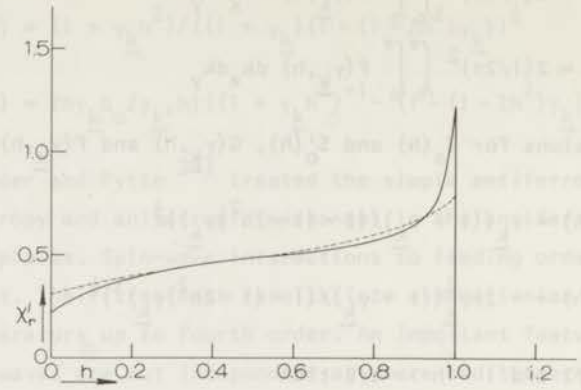

Fig. 5. Zero temperature susceptibility according to different theories.
fully drawn curve: Kanamori as well as Feder and Pytte.
dashed curve : Wang and Callen.

in the Hamiltonian of Feder and Pytte arise from the spin-wave interactions and their effect becomes negligible at zero temperature.

6.2. Comparison with experiment. The experimental results for $CoBr_2 \cdot 6H_2O$ as given in Chapter 5 are compared with the three theories, discussed above, in figures 6, 7 and 8. In all the figures the experiments are represented by circles. Similar comparisons can be made for $CoCl_2 \cdot 6H_2O$; they lead to conclusions which are not essentially different from those for the bromide.

In fig. 6 the data in perpendicular fields is compared with the theories of Kanamori and of Wang and Callen, for three different temperatures. $h_c(T)$ is the experimental transition field in reduced units.

Fig. 7 shows the data in parallel fields for three different temperatures, together with the curves of Feder and Pytte. $h_{c2}(T)$ is the transition field to paramagnetism according to the $T^{3/2}$ law as derived by Feder and Pytte with a fit at the lowest temperatures. h^a_{c1} is the spin flop field.

Fig. 8 shows the data in perpendicular fields, again for three temperatures and also with the theoretical curves of Feder and Pytte.

In these figures the susceptibilities and the fields have been expressed in the same reduced units as in fig. 5, so $h = H/H_c(0)$ and the integral of χ'_r h is equal to $\frac{1}{2}$.

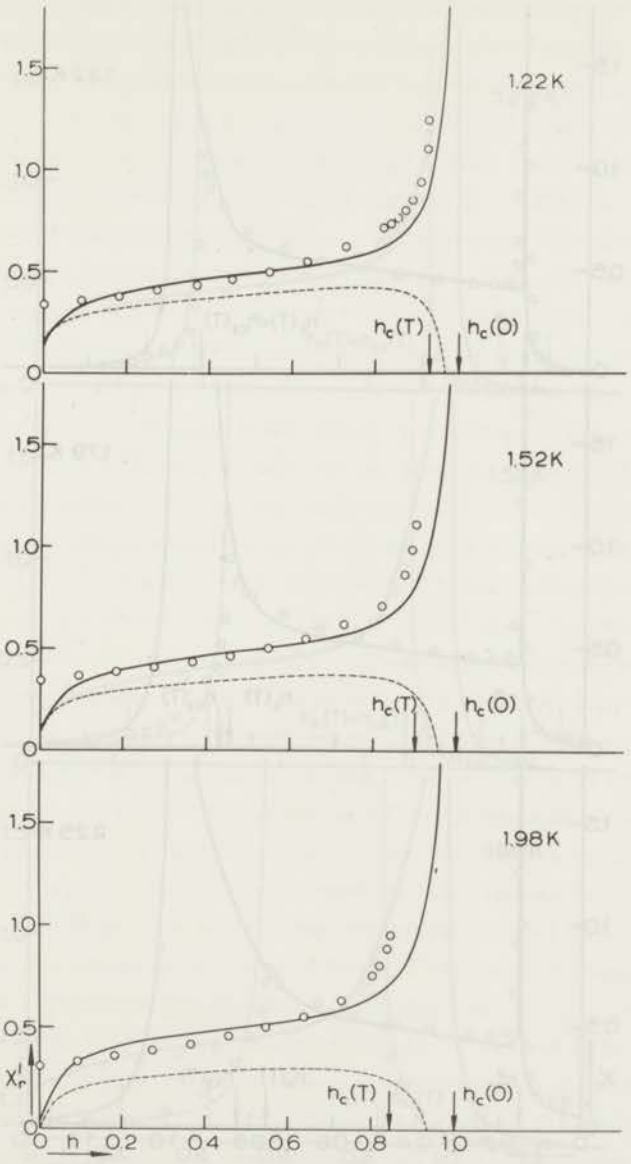

Fig. 6. Experimental perpendicular susceptibility (circles) for $CoBr_2 \cdot 6H_2O$ at different temperatures, compared with the theory as given by Kanamori (fully drawn curve) and Wang and Callen (dashed curve).

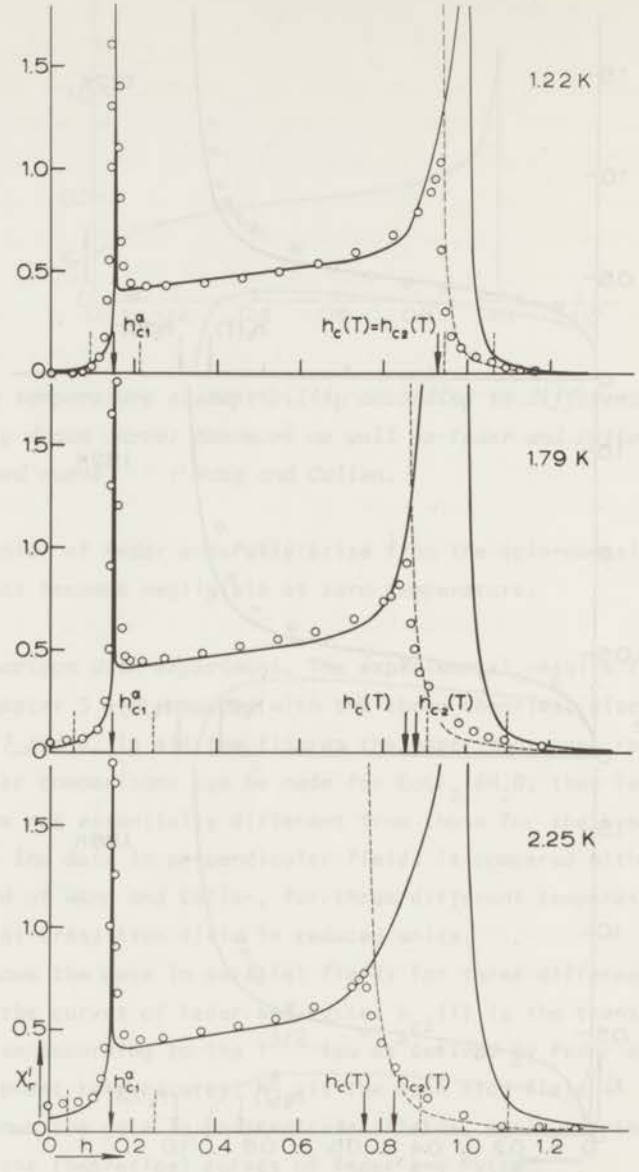

Fig. 7. Experimental parallel susceptibility (circles) for $CoBr_2 \cdot 6H_2O$ at different temperatures, compared with the theory as given by Feder and Pytte (fully drawn curve). The dashed curve is explained in the text.

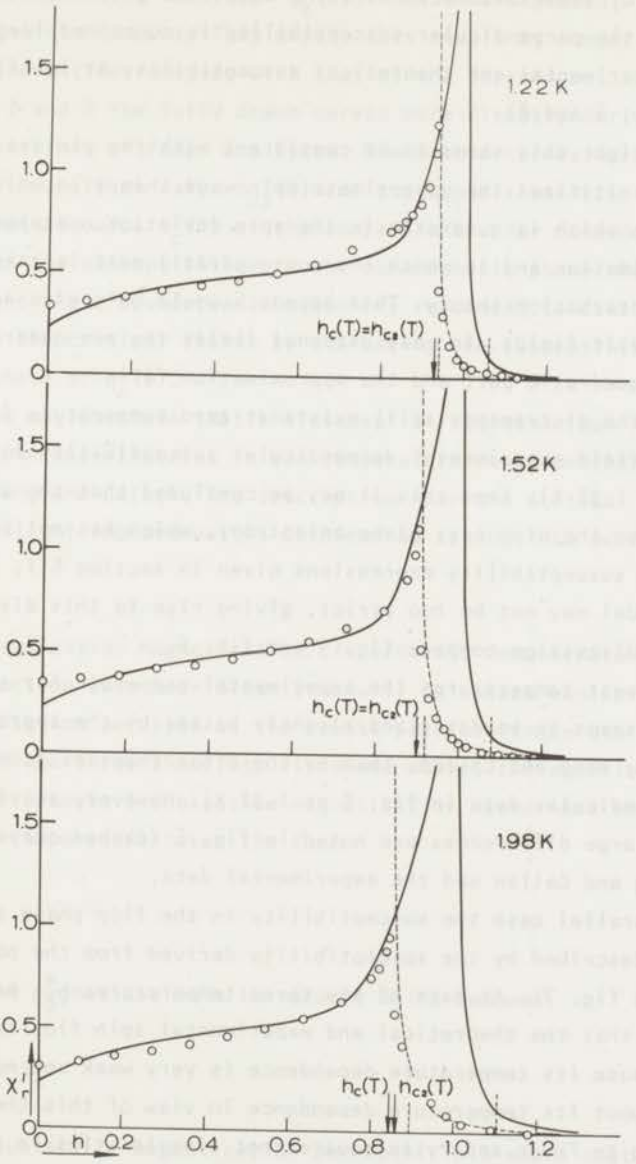

Fig. 8. Experimental perpendicular susceptibility (circles) for $CoBr_2 \cdot 6H_2O$ at different temperatures, compared with the theory as given by Feder and Pytte (fully drawn curve). (The dashed curve is explained in the text.)

Near the vertical dashed lines in figs. 7 and 8, which are located on both sides at distances t/2 from the critical fields the susceptibility has been obtained by interpolating the susceptibility values which were obtained at either side of these dashed lines using equations given in section 6.1.c.

As far as the perpendicular susceptibility is concerned large deviations between the experimental and theoretical susceptibility at low fields are noted (see figs. 6 and 8).

At first sight this seems to be consistent with the picture given by Dyson [27] who criticizes the approximate spin-wave theory in which the part of the Hamiltonian which is quadratic in the spin deviation operators is taken as a first approximation and in which the non-quadratic part is taken into account by means of perturbation theory. This approach would only give reliable results in strong magnetic fields. In weak external fields the non-quadratic part dominates the quadratic part and the approximation fails.

However, the discrepancy still exists at zero temperature (it is supposed that the zero field experimental perpendicular susceptibility does not change any more below 1.22 K). From this it may be concluded that the discrepancy is partially due to the high easy plane anisotropy, which has not been taken into account in the susceptibility expressions given in section 6.1. Also the two-dimensional model may not be too strict, giving rise to this discrepancy. For the preceding discussion compare fig. 5 and fig. 6.

At the lowest temperatures the experimental perpendicular susceptibility in low fields seems to be described slightly better by the approximate theory as developed by Wang and Callen, than by the other theories (compare fig. 5 with the perpendicular data in fig. 6 at 1.22 K). However, at slightly elevated temperatures large differences are noted in fig. 6 (dashed curves) between the theory of Wang and Callen and the experimental data.

In the parallel case the susceptibility in the flop phase seems to be quite nicely described by the susceptibility derived from the paper of Feder and Pytte (see fig. 7). At each of the three temperatures h^a_{c1} has been adapted in such a way that the theoretical and experimental spin flop transitions always coincide, because its temperature dependence is very weak and nothing conclusive can be said about its temperature dependence in view of this theory.

According to Feder and Pytte square root singularities in the susceptibility must be expected near $h^a_{c1}(0)$ and $h_{c2}(0)$. This, however, can obviously not be true for temperatures not equal to zero, because the theory predicts temperature dependent transition fields. This inconsistency must be related to their approximations, in which they take into account spin-wave interactions to

leading order in 1/2S. To this order their transition fields are temperature dependent, whereas to the same order, in their susceptibility expansion terms $(1 - h_c(0))^{-\frac{1}{2}}$ arise. The authors discuss this point also and they conclude that a singularity of the form $(1 - h_c(T))^{-\frac{1}{2}}$ must be expected, if higher order terms are taken into account. They expect this result by comparing the critical behaviour of the antiferromagnet with that of the ferromagnet.

In figs. 7 and 8 the fully drawn curves were directly derived from the theoretical relations of Feder and Pytte. The dotted curves were obtained by replacing the theoretical value $h_{c2}(0)$ for the upper transition field at T = 0 by the experimental value $h_c(T)$ at the temperature under consideration in their expressions for the susceptibility in the paramagnetic phase. Related to the problem near the phase boundaries the authors recommend to calculate the susceptibility at the critical fields by evaluating the susceptibility expressions for the flop phase at $h_c(T)$.

Finally we may conclude that the susceptibility behaviour is satisfactorily described by spin-wave theories in the temperature range considered, except by the one from Wang and Callen. The description near the critical fields is still unreliable. A slight improvement is obtained by taking into account spin-wave interactions.

6.3. The sublattice magnetization. In order to demonstrate the large zero point spin reduction even more clearly we will calculate explicitly the sublattice magnetization per spin at the lowest possible temperature.

In each of the three theories, discussed above, the equilibrium condition for the angle θ between a sublattice magnetization vector and the magnetic field and zero temperature takes the form

$$\cos\theta = h \tag{34}$$

In that case the magnetization m in reduced units becomes

$$m = h\langle S_s \rangle \tag{35}$$

with $\langle S_s \rangle$ the sublattice magnetization per spin. This means that $\langle S_s \rangle$ can be obtained as a function of h by calculating the experimental value of m/h. m can be calculated by integration

$$m(h) = \int_0^h \chi_r' \, dh \tag{36}$$

In this way we can calculate the sublattice magnetization per spin. Above the transition field to saturation the sublattice magnetization and the total magnetization, both in reduced units, are identical.

The quantity as calculated here will not differ significantly from the spin value at zero temperature, corrected for the zero point deviation, if data at 1.22 K are used.

The sublattice magnetization per spin has been plotted in fig. 9 using equations 34, 35 and 36 and the perpendicular susceptibility at 1.22 K for $CoBr_2 \cdot 6H_2O$ (see fig. 8 in Chapter 5).

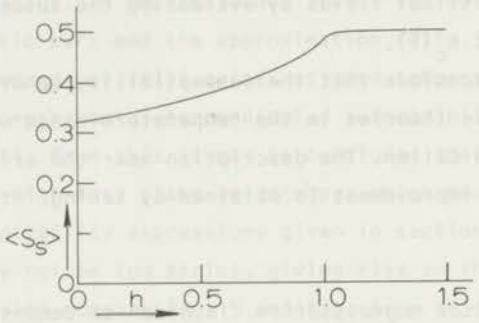

Fig. 9. Sublattice magnetization per spin plotted versus the reduced magnetic field at 1.22 K.

According to the theories given by Kanamori and by Feder and Pytte a zero point spin reduction in zero field of .28 was expected. From Wang and Callen's approach this value would be .19. Both values are derived from fig. 5. These two values may be compared with the value that follows from linear spin-wave calculations using a simple cubic spin structure and which amounts to .08 [19]. In view of the experimental value .17 (see fig. 9) of the zero point spin reduction it seems that the two-dimensional character of the spin arrangement (thus only four neighbours) is corroborated.

References.

1) Shinoda, T., Chihara, H. and Seki, S., J. Phys. Soc. Japan 19 (1964) 1637.
2) Murray, T.E. and Wessel, G.K., J. Phys. Soc. Japan 24 (1968) 738.
3) Date, M., J. Phys. Soc. Japan 16 (1961) 1337.
4) Mizuno, J., J. Phys. Soc. Japan 15 (1960) 1412.
5) Mermin, N.D. and Wagner, H., Phys. Rev. Letters 17 (1966) 1133.
6) Kleinberg, R., J. Chem. Phys. 53 (1970) 2660.
7) Kleinberg, R., Bull. Amer. Phys. Soc. 11 (1966) 759.
8) Haseda, T., J. Phys. Soc. Japan 15 (1960) 483.
9) Flippen, R.B. and Friedberg, S.A., J. Appl. Phys. 31 (1960) 338S.
10) Uryū, N., Skalyo, J. and Friedberg, S.A., Phys. Rev. 144 (1966) 689.
11) Kambe, K., Koide, S. and Usui, T., Prog. Theor. Phys. 7 (1952) 15.
12) El Saffar, Z.M., J. Phys. Soc. Japan 17 (1962) 1334.
13) Nagamiya, T., Yoshida, K. and Kubo, R., Adv. Phys. 4 (1955) 1.
14) Carrara, P., de Gunzbourg, J. and Allain, Y., J. Appl. Phys. 40 (1969) 1035.
15) Lines, M.E. and Jones, E.D., Phys. Rev. 141 (1966) 525.
16) Robinson, W.K. and Friedberg, S.A., Phys. Rev. 117 (1960) 402.
17) Skalyo, J., Cohen, A.F., Friedberg, S.A. and Griffiths, R.B., Phys. Rev. 164 (1967) 705.
18) Fisher, M.E., Proc. Roy. Soc. A254 (1960) 66.
19) Anderson, P.W., Phys. Rev. 86 (1952) 694.
20) Kubo, R., Phys. Rev. 87 (1952) 568.
21) Onsager, L., Phys. Rev. 65 (1944) 117.
22) Bienenstock, A., J. Appl. Phys. 37 (1966) 1459.
23) Kanamori, J. and Yoshida, K., Prog. Theor. Phys. 14 (1955) 423.
24) Feder, J. and Pytte, E., Phys. Rev. 168 (1968) 640.
25) Oguchi, T., Phys. Rev. 117 (1960) 117.
26) Wang, Y.L. and Callen, H.B., J. Phys. Chem. Solids 25 (1964) 1459.
27) Dyson, F.J., Phys. Rev. 102 (1956) 1217.

Samenvatting.

In dit proefschrift wordt het magnetische gedrag van drie antiferromagnetische stoffen beschreven: $LiCuCl_3 \cdot 2H_2O$, $CoCl_2 \cdot 6H_2O$ en $CoBr_2 \cdot 6H_2O$. De overeenkomst tussen deze drie stoffen bestaat hierin dat de magnetische ionen de spinwaarde een half bezitten en dat de anisotropie in de wisselwerking tussen de spins vrij groot is.

Tengevolge van de interactie tussen de spins treden er bij voldoende lage temperaturen (1.2 tot 5 K voor genoemde stoffen) ordeningsverschijnselen op, die op hun beurt weer sterk door een magneetveld beinvloed kunnen worden. Teneinde een groot deel van het veld-temperatuur fasediagram te kunnen onderzoeken, zijn magneetvelden van de orde van 100 kOe nodig, die thans redelijk eenvoudig te verkrijgen zijn met behulp van supergeleidende spoelen. De bouw en het gedrag van een dergelijke spoel met bijbehorende metalen kryostaat is beschreven in hoofdstuk 2. Met behulp van deze magneet is de susceptibiliteit van de drie antiferromagneten gemeten tot ongeveer 110 kOe, waarbij de metingen boven ongeveer 15 kOe geheel nieuw zijn.

De anisotropie in $LiCuCl_3 \cdot 2H_2O$ blijkt, mede op grond van de susceptibiliteitsmetingen die in hoofdstuk 3 vermeld staan, van het Dzyaloshinsky-Moriya type te zijn en dus antisymmetrisch. Hiernaast treedt ook nog een minder belangrijk symmetrisch deel in de anisotropie op. De gegevens uit de literatuur betreffende deze antiferromagneet zijn vrij summier. Niettemin is het in hoofdstuk 4 gelukt enkele opmerkelijke eigenschappen te verklaren. Een hiervan is het bestaan van een extra eerste orde faseovergang ten gevolge van de aanwezigheid van de Dzyaloshinsky-Moriya interactie. Een essentiele eigenschap van die faseovergang is dat het vector product van twee van de vier magnetische onderroosters, welke in $LiCuCl_3 \cdot 2H_2O$ voorkomen, onder invloed van een aangelegd magneetveld, van teken omslaat.

De beide andere stoffen $CoCl_2 \cdot 6H_2O$ en $CoBr_2 \cdot 6H_2O$ blijken in redelijke benadering twee dimensionale anisotrope Heisenberg antiferromagneten te zijn, zoals volgt uit de literatuur gegevens en de susceptibiliteits-metingen, die vermeld staan in hoofdstuk 5. Uit de discussies in hoofdstuk 6 blijkt dat in velden die laag zijn ten opzichte van het spin flop veld de Ising beschrijving redelijk is, terwijl voor hogere velden dit limietgeval van het anisotrope Heisenberg model niet meer voldoet. In het laatste geval is met behulp van spin golf theorie het anomaal gedrag van de susceptibiliteit in de flop fase, zowel als dat van de loodrecht susceptibiliteit, kwantitatief verklaard, hoewel nog moeilijkheden optreden in de buurt van de faseovergangen. De grote nulpunts afwijking van de spin-waarde in veld nul is een verdere kwalitatieve aanwijzing dat in het gedrag van de beide Co-zouten het twee dimensionale karakter een rol speelt.

Op verzoek van de Faculteit der Wiskunde en Natuurwetenschappen volgt hier een overzicht van mijn studie.

Nadat ik het Rembrandt-lyceum in Leiden had doorlopen in de periode 1955-1960 begon ik met mijn studie in de natuur- en wiskunde met als bijvak sterrekunde aan de Leidse Universiteit. Ik legde in 1964 het kandidaatexamen af. Na dit examen ben ik op het Kamerlingh Onnes Laboratorium werkzaam geweest in de werkgroep van Dr. D. de Klerk, waar ik werd ingeschakeld bij het experimenteel onderzoek aan type II supergeleiders van Dr. S.H. Goedemoed. In 1965 kreeg ik van Dr. de Klerk de opdracht de in het laboratorium aanwezige 4 Megawatt installatie zover te verbeteren, dat er fysische experimenten mee gedaan konden worden in velden tot ongeveer 100 kOe. Dit doel werd ten koste van veel inspanning slechts ten dele bereikt en daarom werd in 1967 (mijn doctoraalexamen legde ik eind 1966 af) een aanvang gemaakt met het vervangen van deze installatie door een veel eenvoudiger en moderner opstelling, waarbij het continue magneetveld zou worden opgewekt met behulp van een vrij grote supergeleidende spoel. Deze opstelling werd in 1969 operatief en sindsdien zijn de experimenten uitgevoerd, die in dit proefschrift zijn vermeld.

Naast dit fysisch onderzoek had ik ook een taak bij het onderwijs. Ik assisteerde op het praktikum sinds 1965. In 1971 werd ik hoofdassistent bij het elektronisch praktikum voor tweede jaars studenten.

Voor het tot stand komen van dit proefschrift is de medewerking van vele anderen onmisbaar geweest. In het bijzonder worden Dr. H.W. Capel en Drs. A.E. van der Valk bedankt voor hun bijdrage betreffende de theoretische problematiek rond de discussie en interpretatie van de meetresultaten. Drs. H.A. Jordaan, Drs. J.W. Schutter en Drs. K.R. van der Veen hebben mij bijgestaan bij de voorbereidingen en het uitvoeren van de experimenten. De vele discussies met andere medewerkers zijn hooglijk gewaardeerd.

De illustraties in dit proefschrift zijn op fraaie wijze door de heren W.F. Tegelaar en W.J. Brokaar getekend.

De heren A.F.M. Oosterbaan, J. van den Berg en in het bijzonder T.P.M. van den Burg hebben vele technische problemen weten op te lossen.

Mevrouw M.A. Otten-Scholten heeft het merendeel van de eenkristallen gemaakt, die voor de experimenten nodig waren.

Tenslotte zij vermeld dat de tekst van het proefschrift op vaardige wijze is getypt door mevrouw E. de Haas-Walraven.